Graduate Theses and Dissertations   Graduate School

April 2018

Investigations on FRP-Concrete Bond

Mostfa Al Azzawi
University of South Florida, mostfaalazzawi@gmail.com

Investigations on FRP-Concrete Bond

by

Mostfa Al Azzawi

A dissertation submitted in partial fulfillment
of the requirements for the degree of
Doctor of Philosophy
Department of Civil and Environmental Engineering
College of Engineering
University of South Florida

Co-Major Professor: Rajan Sen, Ph.D.
Co-Major Professor: Gray Mullins, Ph.D.
Autar Kaw, Ph.D.
K Ramachandran, Ph.D.
Abla Zayed, Ph.D.

Date of Approval:
March 30, 2018

Keywords: Composite, Pile, Durability, Testing, Porosity

DEDICATION

To my father, my mother, my wife who supported me throughout this research. And to my children.

ACKNOWLEDGEMENTS

TABLE OF CONTENTS

LIST OF TABLES

LIST OF FIGURES

ABSTRACT

This dissertation presents findings from three separate investigations, a laboratory study and two field studies that evaluated the durability of the Fiber Reinforced Polymer (FRP)-concrete bond. The laboratory study explored the role of porosity on CFRP-concrete bond following immersion in warm water. Two disparate field studies measured residual bond after 20 years outdoor exposure of FRP repairs of full-size masonry walls and after 12 years for partially submerged piles supporting the Friendship Trail Bridge, Tampa Bay.

The ACI 440 code requires the same surface preparation for all externally bonded FRP concrete repairs. This disregards the role of porosity that is a function of the water / cementitious (w/c) ratio. Concretes with high w/c ratios are low strength concretes, have large voids and a more elaborate capillary pore network compared to low w/c, high strength concretes. Epoxies will therefore penetrate deeper into high porosity concretes. As a result, the performance of low strength, high porosity concrete under moisture exposure can be anticipated to be superior. The laboratory study was intended to determine whether this hypothesis was correct or not.

Three different concrete mixes with water / cementitious ratios of 0.73, 0.44 and 0.25 representing high, medium and low porosities were used for the study. The corresponding target compressive strengths were 2,500 psi, 5,000 psi and 7,500 psi respectively. A total of eighteen, 9 in. x 9 in. x 2.5 in. thick slabs, three for each concrete porosity were tested. Slabs were allowed to cure for over 90 days before surfaces were lightly sand blasted to provide the required concrete surface profile (CSP 3). Specimens were then pre-conditioned in an oven for 48 hours to ensure uniform drying.

Concrete porosity was characterized using mercury porosimetry, SEM, 3D surface scanning and images obtained using a portable microscope. Two commercially available CFRP materials were bonded to the oven-dried prepared slab surfaces and the epoxy allowed to cure at room temperature for 4 weeks. Twelve FRP bonded slabs were completely submerged in potable water at 30 ^{o}C (86 ^{o}F) as part of the aging program. The six remaining slabs were used for establishing baseline bond values through destructive pull-off tests. The twelve exposed slabs were similarly tested following 15 weeks of exposure.

Results showed minimal degradation in the high porosity, low strength concrete but over 20% reduction in the low porosity, higher strength concrete. Analysis of the failure plane indicated that the lower porosity of the high strength concrete had limited the depth to which the epoxy could penetrate. This was confirmed from magnified images of the bond line taken using a microscope and from a careful assessment of the failure mode. Findings also suggest that the CSP 3 surface profile (light sand blasting) may be adequate for lower strength concrete but not so for higher strength concrete. For applications where FRP concrete repairs of higher strength concrete are permanently or intermittently exposed to moisture, alternative surface preparation may be needed to allow epoxy to penetrate deeper into the concrete substrate. The viscosity of the resin hitherto not considered may be a critical parameter.

In 1995, two full-scale concrete masonry walls were repaired using three horizontally aligned 20 in. (508 mm) wide uni-directional carbon fiber sheets using different commercially available epoxies. Twenty years later the CFRP-CMU bond was determined through selective pull-off tests that were preceded by detailed non-destructive evaluation. Results showed that despite superficial damage to the top epoxy coating and debonding along masonry joints, the residual CFRP-CMU bond was largely unaffected by prolonged exposure to Florida's harsh environment.

Therein, 99% of samples exhibited in cohesive failure of the CMU or mortar. Pull-off strength was poorer at mortar joints but because the CFRP was well bonded to the masonry surface, its impact on structural performance of the repair was expected to be minimal. Overall, the repairs proved to be durable with both epoxy systems performing well.

The Friendship Trail Bridge linking St. Petersburg to Tampa FL was demolished in 2016. This was the site of three disparate demonstration projects in which 13 corroding reinforced concrete piles were repaired using fiber reinforced polymer (FRP) in 2003-04, 2006, and 2008. The repairs were undertaken using combinations of carbon and glass fiber, pre-preg and wet layup, epoxy and polyurethane resin, and were installed using either shrink wrap or pressure bagging. Residual FRP-concrete bond was evaluated after up to 12 years of exposure through 120 pull-off tests conducted on 10 representative repaired piles. Results showed a wide variation in the measured pull-off strength depending on the type of resin, the number of FRP layers, the prevailing conditions at the time the epoxy was mixed and the method of installation. Epoxy-based systems were found to be sensitive to ambient conditions at installation. Pressure bagging improved performance. The highest residual bond was recorded in pressure bagged piles repaired in 2008. The findings suggest that in marine environments epoxy-based systems installed using pressure bagging can lead to durable repairs.

CHAPTER 1: OVERVIEW

This dissertation presents findings from three separate investigations, a laboratory study and two field assessments evaluating the durability of FRP-concrete bond. The laboratory studies were conducted to understand how durability could be improved in the future while the field studies focused on determining the performance of past repairs. Thus, the two studies linked the past to the future.

Durability of FRP-concrete bond is critically important. It has been, and continues to be, the subject of worldwide research studies. Much has been learned and critical environments identified that are summarized in state-of-the-art reviews, e.g. (Myers, 2007), (Dolan, et al., 2009), (Sen, 2015). These studies evaluated residual bond following exposure to various environments for different combinations of FRP materials and concrete strengths.

An important parameter that appears to have been overlooked is the role of concrete porosity on long term durability. Porosity is a measure of the extent and size of the network of voids present in concrete. The volume of capillary pores present in hydrated concrete is proportional to the water / cementitious (w/c) ratio of the concrete mix, e.g. (Mehta and Monteiro, 1993). The epoxy resin may therefore be expected to penetrate deeper into low strength concrete because of its high porosity compared to high strength, low porosity concrete where penetration will be commensurately shallower. Because permeability is lower in higher strength concrete, it will take moisture longer to reach the bond line. But since epoxy can seal larger voids in lower strength concrete there is a possibility that degradation will occur sooner in high strength concretes.

The laboratory study was set up to explore this hypothesis and is described in Chapters 2 to 8 in this dissertation.

The University of South Florida (USF) has been a pioneer in the application of externally bonded FRP used for masonry settlement repair and for repairing corrosion damage in piles. The use of FRP to repair settlement damage was completed in 1995. Twenty years represents an important mile stone especially since the expected life of a repair is not stated in any specifications. Thus, 2015 was an opportune time to obtain information on FRP-concrete bond. This was evaluated through both non-destructive and destructive testing. The entire manuscript, Al Azzawi et al. 2018 that is awaiting publication in ACI Structural Journal is included as Chapter 9.

The Friendship Trail Bridge has been the site of three disparate studies in which corroding piles were repaired between 2003 to 2008. When a decision was made to demolish this bridge in 2015, Mr. Nils Olsson, Senior Bridge, Hillsborough County Public Works Department, approached USF to conduct studies prior to its demolition. Their offer of assistance and arrangements with the demolition contractor made it possible to complete 80% of the investigation by the time the bridge was demolished in April 2016. The accepted manuscript, Al Azzawi et al. 2018, awaiting publication in ASCE's Journal of Composites for Construction is included as Chapter 10.

To avoid clutter, additional data are included separately in Appendix A.

CHAPTER 2: FRP-CONCRETE BOND-LABORATORY STUDY

The performance of fiber reinforced polymers (FRP) used in structural repair and rehabilitation hinges on the integrity of its bond with concrete. Building codes, e.g. ACI 318-14 have long recognized that better bond is achieved when surfaces are roughened since it significantly increases the contact area between the two bonding surfaces. The required roughening for bonding FRP is defined in ACI 440.2R-17, 6.4.2.1 which states that the "concrete surface should be prepared to a surface profile not less than CSP 3, as defined by ICRI 310.2R". This profile illustrated in Figure 2.1 is achieved by light sand blasting.

Figure 2.1 Concrete surface profiles.
Reprinted from NCHRP 609, Attachment C.
Permission to use from National Academy of Sciences

NCHRP 609 study on construction specifications published in 2008 reported bond results from flexure tests on 26 beam specimens and 10 double shear bond specimens. The target 28-day concrete compressive strength was 5,000 psi. Three different concrete sets and profiles, CSP 1, CSP 2-3 and CSP 6-9 were evaluated. Based on the results, the study concluded that even the "smoothest concrete surface profile …CSP 1 …appeared to provide adequate surface roughness".

Surface profile contributes to bond through mechanical interlock and is commonly considered to provide most of the adhesion with minor contribution from chemical bond. The insensitivity in the NCHRP results suggest that hitherto unrecognized factors may have played an important role. Foremost among these is the porosity of concrete's microstructure. Since concrete uses more water than is needed for hydration, any additional water results in the formation of a network of interconnected voids following evaporation. The extent of the network depends on the amount of water used and on the air content.
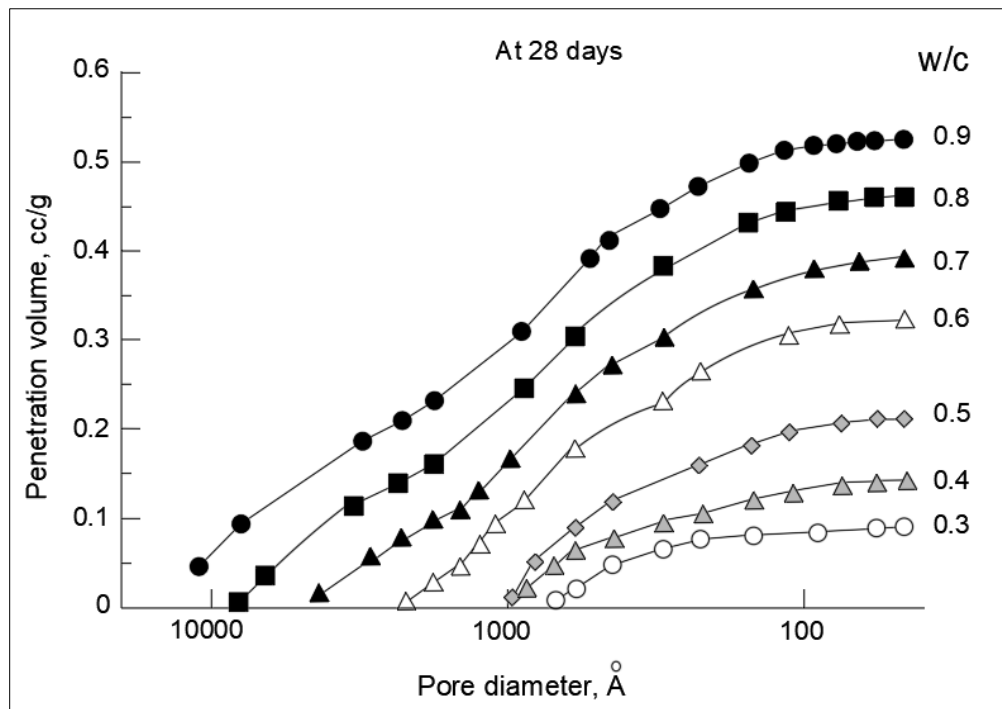
Figure 2.2 Pore diameter, w/c vs penetration volume.
Adapted from Concrete (3rd Edition) p.33 by Mehta and Monteiro, 2006, McGraw-Hill

4
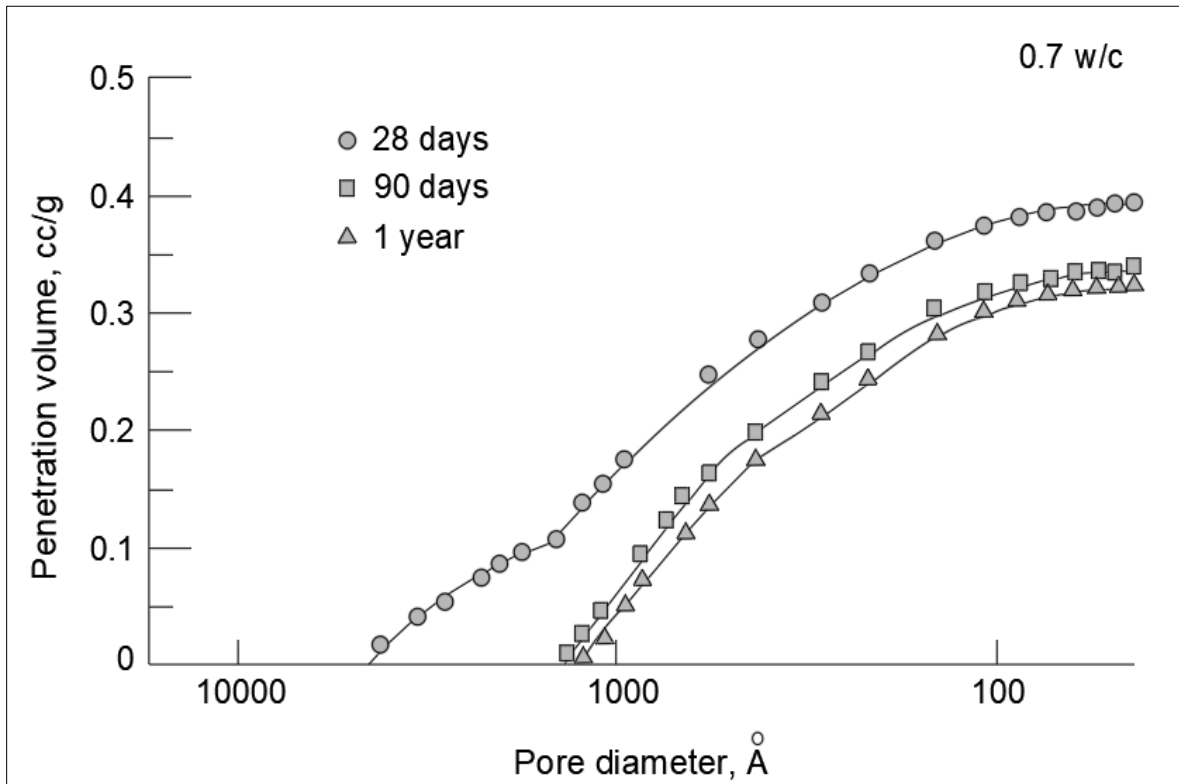
Figure 2.3 Pore diameter, w/c vs penetration volume.
Adapted from Concrete (3rd Edition) p.33 by Mehta and Monteiro, 2006, McGraw-Hill

The maximum average pore size diameter and the distribution of the pores over the bonding surface controls the amount of epoxy that can penetrate into the concrete. Figure 2.2 taken from Mehta and Monteiro 1993 shows the relationship between pore diameter, penetration volume and the water / cementitious ratio. Inspection of Figure 2.2 shows that larger pore diameters and higher penetration volumes are associated with lower strength concrete and vice versa. Figure 2.3 shows the relationship of porosity with age for a w/c ratio of 0.7. The dependence diminishes after 90 days; note that the difference in pore diameters between 90 days and 1 year is much smaller compared to that between 28 days and 1 year. In this study, porosity measurements were made after 90 days.

According to (Mindess, et al., 2003), the water cement ratio for 5,000 psi air entrained concrete is 0.4. For this ratio, the penetration volume is around 0.1 cc/g. The corresponding maximum pore size is 1,000Å but the average is closer to 200Å. For this combination, penetration of the epoxy into the concrete pores is not necessarily optimal. This suggests that the optimal surface profile needs to be tailored to reflect concrete porosity.

Numerous studies have evaluated the role of concrete strength and bond, e.g. (Chajes, et al., 1996), (De Lorenzis, et al., 2001) but their focus was on unexposed specimens. Since epoxies can absorb moisture, water can penetrate into the concrete and react chemically to degrade it. To date, the effect of porosity on long term FRP-concrete durability under moisture exposure has not been systematically evaluated.

2.1 Objectives

The primary goal of the investigation is to understand the relationship between concrete strength, porosity and submerged exposure in potable water. It focuses on specimens whose surface profiles conform to CSP 3 as required by ACI 440.2R-17.

The study can potentially provide new information on the appropriateness of using the same surface profile regardless of concrete strengths or porosity. Since testing will yield results for dry conditions it could provide actionable information on surface preparation needed for both indoor and outdoor applications. This could potentially lead to reduced costs if less intensive surface preparation were found to be necessary.

CHAPTER 3: TEST PROGRAM

Beginning in the late 1990's several laboratory studies were conducted primarily to identify the optimal surface profile for bonding FRP to concrete. These evaluated the effect of variation in bond due to changes in concrete strength and surface preparation techniques that considered water jetting, sand blasting, shot blasting, manual grinding and air chisels. The resulting profiles were mapped optically, e.g. using laser profilometry; bond improvement was established from destructive testing. This typically included lap shear, flexure and pull-off tests, (Chajes, et al., 1996) (Yoshizawa, et al., 1996), (Miller, 1999), (Momber, 1999), (De Lorenzis, et al., 2001), (Maerz, et al., 2001), (Shen, 2002).

The concrete strengths evaluated in the above research studies varied from 2,000 psi to over 8,000 psi, (Jeffries, 2004). Though this spans strengths of interest, because the research focus was on surface profile, porosity was not on the radar. The concern at the time was more on the consequences of damage to the microstructure arising from the different techniques used in surface preparation. These and other studies led to the eventual adoption of ICRI's CSP 3 (Figure 2.1) in ACI's first technical guide published in 2002, ACI 440.2R-02 that became the industry-wide standard. This meant that CSP 3 was used regardless of the concrete strength.

Thanks to advances in concrete technology the average compressive strength of concrete has increased, (Detwiler, et al., 2009). This has profound implications on the future use of FRP and the long term durability of the FRP-concrete bond since higher strength concretes have lower porosity that may require alternative surface preparation techniques to be effective in all environments.

Due to the inverse relationship between strength and porosity, long term FRP-concrete bond characteristics may be expected to differ. This is because the penetration of epoxy into concrete will be smaller in higher strength concretes due to the absence of larger diameter pores and a reduced network of interconnected voids, (Mehta, et al., 2006). This will not impact bond under dry conditions because of the much higher tensile strength of epoxy. However, under wet exposure, water will be able to diffuse through to the epoxy and react chemically leading to irreversible damage to epoxy and accompanying bond degradation after relatively short exposure, e.g. (Büyüköztürk, et al., 2010) reported a 60% reduction in bond after only 8 weeks immersion in 23 ℃ (73 ℉) water.

Since porosity is not being considered, potential corrective measures for making repairs more durable are being overlooked. In the most comprehensive 2009 NCHRP durability study, the performance of over 1,600 specimens bonded to concrete using five different epoxies was evaluated. In contrast, concrete was limited to relatively high strength concrete with compressive strengths ranging from 6,700 to 10,500 psi. Given the expected role of porosity, these findings may need to be re-visited.

The starting point in this research project was the hypothesis that durability of FRP bond in highly porous concrete would differ from that in less porous concrete. The materials evaluated, exposure considered and its evaluation focused such that these differences would be noticeable from the results. If this were demonstrated the way forward will be clearer.

3.1 Compressive Strength

The relationship between porosity and water cementitious ratio provided the basis for selecting target concrete strengths. Lower strength concretes have higher water / cementitious ratios. To provide context, three different concrete strengths were evaluated in the study. Though

researchers have evaluated concrete with a targeted strength of 2,000 psi, (Shen, 2002), this fell below the 2,500 psi minimum strength specified in ACI 318-14, Table 19.2.1.1. An upper target limit for strength was taken as 10,000 psi following the 2009 NCHRP study. An intermediate target strength of 5,000 psi was chosen to allow interpolation. These targets were later revised based on actual strengths achieved (see Chapter 4).

3.2   CFRP System

Three commercially available systems were originally selected. However, since this was a proof of concept study, only the two most widely used systems were utilized in the eventual testing. Since epoxies had to be compatible with the CFRP material, epoxies associated with the respective systems were used.

3.3   Destructive Testing

Pull-off testing provides the simplest and most direct method for comparing changes in the failure mode arising from exposure. Given that epoxy has a higher tensile strength, all failures were expected to be cohesive failures in concrete. The depth of the concrete still bonded to the dolly would allow the depth of epoxy penetration in the substrates of the different concretes to be estimated. It was anticipated that changes would be the least for low strength, high porosity concrete but more noticeable in the higher strength, low porosity concrete.

3.4   Durability Exposure

The NCHRP 2009 durability study identified complete immersion in heated water as the most aggressive environment for FRP-concrete bond. They reported that after 8 weeks immersion in 30°C water, bond reductions from flexure tests were more than 35%. This study adopted a 30°C water temperature since it is also representative of conditions in Tampa Bay where several pile repairs were conducted (see Chapter 10). The exposure period was kept at 15 weeks, that was

9

higher than the 8 week period in the MIT study (Büyüköztürk, et al., 2010). However, provisions were made for a greater period of exposure in case results proved inconclusive.

3.5   Moisture Absorption

The relationship between bond degradation and moisture absorption is critically important. In the study, this was determined from gravimetric testing and is described in Chapter 7.

3.6   Specimen Dimension

Flat specimens such as slabs are the simplest for conducting pull-off tests. The dimensions selected were 9 in. x 9 in. x 2.5 in. These were based on the following (1) ease of fitting slabs into the oven used for drying, (2) sufficient edge distance is provided for isolating side diffusion effects as this experiment was designed to have one dimensional flow, (3) widths reflected repair dimensions used in practice, (4) allowance for 13 possible pull-off locations, and (5) slab depth was comparable to the concrete cover for exterior members and was sufficient to prevent the specimen breaking during testing.

The number of slab specimens was dictated by the test matrix summarized in Table 3.1 through Table 3.3 and shown schematically in Figure 3.1.
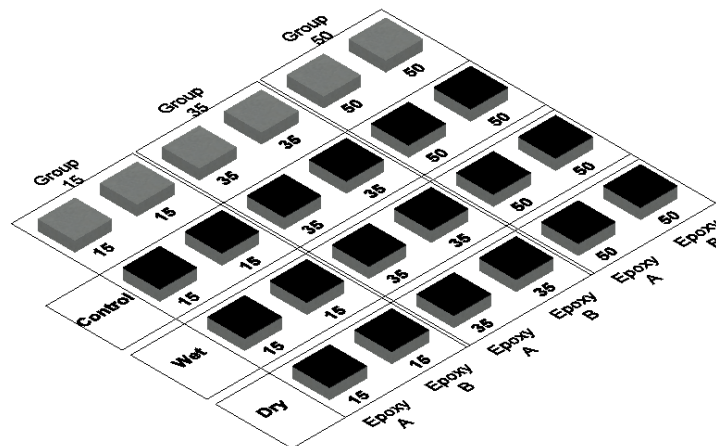
Figure 3.1 Test matrix

The goals of the study were to evaluate bond degradation arising from exposure and to quantify bond recovery upon drying. Three series of tests were planned, one for each concrete porosity and FRP system. The epoxy systems used are identified by the letters A and B in Figure 3.1. The three different concrete grades are identified as 15, 35 and 50 that approximately correspond to compressive strengths measured in MPa. Although 18 concrete slabs were required, two additional slabs were cast for each concrete strength as "spares". A total of 24 slabs were therefore cast.

The three test series were: control, wet and dry. Control (6 slabs) denote specimens that were tested before exposure to provide a baseline value. Wet (6 slabs) represents specimen that were submerged in warm water at $30^{\circ}C$ ($86^{\circ}F$) for approximately 15 weeks. Dry (6 slabs) represents bond recovery specimens. These were allowed to dry at room temperature following removed from water until there was minimal change in weight (0.05%). In each series, six points were tested that exceeded the minimum set of 5 in ASTM D7522. A total of 108 tests were conducted.

Table 3.1 Control specimens

Specimen	Epoxy
A15_control	A
A35_ control	A
A50_ control	A
B15_ control	B
B35_ control	B
B50_ control	B

11

Table 3.2 Wet specimens tested directly after the specimens removed from water

Specimen	Epoxy
A15_wet	A
A35_wet	A
A50_wet	A
B15_wet	B
B35_wet	B
B50_wet	B

Table 3.3 Dry specimens tested after 4 weeks of drying in room temperature.

Specimen	Epoxy
A15_dry	A
A35_ dry	A
A50_ dry	A
B15_ dry	B
B35_ dry	B
B50_ dry	B

CHAPTER 4: SPECIMENS FABRICATION

4.1   Formwork

A total of 24 forms were built using 7 ft long 2 x 3 wood studs. Each form was fabricated using four 10.5 in. length pieces joined with eight 3.5 in. screws, two on each side to create inner dimensions of 9 in. x 9 in. x 2.5 in. as shown in Figure 4.1. The forms were placed on a 1/8 in. thick laminate wood sheet that served as the bottom but more importantly replicated common concrete surface textures.

Figure 4.1 Specimens formwork

4.2   Materials

A total of twenty four 9 in. x 9 in. 2.5 in. slabs and sixty six 4 in. x 8 in. concrete cylinders were cast at Titan America in Riverview, FL. Tables 4.1 to 4.3 provide details on the three mix designs used. Tickets issued by Titan for these mixes are included in Appendix A. Slab specimens were cured by intermittent ponding of water on the exposed surface for 7 days. Cylinders were cured in immersion tanks for 28 days. The compressive strength for each of the three concrete porosities was determined at 28 days in accordance with ASTM C39, using a Forney Testing Machine. The measured strengths were 4,400 psi (Group 15), 4,206 psi (Group 35) and 7,040 psi (Group 50) as compared to the target strengths of 2,500, 5,000 and 10,000 psi. The values for Groups 35 and 50 were each lower compared to target strengths while the Group 15 strength (higher porosity) was unacceptably high. Group 15 slabs and 15 (4 in. x 8 in.) cylinders specimens were therefore re-cast when facilities became available 62 days later. The measured compressive strength was 2,325 psi, somewhat below the 2,500 psi target values. Details in Table 4.4.

Figure 4.2 Casting, curing and testing concrete

4.3 Concrete Mixes (Weight Ratio)

Table 4.1 Group A (batched quantity =0.06 cubic yard)

Cement	1
Cemex Sand (16-078)	3.651709
cemex #57 (87-089)-coarse agg.	4.389744
water/cement (actual weights used)	0.530244
Admixtures	
Master set 961R	20.81 ml
Master air AE90	5.34 ml

Table 4.2 Group B (batched quantity =1 cubic yard)

Cement	1
Cemex Sand (16-078)	2.15873
cemex #57 (87-089)-coarse agg.	2.761905
water/cement (actual weights used)	0.408968
Admixtures	
MasterPozzolith 700N	20 oz.

Table 4.3 Group C (batched quantity =1 cubic yard)

Cement	1
Cemex Sand (16-078)	1.145455
cemex #57 (87-089)-coarse agg.	1.327273
water/cement (actual weights used)	0.208157
Admixtures	
MasterSet R 961	22 oz.
Master Glenium 7920	32 oz.

4.4 Compression Test Result- 4 in. x 8 in. Cylinders

Table 4.4 Compression test results

Group 25 strength results			
specimen ID	Max. Load (lb.)	Fracture Type	Compressive Strength (psi)
25-A	29600	5	2356
25-B	29765	5	2369
25-C	32960	5	2624
Avg. after 5% reduction			2325
Group 35 strength results			
specimen ID	Max. Load (lb.)	Fracture Type	Compressive Strength (psi)
35-A	56995	5	4515
35-B	51430	5	4054
35-C	60110	5	4714
Avg. after 5% reduction			4,206
Group 50 strength results			
specimen ID	Max. Load (lb.)	Fracture Type	Compressive Strength (psi)
50-A	97010	5	7609
50-B	91600	5	7220
50-C	93235	5	7404
Avg. after 5% reduction			7,040

4.5   FRP and Epoxy Specifications

Two commercially available CFRP systems A and B were used. Both were unidirectional carbon fiber systems with their custom made two component epoxies. Manufacturer's specifications for both systems are summarized in Table 4.5.

Table 4.5 FRP and epoxy specifications

System A FRP	
Tensile Strength	550 ksi (3,793 MPa)
Tensile Modulus	34 msi (234.5 GPa)
Elongation at Break	1.5%
Areal Weight	18 osy (611 gsm)
Density	0.065 lbs./in^3 (1.8 g/cc)
Nominal Fiber Thickness	0.0135 in. (0.34 mm)
Fiber Direction	Undirectional
System A epoxy	
Tensile Strength (ASTM D-638)	8,000 psi (55 MPa)
Tensile Modulus (ASTM D-638)	2.5×10^5 psi (1,724 MPa)
Elongation @ Break (ASTM D-638)	3%
Flexural Strength (ASTM D-790)	11,500 psi (79 MPa)
Glass Transition Temperature	+127 °F (53 °C)
Coefficient of Thermal Expansion	6.0×10^{-5} per °C
Flexural Modulus (ASTM D-790)	5×10^5 psi (3,450 MPa)
Cured Laminate Properties (design value)	
Tensile Strength (ASTM D3039)	160.9 ksi (1,110 MPa)
Tensile Modulus (E_f) (ASTM D3039)	10.39 msi (71.7 GPa)
Tensile % Elongation (ASTM D3039)	1.45%
Nominal laminate thickness	0.04 in. (1.0 mm)

Table 4.5 (Continued)

Stiffness (E_f*A) per unit width (ASTM D3039)	6.4 kips/in./ply
System B FRP	
Tensile Strength	580,000 psi (4.0 GPa)
Tensile Modulus	33.4 x 106 psi (230 GPa)
Ultimate Elongation	1.7%
Density	0.063 lbs./in.3 (1.74 g/cm3)
Minimum weight per sq. yd.	19 oz. (644 g/m2)
System B Epoxy Material Properties	
Tensile Strength (ASTM D638)	10,500 psi (72.4 MPa)
Tensile Modulus (ASTM D638)	461,000 psi (3.18 GPa)
Elongation Percent (ASTM D638)	5.0%
Flexural Strength (ASTM D790)	17,900 psi (123.4 MPa)
Flexural Modulus (ASTM D790)	452,000 psi (3.12 GPa)
T_g (ASTM D4065)	180° F (82o C)
Composite Gross Laminate Properties – Design value	
Ultimate Tensile Strength in Primary Fiber Direction (ASTM D3039)	121,000 psi (834 MPa) (4.8 kip/in. width)
Elongation at Break (ASTM D3039)	0.85%
Tensile Modulus (ASTM D3039)	11.9 x 106 psi (82 GPa)
Flexural Strength (ASTM D790)	15,200 psi (104.8 MPa)
Flexural Modulus (ASTM D790)	384,200 psi (2.65 GPa)
Longitudinal Compressive Strength (ASTM D3410)	42,500 psi (293 MPa)
Longitudinal Compressive Modulus (ASTM D3410)	9.5 x 106 psi (65.5 GPa)
Nominal Laminate Thickness	0.04 in. (1.0mm)
Longitudinal Coefficient of Thermal Expansion	3.6 ppm./°F
Transverse Coefficient of Thermal Expansion	20.3 ppm./°F

4.6   Surface Preparation

The concrete surface to which FRP was to be bonded was prepared to achieve a minimum

Concrete Surface Profile 3 (CSP3) as stipulated in ACI-440.2R-17. Light sandblasting was utilized

to prepare the surface. That is also approved by the International Concrete Repair Institute (ICRI).

Surface preparation requires removal of dust, small particles and the creation of a specific surface

roughness that enhances mechanical interlock in the FRP-concrete bond plane.

Samples were sandblasted in the laboratory as shown in Figure 4.3 The spray nozzle was

kept approximately at the same distance from the samples (2.5-3) inches to ensure all samples were

subject to the same pressure. A sweeping motion followed when the sand blasting was carried out.

Subsequently, compressed air was used to clean the surface and remove any small particles.

Figure 4.3 Slabs in sandblaster

4.7   Specimen Drying

To ensure all specimens had the same moisture content before exposure, all specimens

were oven dried for 48 hours at 230 °F as recommended in ASTM C642 for drying concrete.

Figure 4.4 Drying specimens in oven

4.8 Repair with FRP

Following surface preparation, the two FRP systems were bonded to the concrete slabs in accordance with manufacturer's specifications. A total of 18 slabs were repaired, six for each group. Three of the six slabs were repaired with system A and three with system B. The bottom face of the slabs were used for the repair as it simulated conventional beam and slab repair surfaces where the aggregate settles more due to gravity and laitance is absent.

The FRP fabric was cut to 9 in. x 9 in. size. Epoxy components (parts 1 and 2) were mixed for each system (A and B) using an electrical drill with mixing attachment in accordance with the specifications. Epoxy was applied as a primer layer to the prepared concrete surface. The FRP material was then impregnated and applied to the primed concrete surface. Epoxy mixing and FRP application took place in laboratory conditions where the ambient temperature was maintained around 73° F. The repaired slabs were left to cure for four weeks at room temperature inside the laboratory.

CHAPTER 5: SURFACE CHARACTERIZATION

5.1 Mercury Intrusion Porosimetry

Considering the difference in concrete strengths, pore sizes and their distribution should differ (Figure 2.2). Surface voids and porosity affect mechanical bond, composite action, moisture penetration and long term durability. To determine concrete porosity, mercury intrusion porosmetry (MIP) tests were conducted on samples with the three differing compressive strengths.

The MIP test is used to measure capillary pore size and its distribution ranging from10 nm-10000 nm. Capillary pores form an interconnected network of pores (Sidney Mindess, 2003). The samples tested were obtained from 4 in. x 8 in. cylinders that were cut into 0.83 in. slices using a MK-5005S concrete saw as shown in Figure 5.1. A cylindrical sample 0.83 in. high with a radius of 0.45 in. was extracted. It was dried in an oven for 48 hours at 230° F prior to testing. A POREMASTER Automatic Pore Size Analyzer model pm-60-19 (Figure 5.2) from Quantachrome Instruments was used to perform the MIP test. Mercury was pressurized into each sample at a maximum pressure of up to 60,000 psi. The volume of intruded mercury is calculated by deducting the volume of mercury when the machine compartment is unoccupied from the volume of the intruded mercury when machine compartment is loaded with the sample. The intruded volume is then divided by the sample mass to obtain the pore volume (Delagrave, et al., 1979). Results showed that as the concrete strength decreased, that is, as the w/c ratio increased, the mercury intrusion volume increased. These results were consistent with findings reported by (Cho, 2012).

Group A (2,325 psi) had the highest pore ratio with an intruded mercury volume of 0.1085 cm³/g, followed by Group B (4,206 psi) with 0.0922 cm³/g. Group C (7,040 psi) had the lowest pore ratio of 0.0731 cm³/g. The test also reported the threshold pore diameter that represented the maximum pore size that the mercury can penetrate (Aligizaki, 2005). The higher the threshold diameter, the larger the pore size. Machine software converted the applied pressure into pore diameter (Winslow, et al., 1970). As anticipated, Group A had the largest pore size followed by Group B and Group C as shown in Table 5.1 and Figure 5.3.

Figure 5.1 (a) Cut concrete cylinders (b) sample dimension

Figure 5.2 Mercury intrusion testing machine

Table 5.1 Mercury intrusion results

Sample	Total intruded volume (cm³/g)	Threshold pore diameter (nm)
A	0.1085	10000
B	0.0922	200
C	0.0731	150
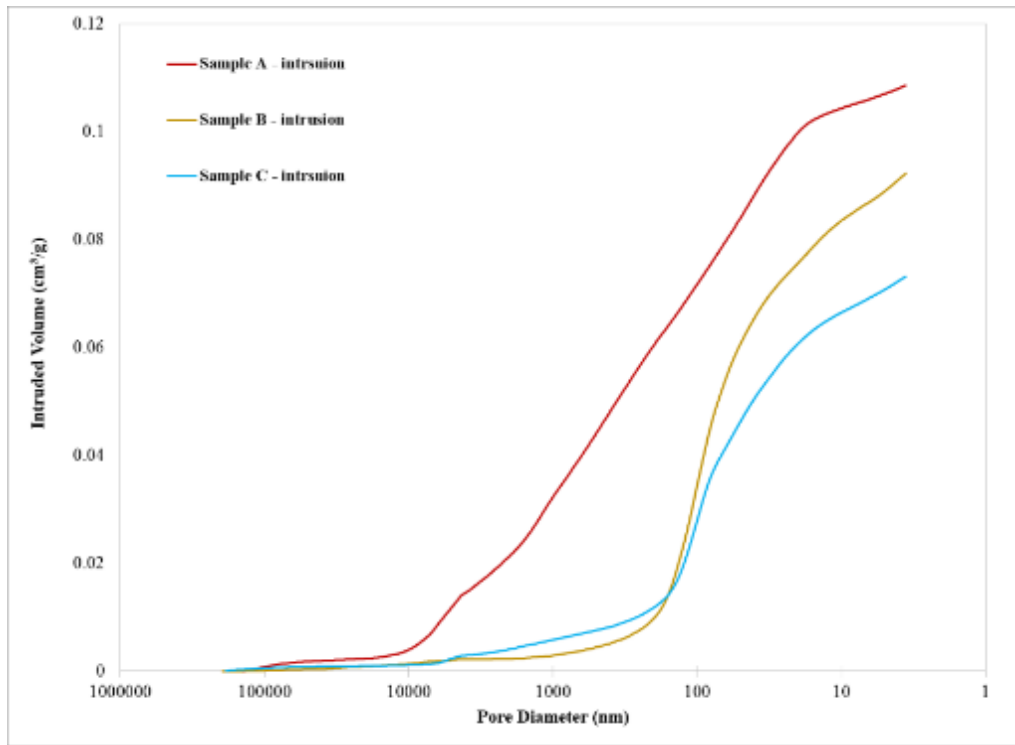
Figure 5.3 Cumulative intrusion curve from intrusion test

5.2   Scanning Electron Microscope

This study focused on capillary pores where the epoxy can penetrate and create mechanical interlock. Surface voids for the three concrete strengths were compared using a Scanning Electron Microscope (SEM). This can differentiate the dissimilarity in void size and distribution for different concrete strengths. SEM produces electron beams that interact with the specimen by penetrating the specimens or backscatter to create signals that are analyzed and converted into images by the SEM machine (Hong Zhao, 1990). SEM is able to capture pores as little as 0.2 µm (Attari, et al., 2016). Images were taken for samples that represented the three concrete strengths.

Cylindrical specimens 0.83 in. high with a radius of 0.45 in. were used for the SEM imaging (see Figure 5.1). Samples were placed in an oven for 48 hours at 230° F prior to testing. The dried samples were then loaded into the SEM machine for imaging. Results showed that void diameters and their distribution were higher for Group A but less distinct for Groups B and C as shown in Figure 5.5. The difference in void sizes and distribution can be attributed to the higher water/cementitious ratios in the low strength concrete (Group A) compared to Group B and C that have higher strength and lower water/cementitious ratios. These results are consistent with the findings from the MIP test.
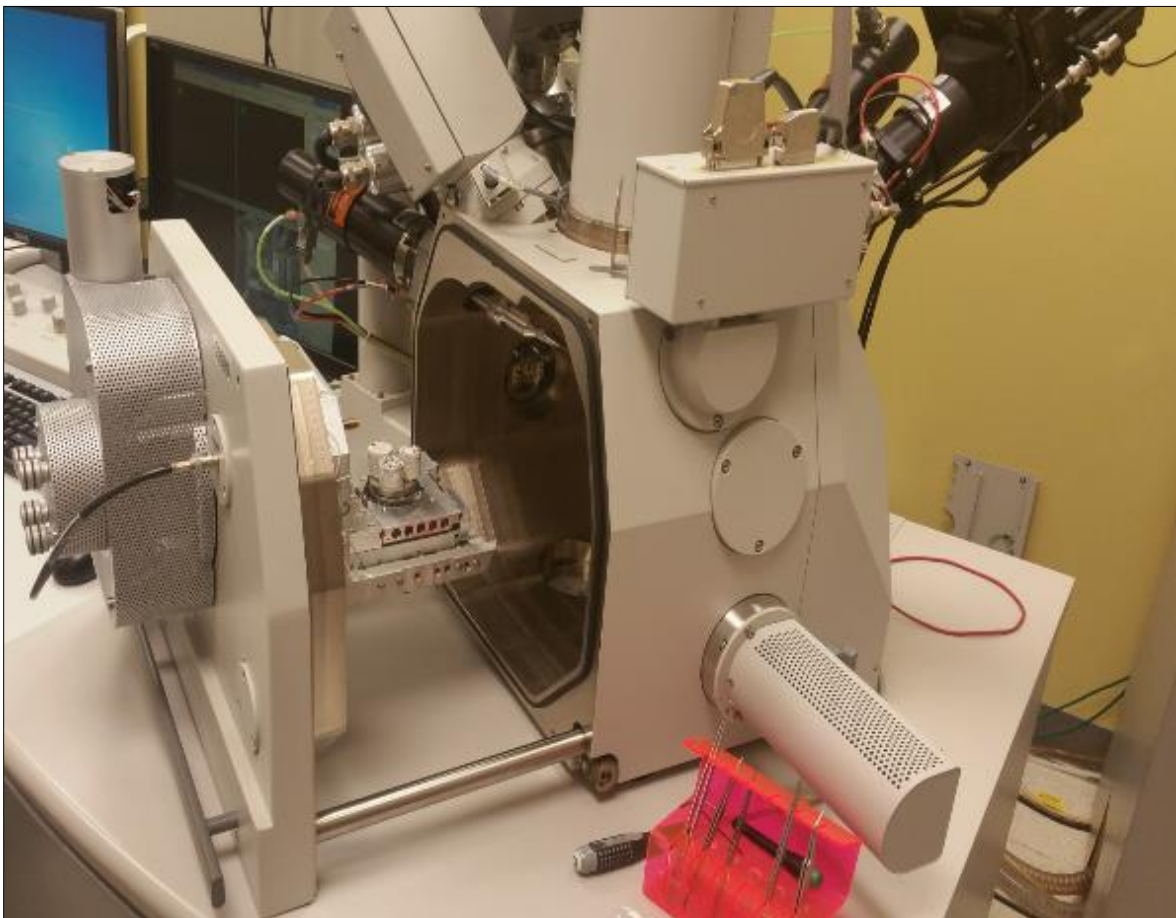
Figure 5.4 Scanning electron microscope machine

Group A (2,325 psi)

Group B (4,206 psi)

Figure 5.5 Scanning electron micrograph (90x)
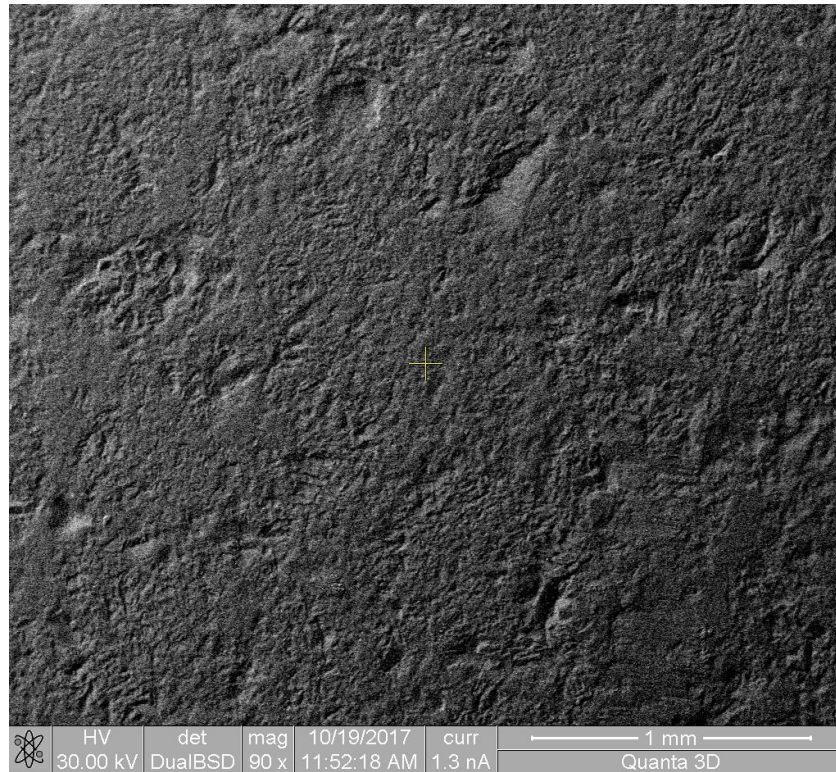
Group C (7,040 psi)

Figure 5.5 (Continued)

5.3 Bond Surface 3D Scan

Bond surfaces for the three strengths were scanned using Artec Eva 3D scanner to identify dissimilarities on the bonding surfaces. Artec Eva 3D is a structured-light handheld scanning device that projects light on the scanned surface and analyzes the distortion to produce images of the surface. Their specifications are shown in Table 5.2.

Three slabs, one for each strength, were scanned at the Digital Heritage & Humanities Collections (DHHC) facilities at the University of South Florida library. The scanned files were converted to 3-d coordinate data points that were then processed in AUTOCAD to obtain the surface void volume. The void volume for Group A was 0.090 in^3, that for Group B was 0.055 in^3 and for Group C it was 0.061 in^3. These results agree with the MIP test data that showed Group A had higher porosity.

26

Figure 5.6 CSP3 ICRI technical guideline No 310-2
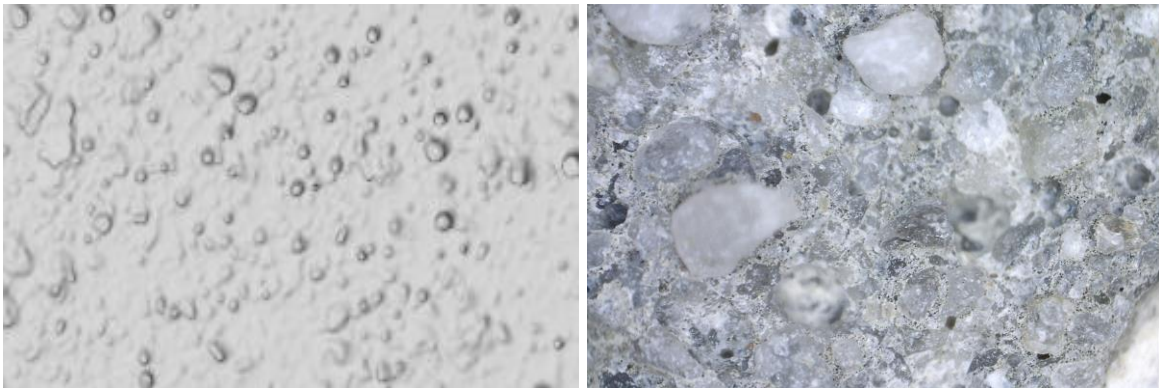
Figure 5.7 Group 15: (left) 3D scan, (right) microscopic photo 60x
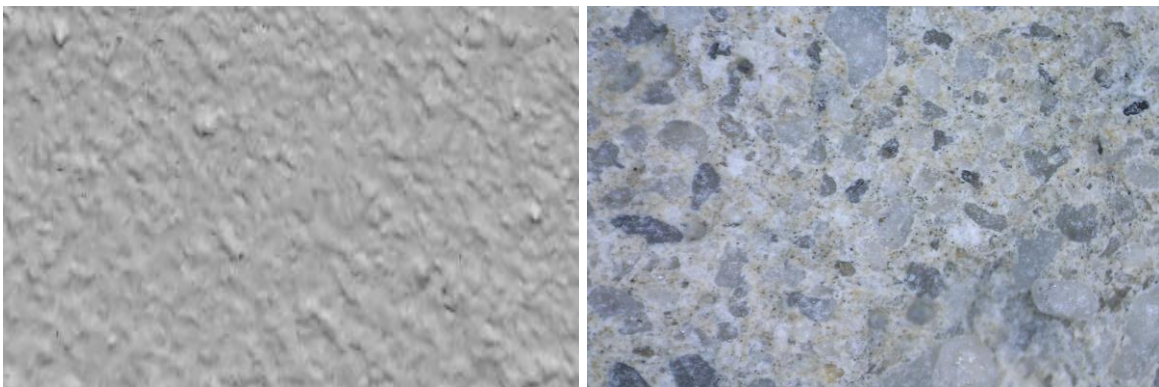
Figure 5.8 Group 35: (left) 3D scan, (right) microscopic photo 60x
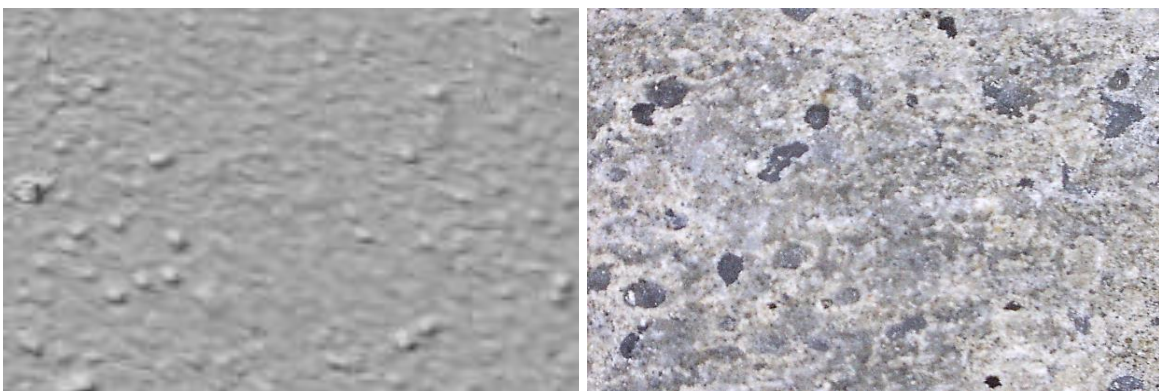
Figure 5.9 Group 50: (left) 3D scan, (right) microscopic photo at 60x

Table 5.2 Artec eva 3d scanner specifications

3D resolution, up to	0.5 mm
3D point accuracy, up to	0.1 mm
3D accuracy over distance, up to	0.03% over 100 cm
Colors	24 bpp
Texture resolution	1.3 mp
Scanning technology	structured light
Structured light source	flash bulb (no laser)
Working distance	$0.4 - 1$ m
Linear field of view, HxW @ closest range	214×148 mm
Linear field of view, HxW @ furthest range	536×371 mm
Angular field of view, HxW	$30 \times 21°$
Video frame rate, up to	16 fps
Exposure time	0.0002 sec.
Data acquisition speed, up to	2 mln points / sec.

Figure 5.10 Artec eva 3D scanner

5.4   Total Void Content

The total void was calculated using constituents of the mix following Neville 2005. This is summarized in Table 5.3. The values confirm that Group A had the highest total void of 17.1% vs 11.4% for Group C.

Table 5.3 Void content

Porosity calculations following Properties of Concrete by Neville, 5th edition, page 280			
	Group 15	Group 35	Group 50
Total void content	17.1%	14.7%	11.4%
Step 1-Weight ratio			
Cement	1	1	1
Fine aggregate	3.5	2.15	1.14
Coarse aggregate	4.3	2.7	1.32
w/c	0.73	0.44	0.25
Air	0.03	0.03	0.03
Step 2-Specific Gravity			
Cement	3.15	3.15	3.15
Fine aggregate	2.66	2.66	2.66
Coarse aggregate	2.46	2.46	2.46
Step 3-Volum ratio			
Cement	7.3	11.4	19.98
Fine aggregate	31.7	29.2	27.12
Coarse aggregate	41.2	40.4	33.9
w/c	16.8	16	15.9
Step 4 -Hydrated cement% Assume 70% have hydrated after 7 days =0.7*Cement volume from step 2	0.7*7.3=5.13	0.7*11.4=7.99	0.7*11.4=14
Step 5 –Volume of Combined water = 0.23* hydrated cementx3.15 (cement specific gravity) (page 26)	0.23*5.13*3.15=3.71	0.23*7.99*3.15=5.79	0.23*14*3.15=10.14

Table 5.3 -continued

Step 6 –Volume of solid products Volume of solid products (cement + water) reduced by 0.254 of combined water volume =volume of hydrated cement(from step 4)+(1-0.254)x volume of combined water (from step 5)	5.13+ (1-0.254)*3.71=7.9	7.99+ (1-0.254)*5.8=12.3	14+ (1-0.254)*10.1=21.5
Step 7 –Volume of gel pores W_g Gel porosity is 28% (page 26) means W_g/(volume of solid products- step 6+ W_g)=0.28 Solve for W_g	3.07	4.79	8.3
Step 8 –Volume of Hydrated cement paste including gel pores volume of solid products of hydration (step 6) + volume of gel pores (step 7)	10.98108	17.1104	29.9487
Step 9 –Volume of dry cement which has hydrated and of mixing water Step 4 + water volume from step 3	21.9682	24.0504	29.9783
Step 10 –Volume of capillary pores Step 9 – step 8	10.987	6.939	0.0295
Step 11 –Total voids content Volume of capillary pores + volume of gel pores + air content	17.1	14.7	11.4

CHAPTER 6: EXPOSURE AND TESTING

6.1 Specimen Coating

Before immersion in heated water, the five exposed surfaces of the FRP repaired slabs were sealed with a water proof coating to ensure water could only diffuse through the FRP. A Behr Basement & Masonry Waterproofer system was used. Two waterproofing layers were applied and the coating allowed to cure for 14 days. This exceeded the 7 days recommended by the manufacturer. Figure 6.1 shows the coated slabs.
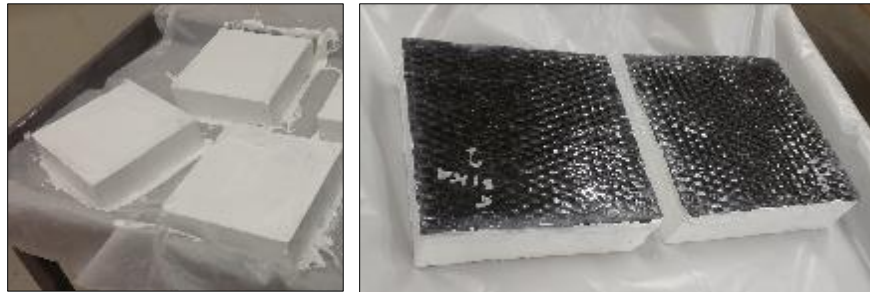
Figure 6.1 Coated specimens

6.2 Exposure

Specimens were immersed in water at 30 °C (86 °F) for 15 weeks (106 days). Specimens were kept in temperature controlled chambers with automatic water heaters as shown in Figure 6.2. The temperature selected replicated conditions for FRP repairs completed in the Tampa Bay area (Chapter 10). Specimens were positioned with the FRP facing up and a 16 in. head of water was on top of the specimens as shown in Figure 6.2.
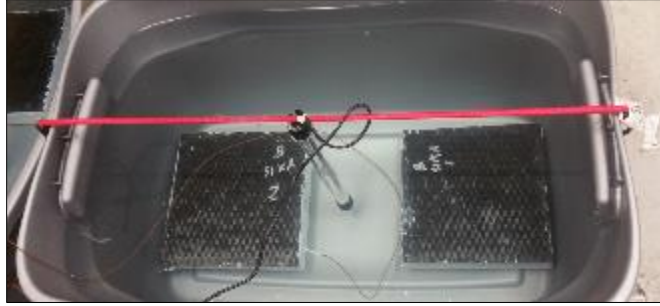
Figure 6.2 Chamber setup
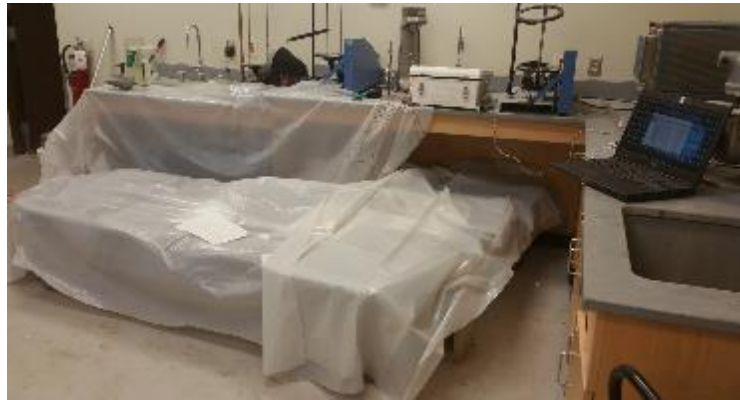
Figure 6.3 Chamber covered with plastic sheet to maintain temperature

6.3 Chamber Setup and Temperature Monitoring

Six plastic containers were used to hold the slabs during exposure. Each was filled with 34 gallons of tap water. A 300W water heater (Uniclife HT-2300) with a heating capacity of up to 80 gallons was attached to each container to maintain the temperature at 86°F (30°C). The heater was suspended from a rubber cable using a zip tie. Thermocouple type T wires were connected to a data logger (CAMPBELL SCIENTIFIC CR1000) and placed inside to record the water temperature every 15 minutes. The average room temperature was 73°F (22.7°C) which was also recorded using the data logger. The average water temperature was 84° F (28.9°C). During exposure a drop in temperature was recorded between days 90 and 100 as outside temperatures dropped in Tampa that led to a drop in the room temperature. This is shown in Figure 6.5.
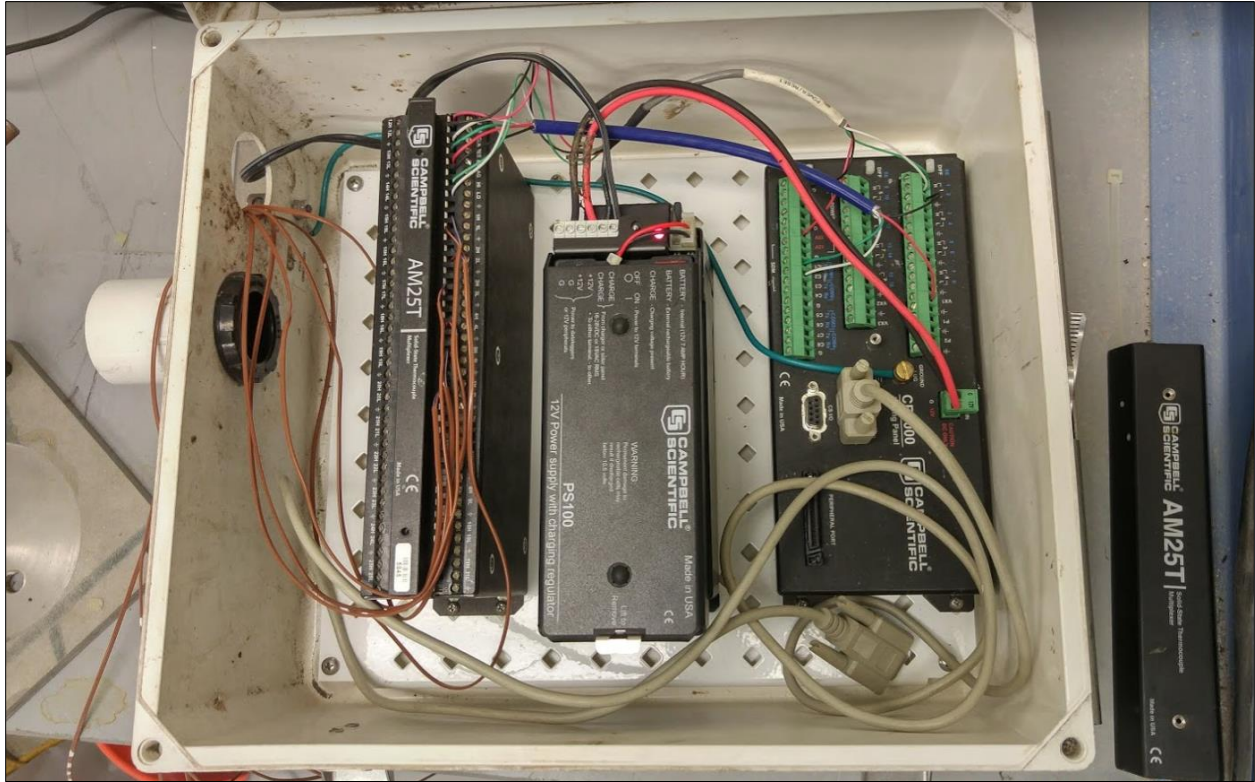
Figure 6.4 Data logger
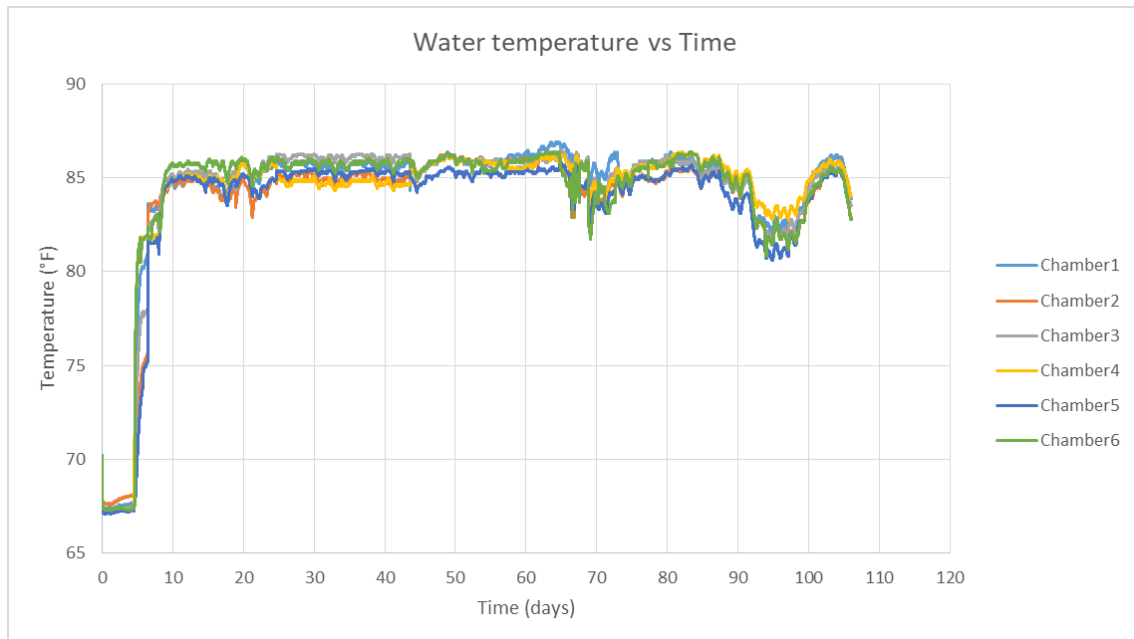
Figure 6.5 Recorded water temperature

6.4 Specimen Series

The specimens were split into three series namely: control, wet and dry. Controls denoted the uncoated samples that were tested before moisture exposure and after being oven dried to obtain the initial bond value. Wet represents samples that were immersed in water for 106 days at 86° F (30 °C). Testing procedure was initiated directly after the specimens were taken out of the water. Dry samples were those left to dry following removal from exposure until there was no noticeable change in weight.

6.5 Testing

A total of 108 points were tested for bond strength. Bond was tested by direct tension (pull-off) in accordance with ASTM D7522-12. Six points, (1-6) in Figure 6.7 were tested for each slab. A template was used to ensure all slabs were tested at identical locations and to optimize the number of points within the available test area. The template was fabricated from a 1 mm aluminum sheet that was cut using a CNC burn table connected to Hypertherm Powermax 65. The dolly surface was roughened by a sandblaster and steel brush then cleaned with compressed air. Dollies were attached to scored locations using 3M Scotch-Weld DP-420 epoxy adhesive. Samples were left to cure for 48 hours before testing. Alignments were checked using a spirit level before the pull-off tests were conducted.

An Elcometer 106 adhesion tester with a 1.25 in. diameter dolly was used. The FRP surface was scored using a 1.25 in. diameter diamond core drill bit to an approximate depth of 0.25 in. into the concrete cover. Test locations were roughened using steel brush attached to a drill to enhance dolly-FRP bond then cleaned with compressed air.

Figure 6.6 Template fabrications
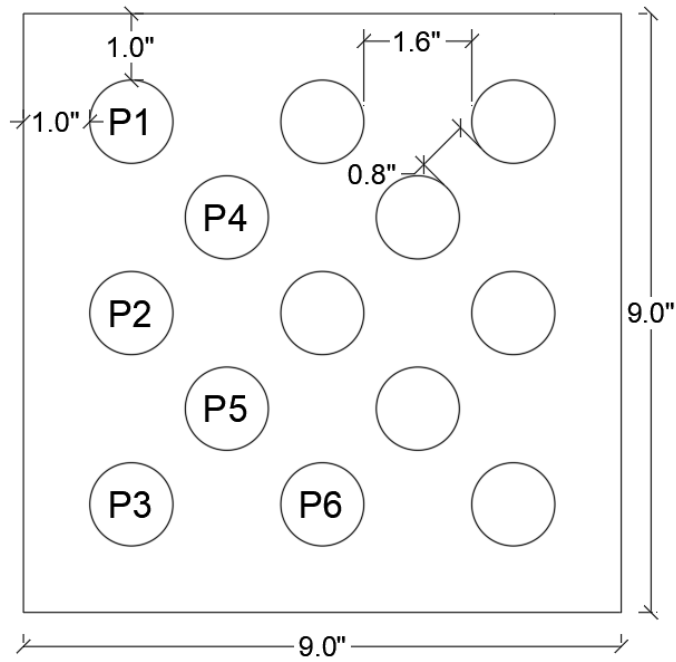
Figure 6.7 Template dimensions

CHAPTER 7: GRAVIMETRIC TESTING

Moisture is the primary factor responsible for degradation of the FRP-concrete bond (Hamilton, 2009) (Karbhari, 2009) (Benzarti, 2010) (Büyüköztürk, 2010) (Hamilton, 2012). Moisture diffusing through to the FRP bond line influences bond strength in two ways: First, it weakens the cross-linked chain and Van der Waals forces between the polymer itself, i.e. between monomers (resins) and co-monomers (hardeners) to cause permanent damage, e.g. cracking and changes to physical properties, e.g. glass transition temperature; Second, by weakening the hydrogen bond between the polymers and concrete at the bonding plane (Büyüköztürk, 2010) (Jean-Pierra Pascault, 2010). Diffused moisture can be chemically bonded to epoxy or remain as free water after reaching equilibrium. Thus, it is important to quantify the moisture absorbed.

The gravimetric method is widely used to quantify moisture absorption in concrete, epoxy and the laminate. In this method, a specimen is weighed before and after exposure. The difference in weight provides moisture absorption. Hamilton 2009 used the gravimetric method to determine moisture absorption in concrete slices 4 in. x 4 in. x 1 in. with compressive strength varying from 7-10 ksi. His results showed that concrete immersed in 30°C for 60 days absorbed up to 3.2% water by weight. The corresponding weight gain in the epoxy specimens was up to 2.9%. In 2010 (Denvid Lau, 2010) utilized the gravimetric method to determine moisture absorption for repaired concrete beams (4 in. x 1.5 in. x 1.5 in. blocks and 8 in. x 8 in. x 4 in sandwich specimens fabricated from beams) having a concrete strength of 5,800 psi. The concrete had been oven dried for 3 days at 122 °F. Specimen moisture uptake after 10 weeks of exposure at 23 °C and 50 °C was up to 5%.

Tests on neat epoxy (Jelinski, 1985) recorded up to 5 % weight gain for 2 mm x 2 mm x 2 mm epoxy cube specimens immersed at room temperature water for one week. The water content was determined by gravimetric testing.

In this study, 12 specimens were oven dried prior to FRP application. Six of these were part of the exposure study and are referred to as "wet". Six others were part of a study that attempted to determine the extent of bond recovery following removal from exposure and were permitted to dry under ambient conditions. These are referred to as "dry" specimens. An A&D HP-12K electric weighing scale with a maximum capacity of approximately 26 lb. was used to weigh the specimens.

For the wet slabs, weights were recorded before and after exposure while for the dry slabs, weights were recorded before exposure and at periodic intervals until the weight change reduced below 0.05%. Moisture uptake values were 5.2%, 4.9% and 4.3% for Groups 15, 35 and 50, respectively after 15 weeks immersion. Measurements are summarized in Table 7.1 and results plotted in Figure 7.1.
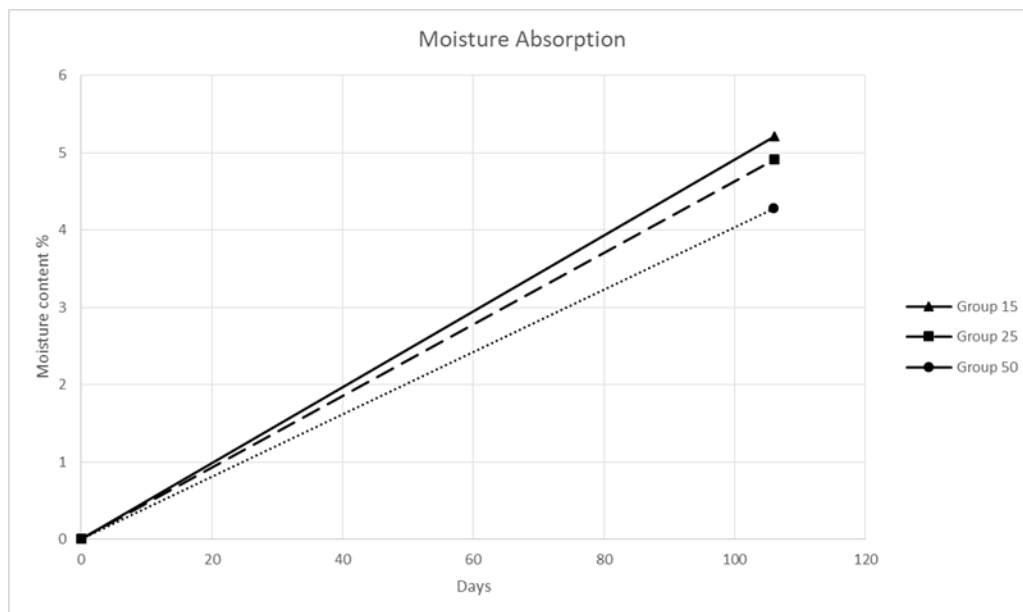
Figure 7.1 Moisture uptake

Table 7.1 Specimen weights before and after moisture exposure

	dry weight (lb)	wet weight (lb)	Uptake %
A-15-wet	15.27	16.07	5.28
B-15-wet	15.65	16.46	5.19
A-15-dry	15.88	16.73	5.34
B-15-dry	15.44	16.22	5.04
Average uptake %		5.21	
A-35-wet	15.78	16.53	4.79
B-35-wet	16.09	16.90	5.01
A-35-dry	16.30	17.09	4.88
B-35-dry	16.50	17.32	4.96
Average uptake %		4.91	
A-50-wet	16.83	17.53	4.17
B-50-wet	16.95	17.66	4.15
A-50-dry	16.41	17.12	4.33
B-50-dry	17.53	18.31	4.45
Average uptake %		4.27	

CHAPTER 8: RESULTS AND DISCUSSION

8.1 Introduction

The underlying premise of the research study was that porosity was critically important for ensuring the integrity of the FRP-concrete bond. The test program was designed to allow direct comparison of the performance of identical specimens with significantly differing porosities following identical exposure. Degradation was quantified through destructive pull-off tests conducted at identical locations. Subsequent investigations comparing failure modes, the condition of the failure plane of tested samples and the location of the epoxy bond line were undertaken to validate or deny the correctness of the original hypothesis.

Results from the destructive testing are summarized in Section 8.2. A comparison of the failure modes appears in Section 8.3. This section also contains information on the failure surface and includes images taken with a microscope to compare the depth of penetration of the epoxy in the concrete substrate with differing porosities. The main conclusions and recommendations are summarized in Section 8.4.

8.2 Pull-off Results

Three series of tests were conducted on controls, exposed specimens, and specimens that were dried following exposure and re-tested. Specimens are identified by a letter (signifying the epoxy type A or B) followed by a number (signifying approximate concrete strength in MPa as 15, 35, 50). Because of the inverse relationship between porosity and strength, the highest porosity specimens are A15 and B15; the corresponding lowest porosity specimens are A50 and B50.

The same relative locations identified as P1 to P6 in Figure 8.1 were tested in all cases. To minimize edge effects, points were offset by an inch from the corresponding edge as shown. These locations are referenced in the results summarized in Table 8.1 through Table 8.3 and in subsequent figures.
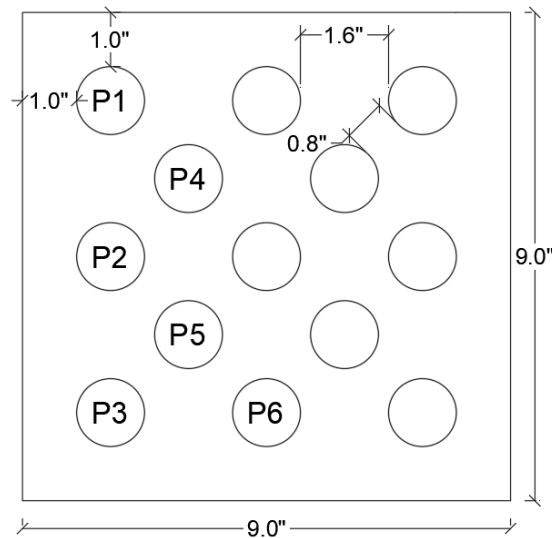
Figure 8.1 Location of test points

8.3 Controls

Baseline values for pull-off bond were first established. These were obtained from tests conducted prior to exposure but after the FRP had been bonded to the concrete surface and the epoxy allowed to cure for 4 weeks. For the two epoxy systems A and B, three concrete porosities (identified by the numerals 15, 35, 50), and six test locations P1 to P6 were tested making a total of 36 tests for the series. Because of the size of the slab, equipment used to score the FRP surface for attaching the dollies dictated the positions that were available for testing.

Test results are summarized in Table 8.1. Since all failures were cohesive, that is, they failed in the concrete, pull-off values reflect concrete's tensile strength. The table also shows calculated means and standard deviation values. The variation in average values was small. Individual results can show larger variation if the aggregate were engaged, Mostfa et al. 2018.

41

Table 8.1 Pull-off result summary for controls- all failures were cohesive

High Porosity Concrete Control Group 15				
Point	Epoxy A		Epoxy B	
	psi	MPa	psi	MPa
P1	225	1.55	266	1.84
P2	246	1.7	246	1.70
P3	246	1.7	287	1.98
P4	287	1.97	246	1.70
P5	266	1.8	266	1.84
P6	246	1.7	246	1.70
Mean (psi)	253		260	
Standard deviation (psi)	21		17	
Intermediate Porosity Concrete Control Group 35				
Point	Epoxy A		Epoxy B	
	psi	MPa	psi	MPa
P1	225	1.55	287	1.98
P2	369	2.54	369	2.54
P3	328	2.26	266	1.84
P4	225	1.55	266	1.84
P5	307	2.12	266	1.84
P6	328	2.26	307	2.12

Table 8.1 (Continued)

Mean (psi)	297		294	
Standard deviation (psi)	59		40	
Low Porosity Concrete Control Group 50				
Point	Epoxy A		Epoxy B	
	psi	MPa	psi	MPa
P1	328	2.26	369	2.54
P2	348	2.40	389	2.68
P3	369	2.54	348	2.40
P4	410	2.83	410	2.83
P5	389	2.68	348	2.40
P6	410	2.83	410	2.83
Mean (psi)	376		379	
Standard deviation (psi)	33		28	

For the concrete with the highest porosity, Group 15 (2,325 psi), the average pull-off value was 253 psi for epoxy A and 260 psi for epoxy For the intermediate porosity concrete, Group 35 (4,206 psi), the average pull-off strength was 297 psi for epoxy A and 294 psi for epoxy B. For the lowest porosity concrete, Group 50 (7,040 psi), the corresponding pull-off values were 376 psi for epoxy A and 379 psi for epoxy B.

The disparity in test values reflect the relationship between concrete's compressive and tensile strength reported as $5\sqrt{f'c}$ (psi) in ACI 318-14, Eq. 14.5.2.1a for plain concrete in flexure.

The corresponding coefficients calculated using the average test values in Table 8.1 are 5.33 (Group 15), 4.56 (Group 35) and 4.49 (Group 50).

8.4 Wet Series

The specimens tested in this series were also part of a gravimetric study geared towards measuring moisture absorption at the bond line. To ensure moisture could only enter through the FRP, all other concrete surfaces at the sides and the bottom were sealed using a water proof coat. Details are included in Section 6.1.

The water temperature was selected as 30°C (86°F), comparable to the average Tampa Bay water temperature. More importantly, previous studies such as those at MIT and in the NCHRP study had indicated that bond degraded in as little as 8 weeks under this exposure. Specimens were submerged for 15 weeks but there were provisions for additional exposure should results prove inconclusive.

Test results are summarized in Table 8.2. Since the failure mode changed because of the exposure, information on the failure mode is provided in the table. The codes G, E and F used correspond to ASTM D7522 definition of the failure mode and are identified in Figure 8.2.

Table 8.2 Pull-off result summary after immersion for 15 weeks

High Porosity Group 15 – Wet						
Point	Epoxy A		Mode	Epoxy B		Mode
	psi	MPa		psi	MPa	
P1	205	1.41	F	246	1.70	G
P2	287	1.98	G	266	1.84	G
P3	266	1.84	G	246	1.70	G
P4	246	1.70	G	246	1.70	G

Table 8.2 (Continued)

P5	225	1.55	G	307	2.12	G
P6	246	1.70	G	266	1.84	G
Mean (psi)	246			263		
Standard deviation (psi)	29			24		
Intermediate Porosity Group 35- Wet						
Point	Epoxy A		Mode	Epoxy B		Mode
	psi	MPa		psi	MPa	
P1	266	1.84	F	246	1.70	F
P2	307	2.12	G	266	1.84	F
P3	246	1.70	F	266	1.84	F
P4	225	1.55	E	307	2.12	F
P5	225	1.55	F	287	1.98	F
P6	307	2.12	G	225	1.55	E
Mean (psi)	263			266		
Standard deviation (psi)	38			29		
Low Porosity Group 50-Wet						
Point	Epoxy A		Mode	Epoxy B		Mode
	psi	MPa		psi	MPa	
P1	369	2.54	G	307	2.12	F
P2	225	1.55	E	266	1.84	F

Table 8.2 (Continued)

P3	266	1.84	F	328	2.26	F
P4	225	1.55	E	225	1.55	F
P5	410	2.83	G	225	1.55	F
P6	348	2.40	G	307	2.12	F
Mean (psi)	307			277		
Standard deviation (psi)	79			44		

G=Substrate, E=Bond plane, F=Mixed Mode (ASTM D7522)

Excepting for the high porosity Group 15 that showed minimal reduction in average bond strength, the reduction in bond varied with porosity as anticipated. The reduction in the average pull-off bond was only 1% for the high porosity, low strength concrete (Group 15 – 254 psi vs 256 psi for controls). It was higher for the intermediate porosity concrete where the average reduction was 11% (Group 35 - 264 psi compared to 295 psi). The greatest reduction was in the low porosity, high strength Group 50 specimens. Here bond reduction was 23% dropping from an average value of 377 psi to 292 psi.

The failure mode changed from cohesive failure in the high porosity group to mixed cohesive adhesive failures to adhesive failures. Information on the failure modes is included in Table 8.1 and Figure 8.2. A detailed discussion on the failure mode is presented in Section 8.3.

Comparison of the relative performance of two epoxies indicated that Epoxy A was better for the low porosity concrete (high strength concrete) whereas epoxy B performed better for the low and intermediate porosity concretes (low to medium strength concrete). This finding was consistent with those reported previously in the literature, (Sen, 2015). Results in Table 8.1 and Table 8.2 are shown as bar plots in Figure 8.3 and Figure 8.4.

Figure 8.2 Failure mode after moisture exposure.
Failure Mode: G (Concrete Substrate failure), E (FRP/concrete interface), F (mixed mode G and mode E)
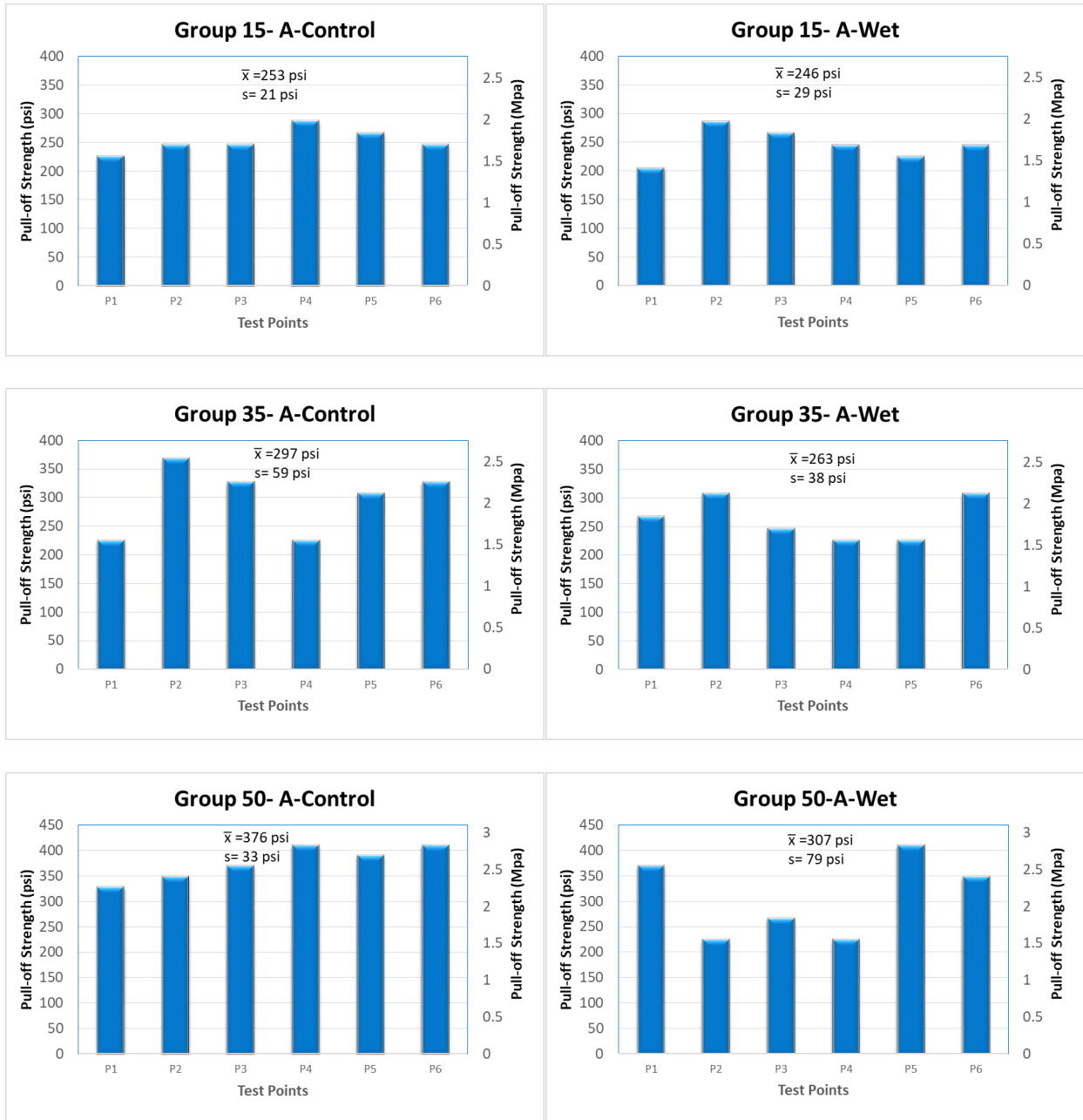
Figure 8.3 Overview of results for epoxy A.
($\overline{x}$= sample mean, s=sample standard deviation)
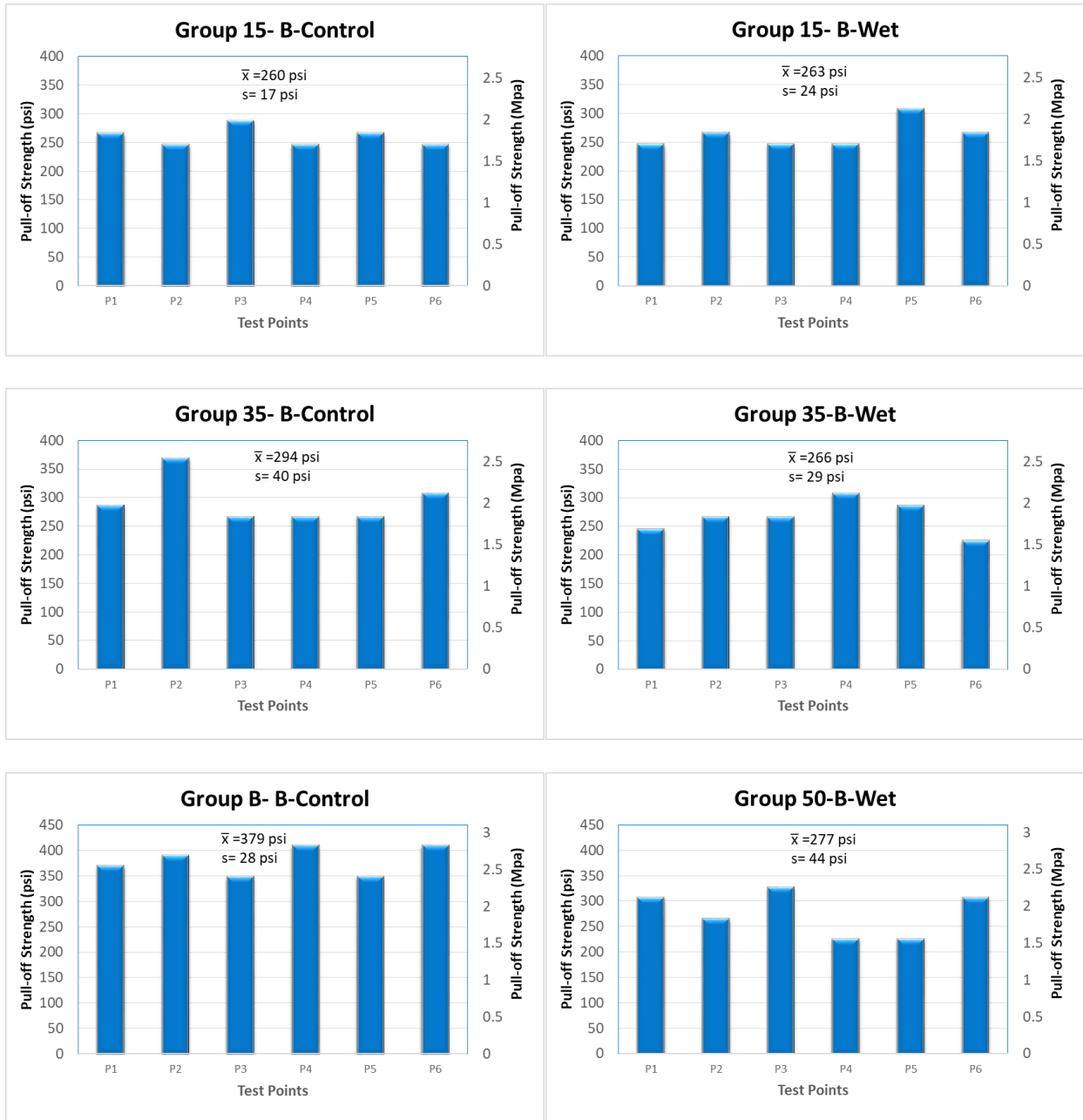
Figure 8.4 Overview of results for epoxy B.
($\overline{x}$= sample mean, s=sample standard deviation) exhibited

8.5 Dry Series

To obtain a measure of bond recovery, exposed specimens were left to dry and their weight measured periodically until the change in weight fell below 0.05%. As before, six slabs, two for each porosity were tested. The same six locations in Figure 8.1 were tested for the three concrete strengths and the two epoxies. Results are summarized in Table 8.3. A comparison of the results from the wet and re-dry tests is shown graphically as bar plots in Figure 8.5 and Figure 8.6.

Regain was lower in the low porosity specimens followed by that in the concrete with the highest porosity. The greatest gain was in the specimens with intermediate porosity. For the high porosity specimens the average re-gain was 4% (Group 15 (2,325 psi) average was 266 psi compared to wet series average of 255 psi). For the intermediate porosity specimens the regain was 10% (Group 35 (4,206 psi) average was 292 psi compared to the wet series average of 264 psi). For the low porosity specimens the regain was just 2% (Group 50 (7,040 psi) average was 299 psi compared to the wet series average of 292 psi.

For the high porosity concrete (Group 15), the low percent regain is not surprising since the failure mode was unaffected by exposure. The epoxy strength continued to exceed that of the concrete resulting in cohesive failure. The intermediate porosity concrete (Group 35) recorded the highest strength regain with a mixed failure mode. Unlike the high porosity concrete where the epoxy sealed the capillary network, its lower porosity permitted water to evaporate and improve mechanical interlock bond as was observed in the NCHRP study, Dolan et al. 2009. Nonetheless, the epoxy had degraded sufficiently so that its strength was comparable to concrete's tensile strength that led to a mixed mode failure. The lowest regain was observed for Group 50 (2%) where the epoxy experienced irreversible damage. Limited re-gain was possibly due to improved mechanical interlock. An overview of all the results is shown in Figure 8.7 to Figure 8.8.

Table 8.3 Pull-off result summary after re-dry

Point	Epoxy A		Mode	Epoxy B		Mode
	psi	MPa		psi	MPa	
High Porosity Group 15- Re-Dry Results						
P1	328	2.26	G	225	1.55	F
P2	246	1.70	G	246	1.70	F
P3	225	1.55	G	287	1.98	G
P4	266	1.84	G	328	2.26	G
P5	205	1.41	G	246	1.70	G
P6	266	1.84	G	328	2.26	G
Mean (psi)	256			277		
Standard deviation (psi)	42			44		
Intermediate Porosity Group 35- Re-Dry Results						
P1	410	2.83	G	246	1.70	F
P2	246	1.70	E	287	1.98	F
P3	287	1.98	F	369	2.54	G
P4	328	2.26	G	348	2.40	G
P5	225	1.55	E	246	1.70	F
P6	266	1.84	F	246	1.70	E
Mean (psi)	294			290		

Table 8.3-Continued

Standard deviation (psi)	67			56		
Low Porosity Group 35- Re-Dry Results						
Point	Epoxy A		Mode	Epoxy B		Mode
	psi	MPa		psi	MPa	
P1	287	1.98	E	389	2.68	F
P2	266	1.84	E	246	1.70	F
P3	328	2.26	F	246	1.70	F
P4	266	1.84	E	307	2.12	F
P5	348	2.40	F	328	2.26	F
P6	287	1.98	F	287	1.98	F
Mean (psi)	297			301		
Standard deviation (psi)	34			54		

G=Substrate, E=Bond plane, F=Mixed Mode (ASTM D7522)
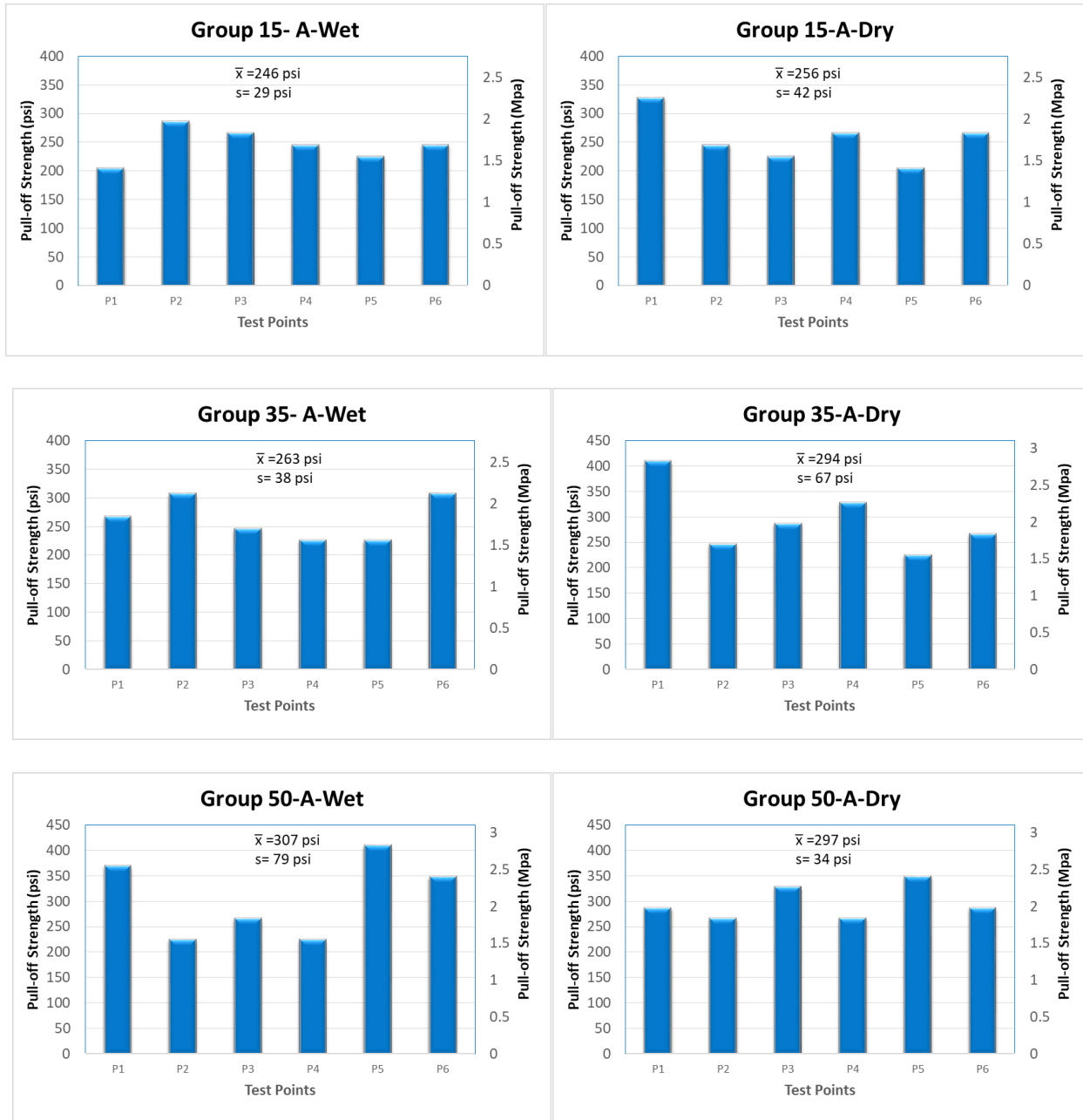
Figure 8.5 Overview of strength regain results for epoxy A.
($\overline{x}$= sample mean, s=sample standard deviation)

53
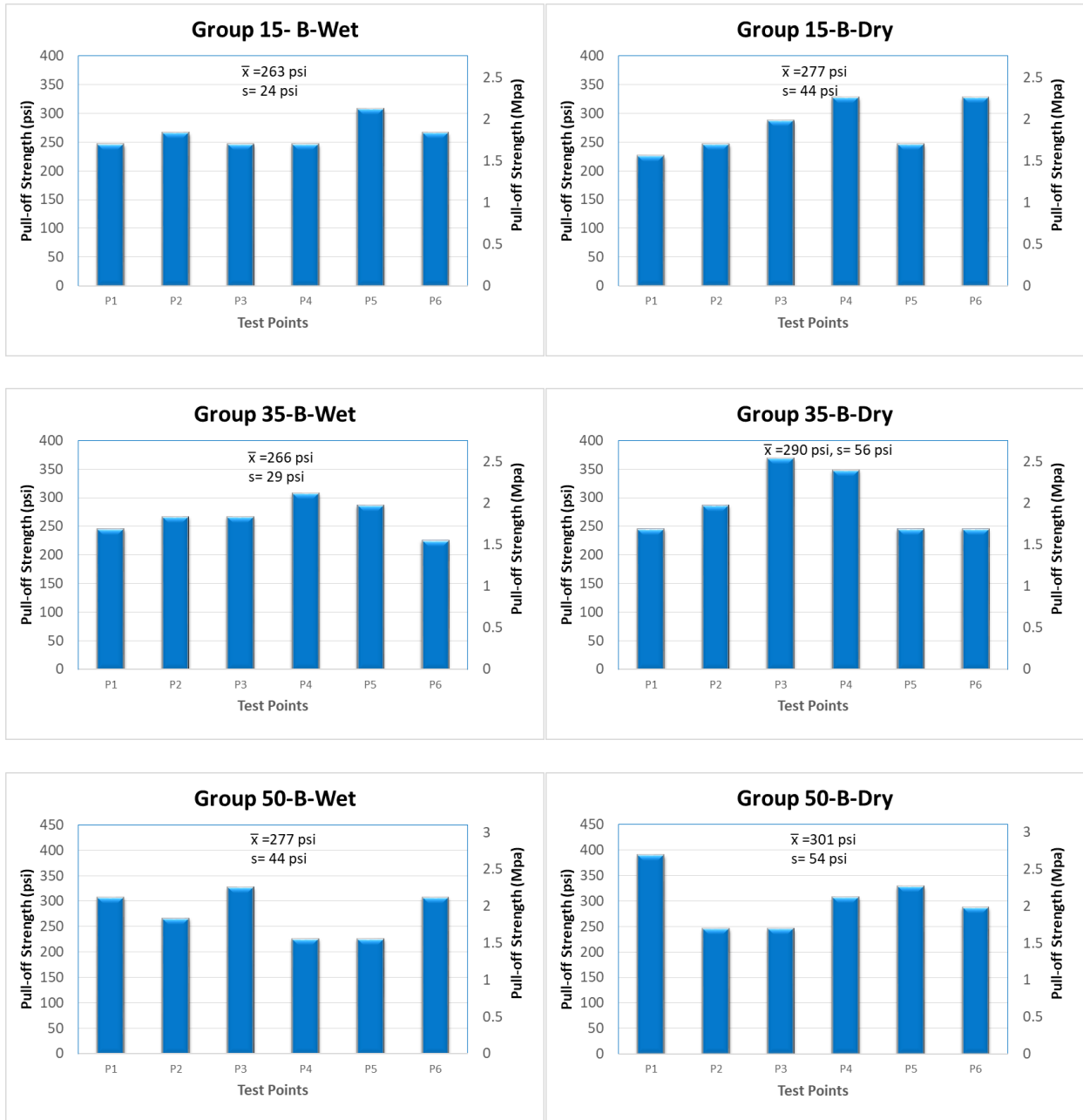
Figure 8.6 Overview of strength regain results for epoxy B.
($\overline{x}$= sample mean, s=sample standard deviation)
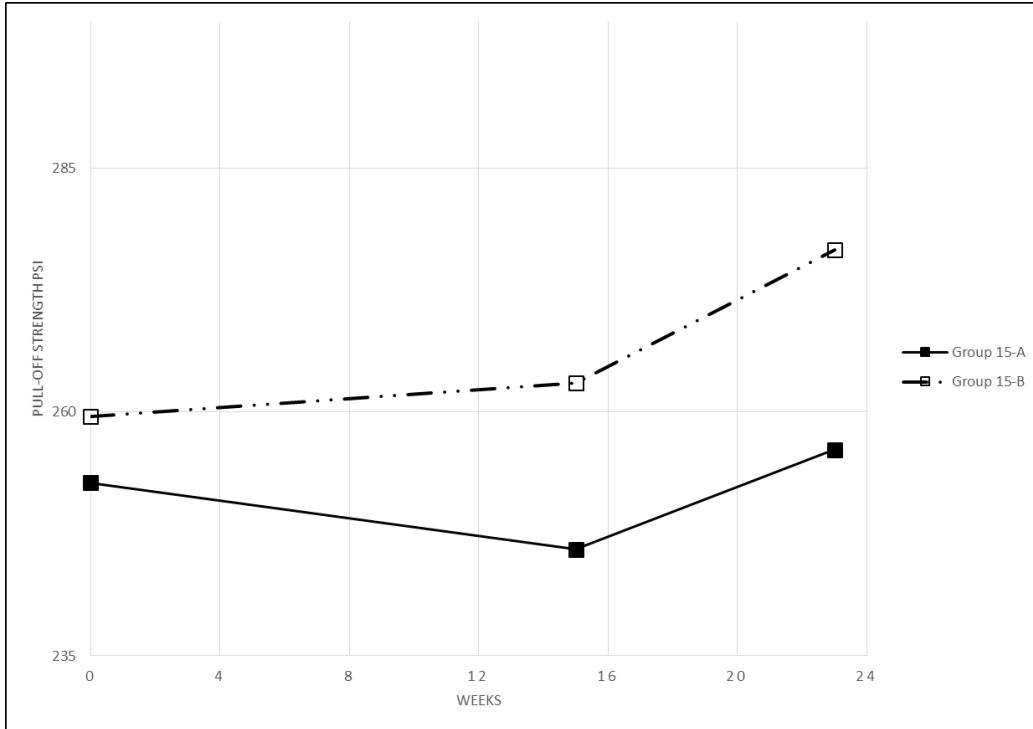
Strength with time-Group 15
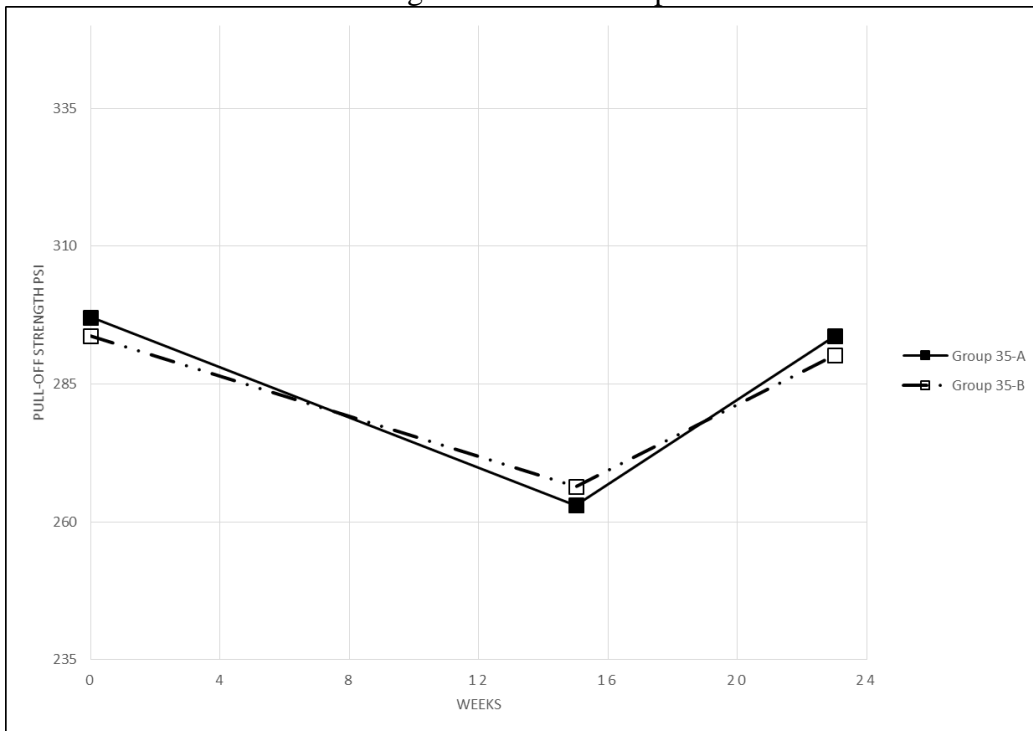
Strength with time-Group 35
Figure 8.7 Overview of results from control, wet and dried tests
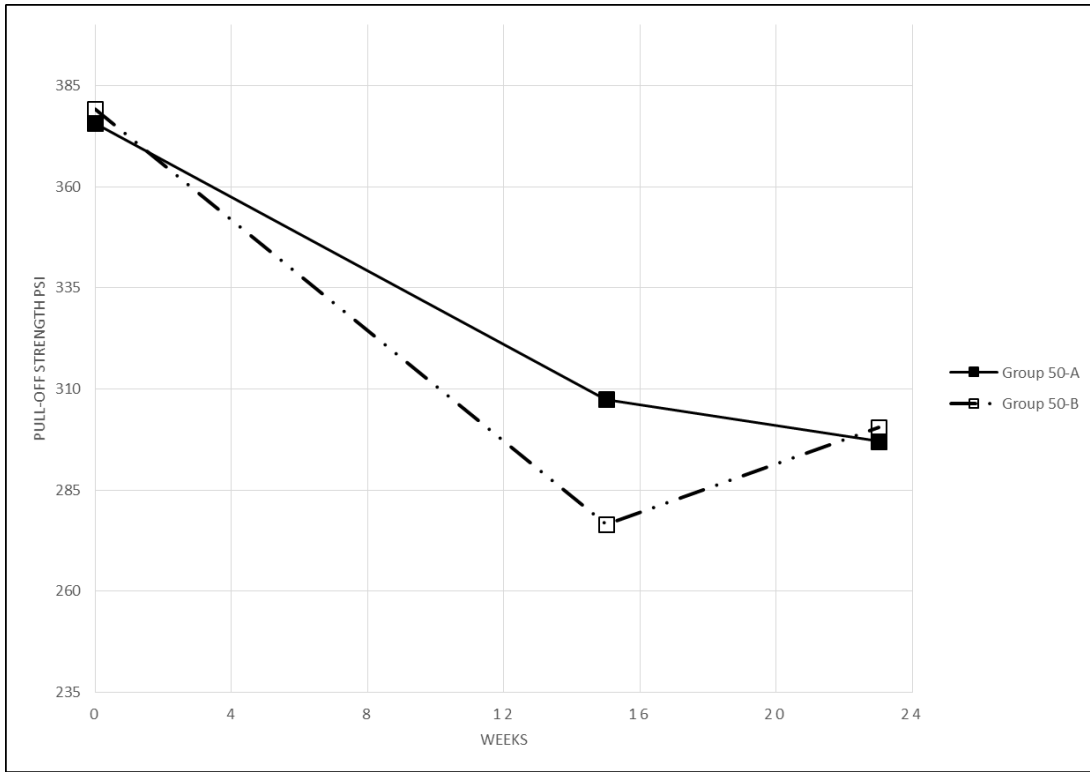
Strength with time-Group 50

Figure 8.7 (Continued)
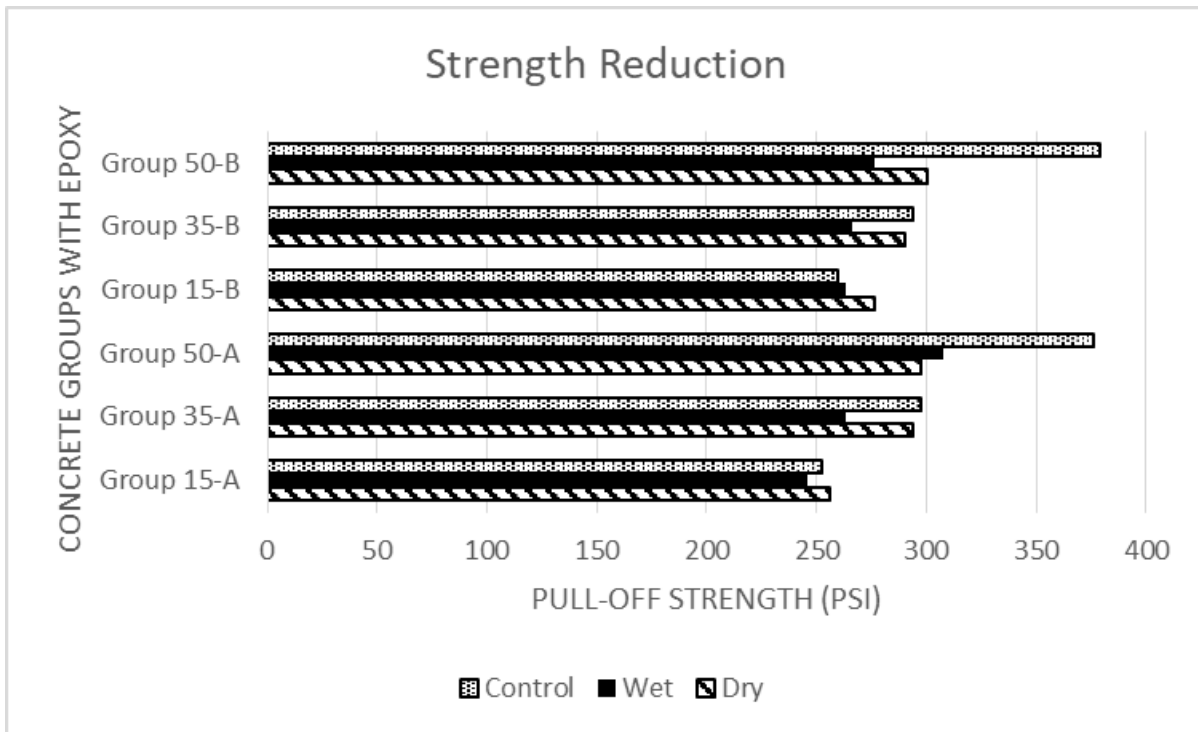
Figure 8.8 Role of epoxy in degradation

8.6   Failure Mode Comparison

The results from the pull-off tests showed markedly greater degradation in the low porosity concrete compared to the high porosity concrete. This section presents findings from investigations that compared the failure mode for the different porosities and results of the measurement of the approximate depth of penetration of epoxy into the various concrete substrates. They are based on an analysis of photographic images taken using a digital camera and a portable microscope. In this section, selection of these images are presented. The rest may be found in Appendix A.

8.7   Concrete Bonded to Dolly

The depth of concrete bonded to the dolly is an indirect measure of the porosity of the concrete. For concretes with low porosity, epoxy can be expected to penetrate deeper into the substrate. Therefore, an examination of the failure plane could show traces of epoxy, evidence of open pores and pores that were filled with epoxy. In high porosity concrete, epoxy was unlikely to be present in the failure plane and pores would not as visible.

Figure 8.9 and Figure 8.10 compare the depth of concrete attached to the dolly from tests conducted on controls and wet specimens. In these plots, failure in high porosity (low strength concrete) is compared to that of intermediate (Figure 8.9) and low porosity concrete (Figure 8.10). In each set of these photos, the average depth from the three points shown is provided.

Inspection of Figure 8.9 - Figure 8.10 shows that the depth of concrete attached to the dolly was considerably greater for the high porosity concrete from both dry and wet tests. The distinction between the medium and low porosity concrete was evident. Interestingly, the reduction in the depth between dry and wet states was similar in all cases (about 6 mm). The results suggest that epoxy penetrated deeper into the substrate in high porosity concrete.

15-Dry 16mm

15-Wet 10mm

35-Dry 10 mm

35-Wet 4 mm
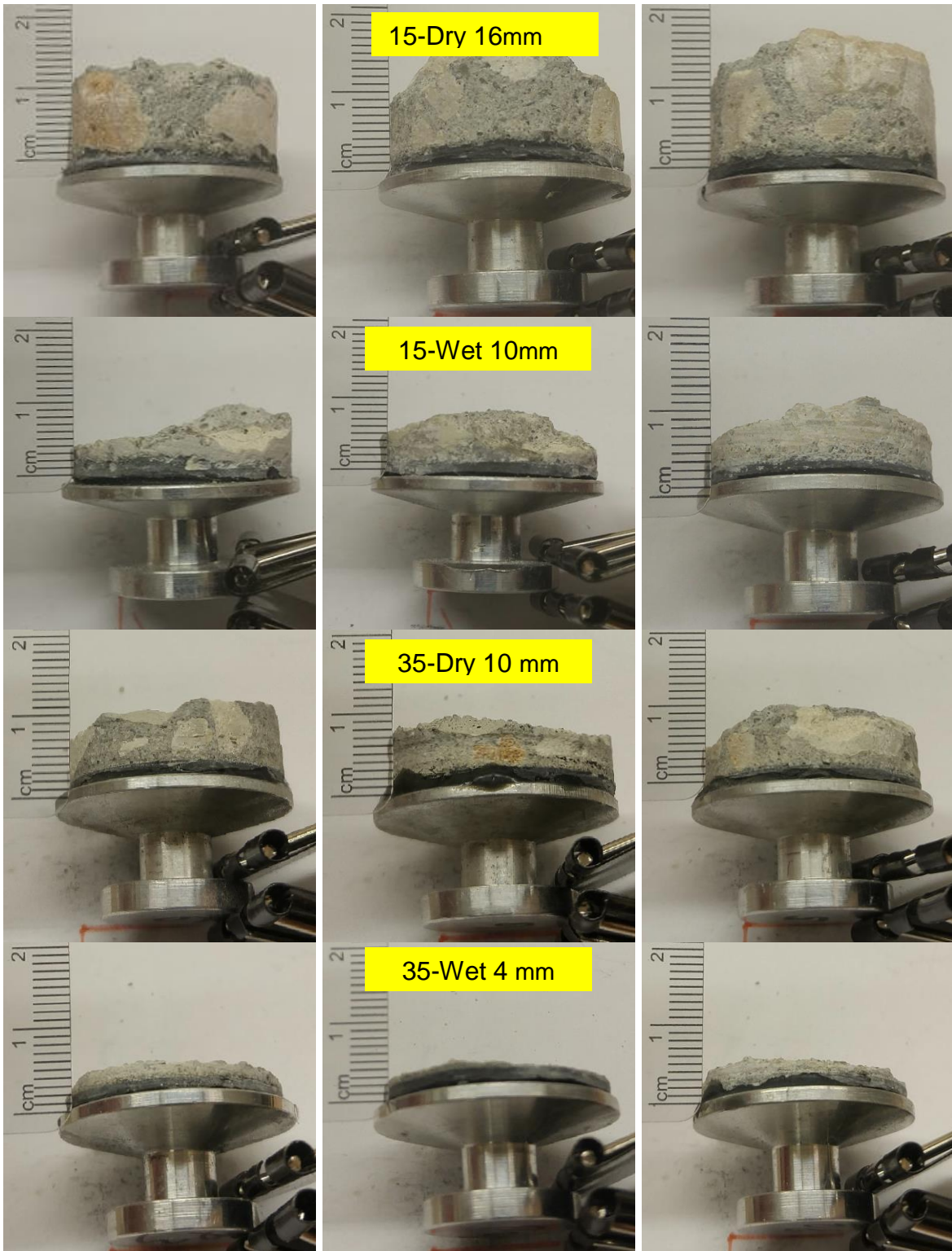
Figure 8.9 Role of epoxy in degradation
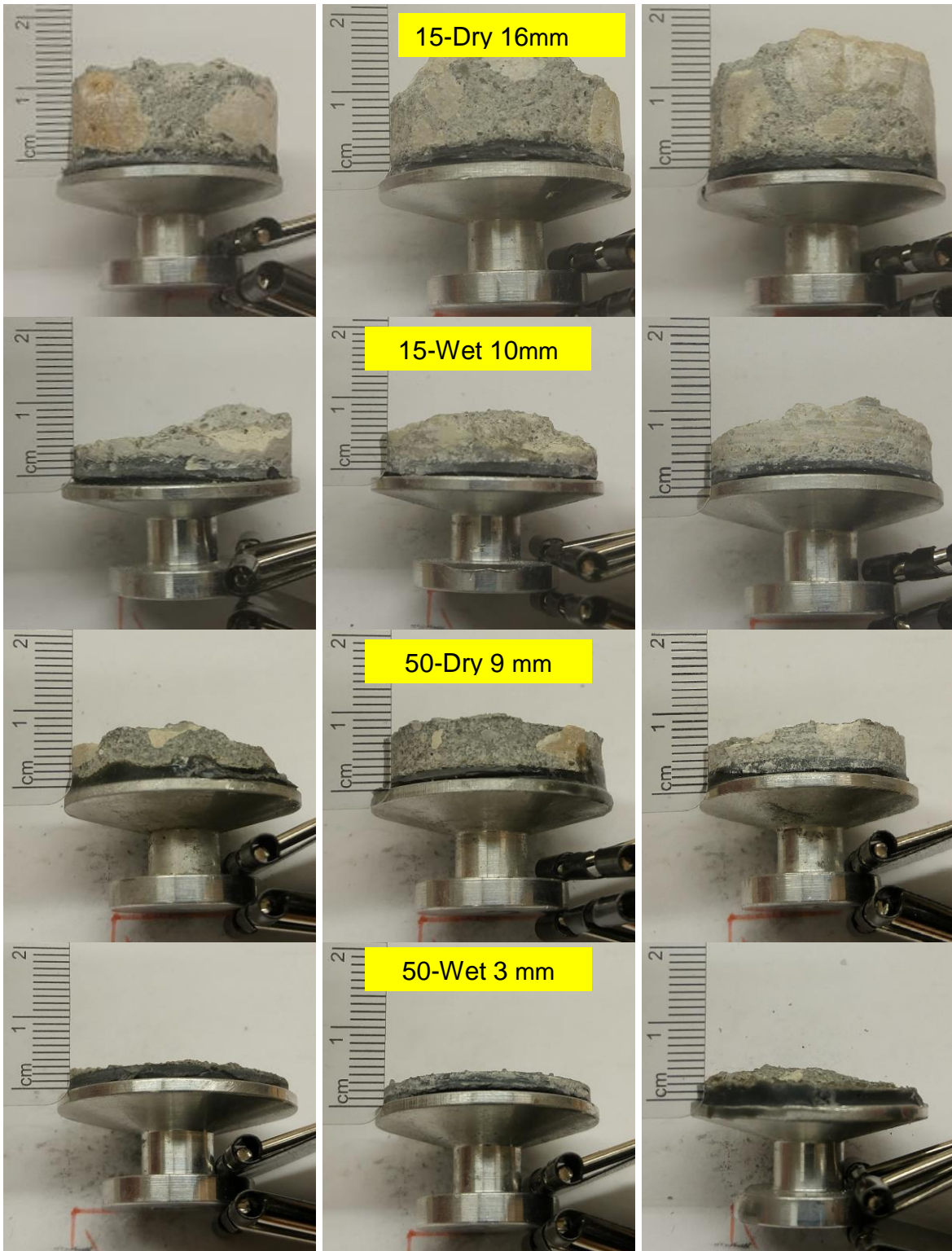
Figure 8.10 Role of epoxy in degradation

8.8 Failure Plane

The failure plane of the tested specimens were photographed to find evidence of epoxy penetration into the substrate. Figure 8.11 compares the failure planes from low, medium and high porosity concretes taken from dry specimens. Inspection of Figure 8.11 shows evidence of epoxy and voids only in the high porosity concrete even at a considerably deeper depth (16 mm vs 10 mm for the lower porosity concrete).

The greater depth of penetration of the epoxy meant that water could not extend below the bond line for the high porosity concrete. Given epoxy's greater tensile strength, bond was not affected after 15 weeks of exposure. However, degradation could be expected if the immersion period were longer.

Low Porosity -Dark circled area shows epoxy penetration, More pores visible

Medium Porosity – some pores visible but no epoxy
Figure 8.11 Dolly plan-view from control specimens

Low Porosity – similar to medium porosity
Figure 8.11 (Continued)

8.9   Epoxy Penetration Depth

Magnified photographic images of the bond line can provide compelling evidence of the role of porosity that may also help to explain why the NCHRP study did not find much difference in the performance of surfaces prepared to a CSP 1 and CSP 3 profile, NCHRP.

The location of the bond line cannot be obtained by saw cutting because the grinding action of the saw spews out dust that can form a coating on the cut surface. It was discovered that this problem could be overcome by breaking open the specimen. This revealed locations where it was possible to take magnified images using a microscope.

The magnification used to obtain the images was approximately 60x (a third of the scale). Prior measurement of the thickness of the FRP using a digital caliper had indicated that its thickness was approximately 1.5 mm. Using this value as a reference, the images were processed using AUTOCAD to introduce a local scale that could be used for comparison.

A total of nine images were taken – three of these corresponding to high, medium and low porosity are shown in Figure 8.12. Each picture is accompanied by its own local scale. The FRP material is clearly visible at the top.

.
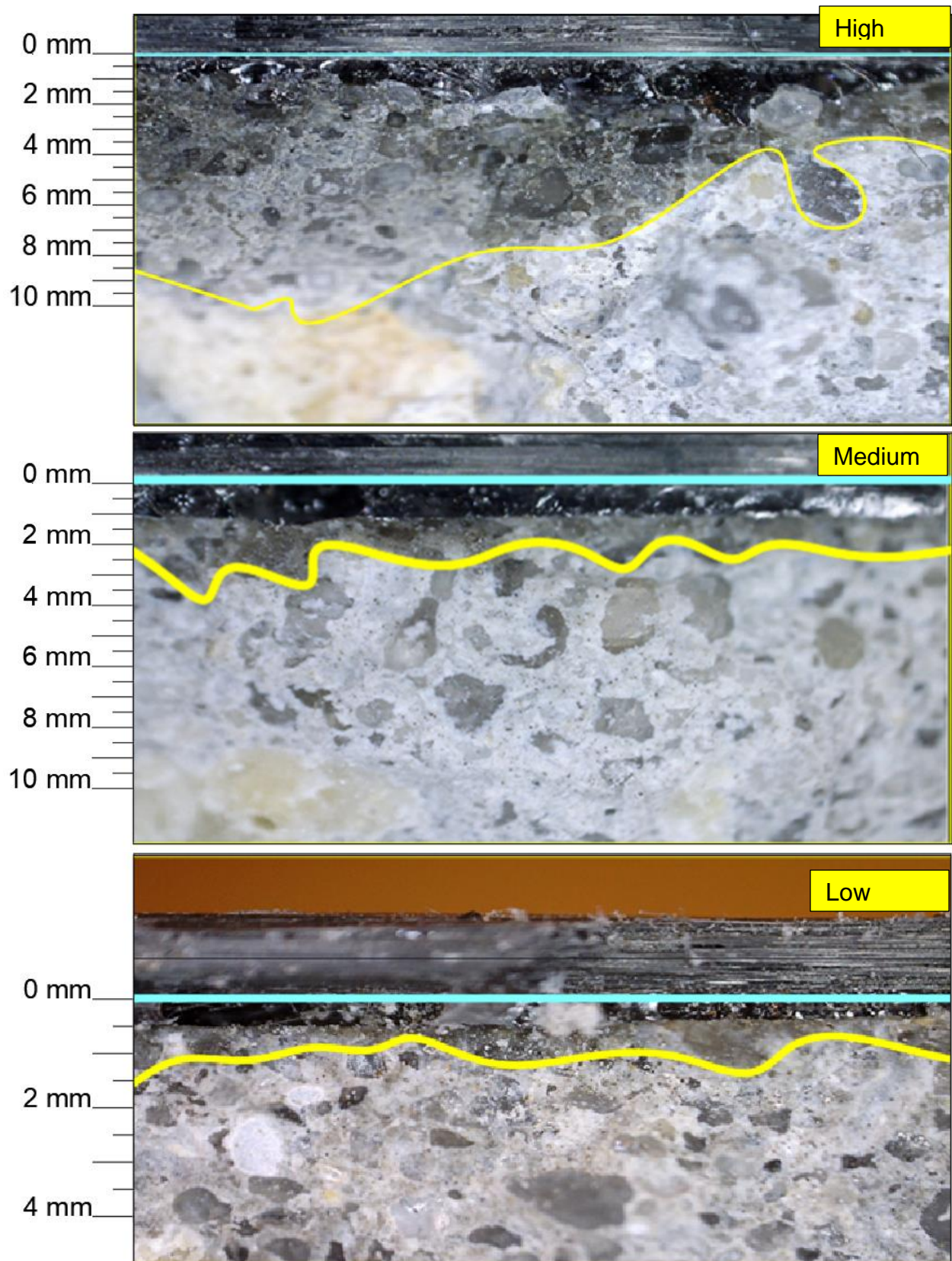
Figure 8.12 Relative depth of epoxy penetration

Inspection of Figure 8.12 shows the variability of the epoxy penetration depth that is a reflection of the network of voids present in the concrete. The depth of penetration of the epoxy is significantly greater for the high porosity concrete. The top photo also shows locations where the epoxy filled the voids.

8.10 Conclusions

This chapter provides evidence that helps to improve our understanding on the role concrete porosity on FRP-concrete bond. The tests clearly demonstrate that FRP durability in a wet environment is strongly influenced by porosity. High porosity, low strength concrete performed significantly better than the low porosity high strength concrete.

In the study, the bonding surfaces were prepared by sand blasting to achieve a target CSP 3 finish though complete conformity with this target is difficult to prove as was pointed out in the NCHRP 609 study. Nonetheless, since all specimens were identically prepared in the same manner by the same individual there was consistency in the surface preparation. The study suggests that the long term performance of the FRP-concrete bond could be improved if the epoxy could be made to penetrate deeper. Such preparation will be needed only for applications where FRP-bond was subjected to intermittent immersion in water.

8.11 Future Work

The immediate need is to conduct a systematic investigation of practical surface preparation techniques and epoxy viscosities that can ensure deeper penetration of the epoxy in higher strength concretes. The technique selected should minimize micro-cracking damage since this can reduce the effectiveness of the FRP-concrete bond.

CHAPTER 9: CFRP-CMU BOND IN OUTDOOR EXPOSURE

9.1   Note to Reader

This chapter has been accepted for publication in ACI, Structural Journal and is reproduced with permission from the publisher ACI.

9.2   Abstract

Two full-scale concrete masonry walls were repaired with three horizontally aligned 20 in. (508 mm) wide uni-directional carbon fiber sheets using different commercially available epoxies. Twenty years later the CFRP-CMU bond was determined through selective pull-off tests that were preceded by detailed non-destructive evaluation. Results showed that despite superficial damage to the top epoxy coating and debonding along masonry joints, the residual CFRP-CMU bond was largely unaffected by prolonged exposure to Florida's harsh environment. Therein, over 90% of the failures were in the concrete substrate. Though bond was poorer at mortar joints because the CFRP was well bonded to the masonry surface, its impact on structural performance of the repair was expected to be minimal. Overall, the repairs proved to be durable with both epoxy systems performing well.

9.3   Introduction

The application of FRP for masonry repair is recent compared to concrete. As a result, there are no durability studies on the performance of its bond comparable to that available for reinforced concrete, e.g. (Dolan, et al., 2009) (Sen, 2015). This study provides the first data set on the performance of CFRP-CMU repairs exposed for over 20 years to Florida's aggressive environment. Since its original installation, no protective UV coating was applied to the CFRP

material. Thus, the results provide a measure of the likely performance of neglected repairs without external intervention over an extended period of time.

9.4   Background

Concrete masonry units (CMU) are widely used in residential construction particularly in the southeastern United States where walls constitute the most common structural element. In low seismic regions such as Florida or Texas, walls are designed and detailed to withstand bending moments and shear force due to hurricane force winds. Experience has shown that walls can also sustain settlement damage when supported by soils containing decaying organic material such as tree limbs or roots that lie buried below the foundation. Settlement manifests itself in characteristic stair-step cracking along mortar joints as shown in Figure 9.1.

Figure 9.1 Characteristic stair-step cracking in CMU wall.

Figure 9.2 Walls labeled 2 and 3 were repaired using CFRP and tested

To explore the feasibility of carbon fiber repair, the University of South Florida created a test setup simulating foundation settlement. Four full-size 20 ft. (6.1 m) long, 8 ft. (2.43m) high and 8 in. thick (203 mm) concrete masonry walls were constructed, Figure 9.2. The free ends of the walls were supported on screw jacks that could be adjusted to induce settlement. An overhead structural frame was used to apply simulated roof loads, Hartley et al.,[13].

The walls were built using 1900 psi (13 MPa) concrete masonry blocks and 1800 psi (12.4 MPa) type S mortar. Vertical reinforcement varied to reflect changing code provisions and construction practice in Florida over the past 40 years, (Mullins, et al., 2000). Reinforced cells were grouted using code specified 2500 psi (17 MPa) grout. Since owners of local masonry contracting companies built the walls, construction reflected the very best practice.

Two of the weakest walls, identified here as Walls 2 and 3 represented design and construction practice prior to Hurricane Andrew when requirements for vertical reinforcement were lax. Mortar joints separating courses were laid in running bond in which vertical joints do not line up. This contrasts with laboratory investigations[8] in which the verticals joint line up (stacked bond). The weakest wall (Wall 3) was only reinforced at its ends whereas the second weakest wall (Wall 2) had two additional intermediate vertical bars located 8 ft. (2.43 m) from each end Figure 9.3. Thus both walls would be classified as unreinforced in code parlance because the reinforcement spacing exceeded six times the wall thickness. Simulated settlement and roof loading resulted in tell-tale in-plane stair-step cracking in both walls, (Hartley, et al., 1996). The damaged walls were repaired using unidirectional carbon fiber sheets and re-tested under the same load setup. The results showed that the CFRP repair was effective. At the end of the testing, loads were removed and the walls left exposed to the elements.
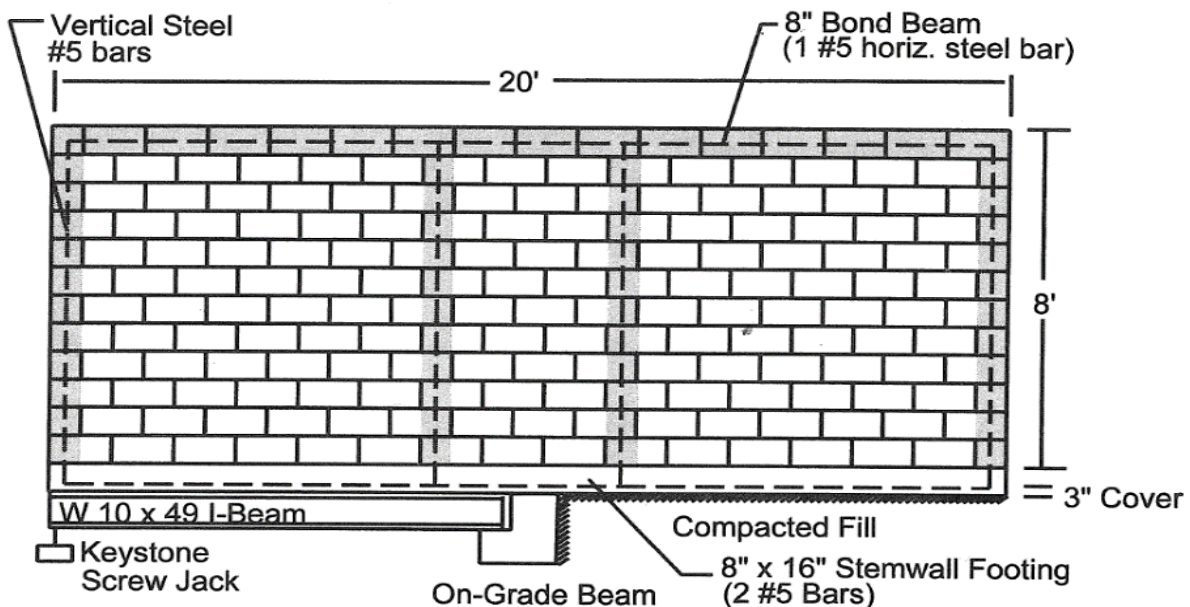
NOTE: Intermediate Vertical Reinforcement Omitted in Wall 3

Figure 9.3 Wall 2 reinforcement details and test set up for settlement simulation

9.5   Objectives

The primary goal of the study was to quantify CFRP-CMU bond through destructive pull-off testing. Because of the age of the repair, extreme care was exercised to ensure only limited portions of the two 100 sq. ft. (9.3 sq. m) CFRP bonded surfaces were used in the testing. The untested area was earmarked for future tests that could be conducted in five to ten years. Since the walls were evaluated non-destructively, the extent to which the NDT technology was able to predict regions of good or bad bond became an important secondary objective.

In the 20 years following the original repair the walls were left unattended. No maintenance was carried out nor was coating applied to the CFRP surface to protect against solar radiation. Thus, the results provide a worst-case scenario for assessing CFRP bond performance under exposure to a very aggressive environment.

9.6   Research Significance

Long term performance data on new materials are critically important for advancing the state of knowledge and fine tuning industry practice. This study provides the first quantitative data set on the durability of CFRP-CMU bond after over 20 years exposure to hot, humid conditions. This will make it possible to calibrate available models[8]. Most results, such as the durability of mortar joints laid out in running bond, are new. Spatial temperature data comparing ambient to CFRP / CMU surface temperature are also new and can impact specifications addressing hot weather installation. Findings from non-destructive testing provide useful insights on its effectiveness in evaluating and inspecting CFRP-repaired elements.

9.7   Governing Codes

No FRP codes were in existence at the time the repair was carried out in 1995. ACI published its first FRP guide in 2002 and its first code, ACI 440.2R-08, in 2008. The first FRP-

Masonry code was issued in 2010, ACI 440.7R-10. The relevant code for masonry design and construction at the time the walls were built was ACI 530-92.

ACI 440.2R-08, specifies (provision 1.3.4) "FRP systems should not be used when the concrete substrate has a compressive strength f'c less than 2500 psi (17 MPa)". Additionally, it requires tensile strength to be at least 200 psi (1.4 MPa) to ensure concrete had sufficient strength to allow force transfer to the FRP.

ACI 440.7R-10 recognizes the lower strength of concrete masonry but does not stipulate minimum strengths. Instead, requirements are qualitative, e.g. provision 6.2.5 states that "Tension adhesion tests should exhibit failure of the masonry substrate" while 11.2.1 states that "the weak link in the masonry/FRP interface is the masonry. The quality and tensile strength of the substrate will limit the overall effectiveness of the bonded FRP system".

9.8 Details

Masonry walls are characterized by a network of mortar joints that constitute well-defined planes of weakness. Horizontal joints are classified as "bed" joints and vertical joints as "head" joints. Joints where bed and head joints intersect are referred to here as intersecting joints. They are illustrated in Figure 9.4.

Tensile resistance of a mortar joint depends on the direction of the load. In weak axis bending, that is, bending under wind loads perpendicular to the wall face, the allowable tensile stress normal to the bed joints in hollow units for type S mortar was 25 psi (0.17 MPa); it was 50 psi (0.34 MPa) for tension parallel to the bed joint, ACI 530-92,4. These values were permitted to be increased by 33% for load combinations involving wind.

69
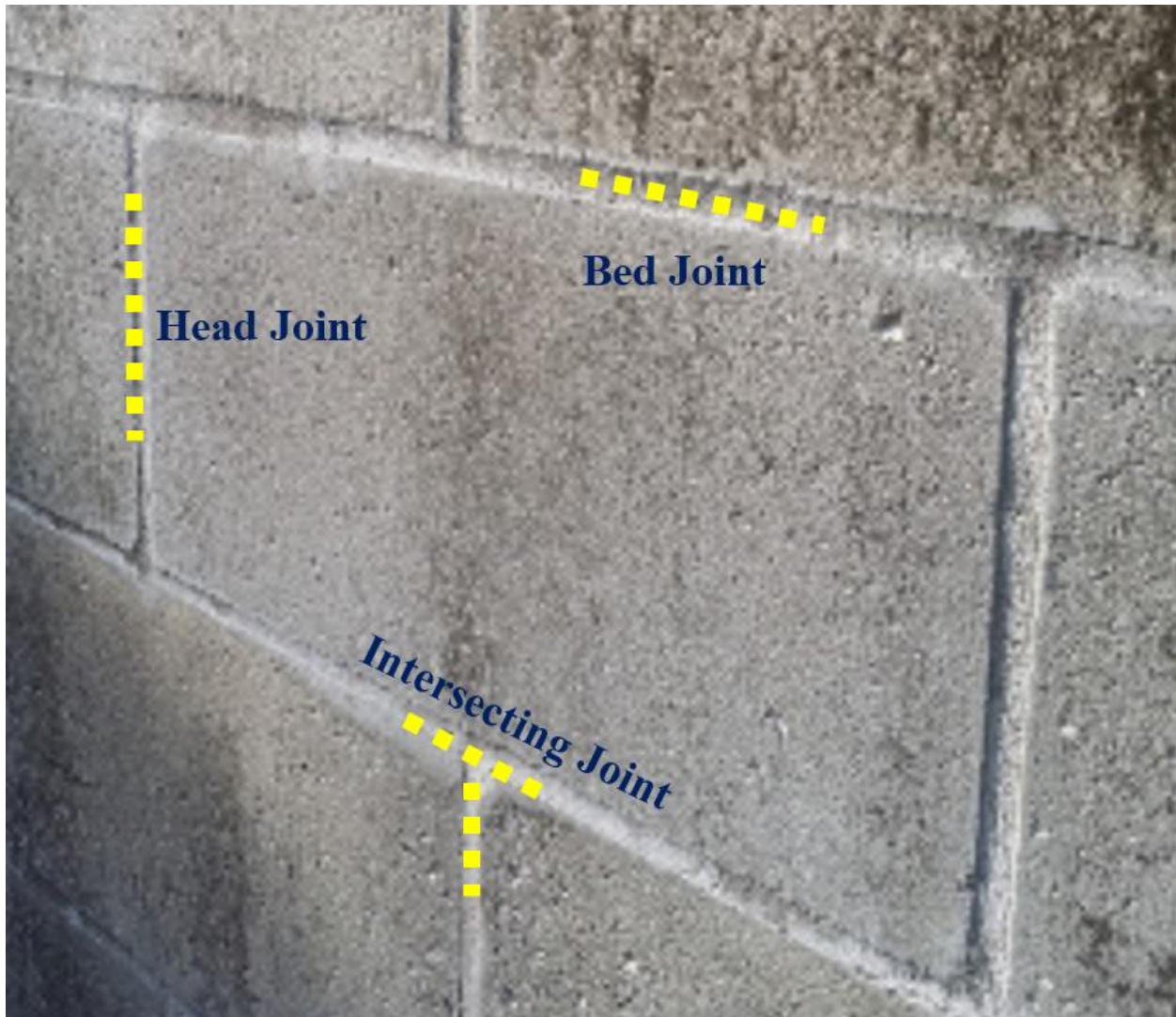
Figure 9.4 Mortar joint definition

9.8.1 CFRP Repair Details

A single layer uni-directional carbon fiber sheeting (FTS-C1-120) was used for the CFRP repair. Two commercially available epoxies were used as adhesives; these were from Henkel and Tonen. Material properties of the carbon fiber and the epoxies as reported by the manufacturer are summarized in Table 9.1, (Hartley, 1995).

The carbon fibers were oriented horizontally since the intent was to provide shear strengthening under in-plane settlement forces. Three 20 ft. (6.1 m) long strips each 20 in (50.8

cm) wide were placed side-by-side to repair each wall. Thus the CFRP bonded area was 20 ft. x 5 ft. (6.1 m x 1.5 m) leaving a 20 ft x 3 ft. (6.1m x 0.9 m) height of unrepaired wall below. Finite element modeling suggested that strengthening would have been equally effective if the repair width were narrower than 5 ft (1.5m), (Engebretson, et al., 1996).

Table 9.1 Material properties of CFRP and epoxy

CFRP- FTS-C1-20 Tonen Co. Japan	
Fiber thickness	0.00433 in
	(0.1099 mm)
Fiber modulus	33,000,000 psi
	(220 GPa)
Tensile strength	2183.9 lb/in
	(382 kN/m)
Layers	1
Resin-wall 2: Henekel Co. of Kankakee, IL	
Primer	13-283/13-284
Resin	13-285/13-286
Resin Tension	8.1 ksi
	(55 MPa)
Resin-wall 2:Tonen Primer and Resin	
Primer	FP-NS
Resin	FR-E3P
Resin Tension	6.8 ksi
	(46 MPa)
Finish Layer: Resin paint	

The mortar joints were not flush with the concrete surface in either wall Figure 9.4. This unevenness of the repair surface was allowed to remain. In the repair, wall surfaces were cleaned and a wetting coat of epoxy applied with a roller. With the resin still wet, precut Tow Sheet pieces 20 ft x 20 in. wide (6.1 m x 508 mm) were positioned onto the wet surface, pressed in place and a second coating of resin applied. Full impregnation was achieved by working the resin into the sheet Figure 9.5.

9.9   Selection of Locations for Pull-off Testing

To provide a rational basis for selecting locations for destructive testing, the two CFRP repaired walls were carefully evaluated using non-destructive methods. Initially simple methods such as visual inspection, touch and tap tests were used. These were subsequently complemented by thermal imaging7 in which both passive and active systems were used. In passive methods, no external heat is applied prior to thermal imaging. In active methods, the surface is heated and an image showing heat diffusion/dissipation taken immediately thereafter. Regions where bond was poor were identified as "hot spots" indicating that because of voids, entrapped air, or de-bonding, heat could not be conducted away from the CFRP material.

Preliminary non-destructive assessments were first made by (Ross, 2013). Destructive tests were however deferred until later when more elaborate non-destructive evaluations were completed. Predictions of bond degredations from the latter effort were used to establish locations for the destructive pull-off tests.

9.10   Environmental Exposure

Data from the nearest weather station showed that the maximum ambient temperature over the period 1995 to 2016 was 99F (37.2C) and the minimum, 25F (-3.9C), NOAA GHCN 2016. (Ross, 2013) Reported that the average annual rainfall was 34 in. (0.86 m) and the average annual humidity 87%.

To assess the validity of the weather station data, (Ross, 2013) used 25 thermocouples to monitor ambient temperature and the spatial variation in surface temperature in CFRP and masonry. Initially only one face of the wall was instrumented; later both faces were instrumented but it was found that there was little difference in temperature between the two surfaces.

Figure 9.5 CFRP installation on epoxy wetted surface

Sixteen thermocouples were attached to the CFRP surface, eight to the masonry. The last thermocouple #25 was used to monitor ambient conditions. According to the equipment, temperature measurements were accurate to 0.06% of the recorded value. This corresponds to ±0.04F at 60F (±0.02F at 15.6C) and ±0.06F at 100F (±0.03C at 37.7C). Temperature was recorded at 15 minute intervals over two separate time frames in April and August 2012. Comparisons of temperature data taken at the site with that from the weather station were found in close agreement.

9.10.1 Spatial Variation in Wall Temperature

The surface temperature of CFRP and concrete masonry were expected to differ from the ambient temperature because of their differing emissivity. Temperature readings recorded using thermocouples are displayed in Figure 9.6.

This shows the variation in maximum, minimum and mean temperature over one week from March 31 to April 7, 2012. Thermocouples #1-16 identify locations on the CFRP surface and #17-24 the locations on the bare masonry. Thermocouple #25 recorded ambient conditions and its data are presented outside the wall outline in Figure 9.6.

Inspection of Figure 9.6 shows that the maximum CFRP temperature could be more than 10F (5.5C) higher than The ambient temperature (compare ambient thermocouple reading with that of thermocouple #8). Temperature readings were generally higher for CFRP and temperatures typically increased from left to right. This difference was a measure of the amount of sunlight falling on the CFRP. Thus, spatial distribution of damage caused by differing solar radiation exposure was recognized to be an important variable.

Figure 9.6 shows an infrared thermograph superimposed over a perspective sketch of Wall 2 which shows the temperature variation caused by solar heating (blue cold; white hot). The filled cells at mid-day (12:00pm) when the image was taken lagged the diurnal warming trends due to the increased grout mass. Also the cooler soil to the left provided a thermal sink which again slowed the diurnal effects.

■1	■2	■3	■4	■5	■6	■7	■8
Max: 99.5°F	Max: 100.2°F	Max: 100.1°F	Max: 100.9°F	Max: 98.0°F	Max: 103.1°F	Max: 103.4°F	Max: 102.5°F
Min: 62.5° F	Min: 61.3° F	Min: 61.2° F	Min: 61.2° F	Min: 62.4° F	Min: 59.6° F	Min: 59.5° F	Min: 59.1° F
Mean: 79.4°F	Mean: 79.2°F	Mean: 79.3°F	Mean: 79.5°F	Mean: 79.5°F	Mean: 79.2°F	Mean: 79.2°F	Mean: 79.1°F
■9	■10	■11	■12	■13	■14	■15	■16
Max: 99.7°F	Max: 99.5°F	Max: 100.2°F	Max: 100.4°F	Max: 97.2°F	Max: 102.3°F	Max: 102.6°F	Max: 102.8°F
Min: 62.9° F	Min: 61.8° F	Min: 61.5° F	Min: 61.7° F	Min: 62.8° F	Min: 60.4° F	Min: 59.9° F	Min: 59.6° F
Mean: 79.3°F	Mean: 78.9°F	Mean: 79.2°F	Mean: 79.4°F	Mean: 79.3°F	Mean: 79.0°F	Mean: 79.1°F	Mean: 79.1°F
■17	■18	■19	■20	■21	■22	■23	■24
Max: 96.0°F	Max: 94.7°F	Max: 90.8°F	Max: 98.0°F	Max: 96.8°F	Max: 100.9°F	Max: 100.9°F	Max: 102.0°F
Min: 63.8° F	Min: 63.2° F	Min: 63.3° F	Min: 62.2° F	Min: 63.5° F	Min: 61.0° F	Min: 60.5° F	Min: 60.0° F
Mean: 78.2°F	Mean: 77.4°F	Mean: 77.3°F	Mean: 78.1°F	Mean: 78.9°F	Mean: 78.4°F	Mean: 78.2°F	Mean: 78.4°F

■ **25 Ambient Temperature,** *Max: 90.8°F, Min: 63.3°F, Mean: 74.8°F*
■ **Thermocouple**

(a).Summary temperature data for wall 2 north side – 3/31/12 to 4/7/12
Figure 9.6 Temperature data and infrared image.
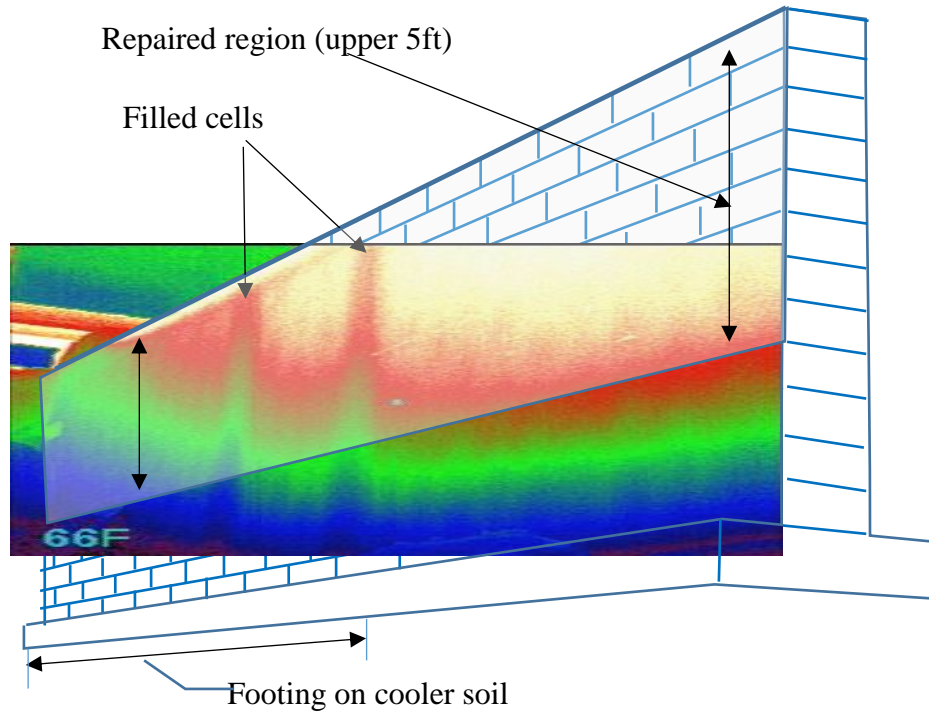
(b) - Infrared image of Wall 2 showing warmer temperatures near the sun-exposed corner

Figure 9.6 (Continued)

9.11 Test Program

The assessment of the long term performance of the CFRP-CMU bond necessitated: (1) the non-destructive evaluation of the two strengthened walls, (2) destructive pull-off testing to establish the baseline strength of concrete masonry and its mortar joints (bed, head, intersecting), and (3) destructive pull-off testing to characterize CFRP-CMU bond over masonry surface and across mortar joints. Locations selected for destructive testing were based on findings from the non-destructive evaluation.

9.11.1 Non-Destructive Evaluation

As noted, the repaired portions of the walls were readily accessible and preliminary non-destructive evaluation consisted of visual inspection, tap and tactile tests, complemented by thermal imaging. The intent was to identify potentially problematic regions for destructive testing.

For visual inspection, The CFRP surfaces on the two walls were examined to identify changes in color, cracking, debonding, voids or any unusual signs that signified degradation. This involved a side-by-side photographic comparison from their initial state using images taken at the time of the original CFRP installation (Figure 9.5). A portable microscope was used to obtain magnified images of problem areas.

Discoloration of the CFRP was noticeable though there was minimal deterioration at the mortar joints. Sunlight was believed to be the likely cause of the discoloration. Close-up photos of these regions at 60 and 160 magnifications provided conclusive evidence of a disintegrating top epoxy coating that revealed the underlying carbon fiber (Figure 9.7). These locations correlated well with the spatial temperature variation shown in Figure 9.6 As a result, the destructive pull-off tests were targeted for shaded and sunny regions on the CFRP surface to allow quantification of the difference, if any, in residual bond.

Figure 9.7 Comparison of images for wall 2 and wall 3.
At installation and after exposure

Tap tests were conducted using a small hammer. A hollow sound identified de-bonded regions. Some de-bonding was detected along the mortar joint. Surface irregularities were also noticed and voids could be detected by depressing the surface by hand. Thermal imaging: Active Infrared Thermography (AIT) methods employ heat to identify de-bonded locations. In general a heat source is used to apply heat to a surface. Changes in the measured surface temperature indicate changes in diffusion/conduction rates and identify possible regions of concern. Passive Infrared Thermography (PIT) uses the same basic principles but instead the naturally occurring changes in surface temperature from diurnal temperature changes provide the heat energy source. While

Figure 9.6 (taken with a FLIR model Tau 320 camera) shows some faint warmer stripes that coincided with the presence of mortar joints, PIT is highly affected by the time of day or the past air temperature changes and is therefore less controllable / reliable. Figure 9.9 shows the passive thermograph at 8:00am where no issues where identified.

Sun (60x magnification)   Sun (160x magnification)
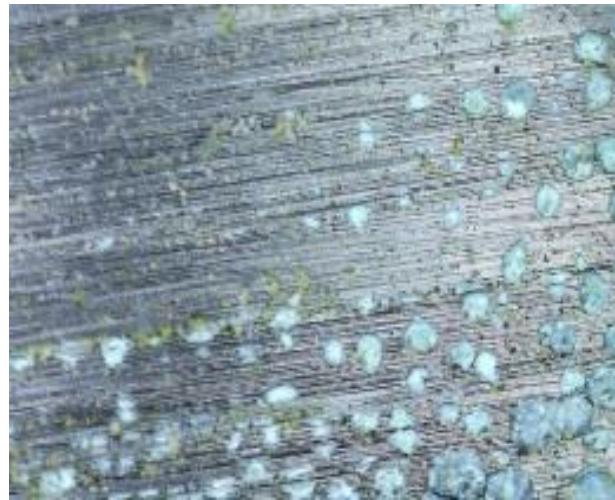
Shade (60x magnification)   Shade (160x magnification)

Figure 9.8 Microscope photos.
(top) sun exposure (disintegrating coating) and shade (coating intact)

AIT was performed immediately following PIT using the step heating method where a 350 watt lamp was placed within 2-3 in. (5-7.5 cm) from the wall surface and two infrared cameras

were used to capture the thermal images: FLIR model Tau 320 and Seek compact thermal imager. Hot spots were detected along some mortar joints as shown in Figure 9.9. This correlated well with the tap test findings and indicated the presence of voids.
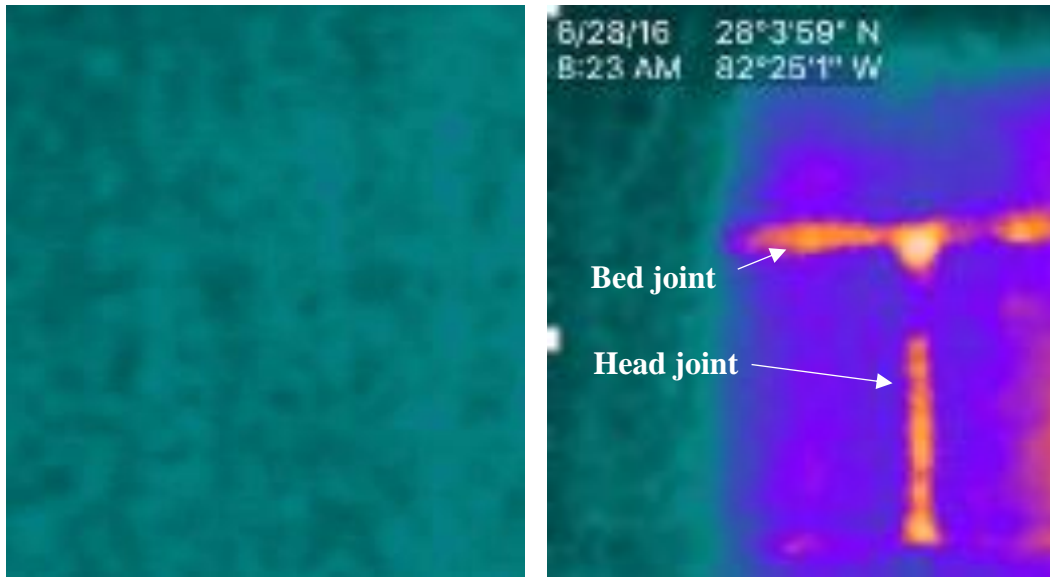
Figure 9.9 (a) Passive thermal image, left (b) active thermal image, right

9.11.2 Destructive Testing

To quantify bond, pull-off tests were conducted on the block surface and also across bed, head and intersecting joints in both the exposed CMU and the CFRP strengthened wall areas. All testing was conducted in accordance with ASTM D 7522 using a 1.25 in. (3.17 cm) circular dolly. Fast setting epoxy (3M Scotch-Weld DP-420) was used and bonded dollies were kept in place using duct tape. A total of 119 pull-off tests were conducted, 21 were on the bare CMU wall and 98 on the CFRP strengthened regions.

9.12 CMU Wall

A summary of the results of the 21 pull-off tests is given in Table 9.2. Individual results are plotted in Figure 9.10. There is variation in the values depending on whether aggregates were

engaged or not. Values were higher when aggregates were part of the substrate that stuck to the dolly. This increased contribution of exposed aggregates is recognized in ACI 503.5R-92. Failure modes are collectively discussed later after all results have been presented.

Table 9.2 Results of pull-off tests on CMU wall face and mortar joints

Description	Face	Bed Joints	Head Joints	Intersecting
# of Tests	6	5	5	5
psi	234	167	107	115
MPa	1.6	1.15	0.7	0.8

9.12.1 CMU Wall Face

The average pull-off strength from the six tests on the wall face was 234 psi (1.61 MPa) even though the unit strength of the masonry block was 1900 psi (13 MPa). This average exceeded the 200 psi (1.37 MPa) minimum tensile strength requirement for 2500 psi (17 MPa) concrete specified in ACI 440.2R-08.
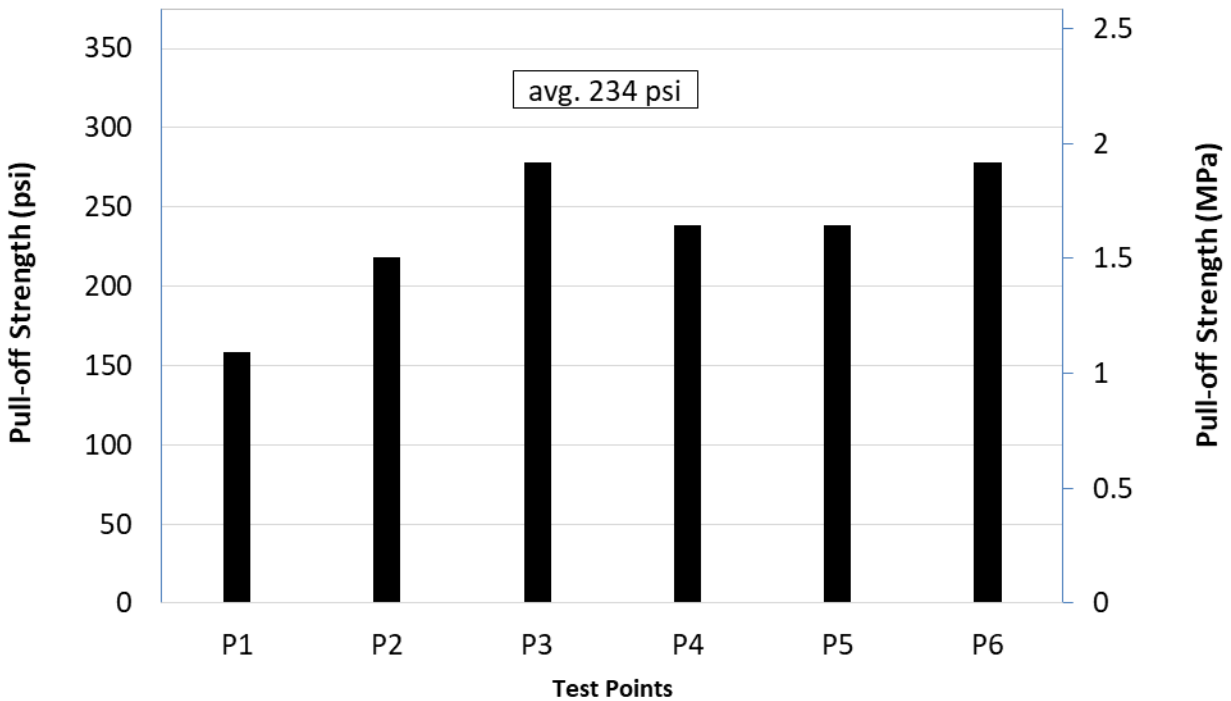
Figure 9.10 CMU surface pull-off strength

9.12.2 CMU Mortar Joints

Individual results and average values from the pull-off tests on mortar joints are shown in Figure 9.11. The average strength was highest for bed joints, 167 psi (1.15 MPa) and lowest for head joints, 107 psi (0.7 MPa). Intersecting joint values were in-between, 115 psi (0.8 MPa). Since a mortar joint is only 3/8 in. (0.95 cm) wide and the dolly diameter 1.25 in. (31.7 mm) diameter, the dolly was partially adhered to the surrounding block surfaces. Therefore the results do not purely reflect tensile strength of the mortar joint. Nonetheless, the distinctly higher value for bed joints compared to head joints suggest that the weight of the blocks supported by the bed joint may have contributed to its increased strength.
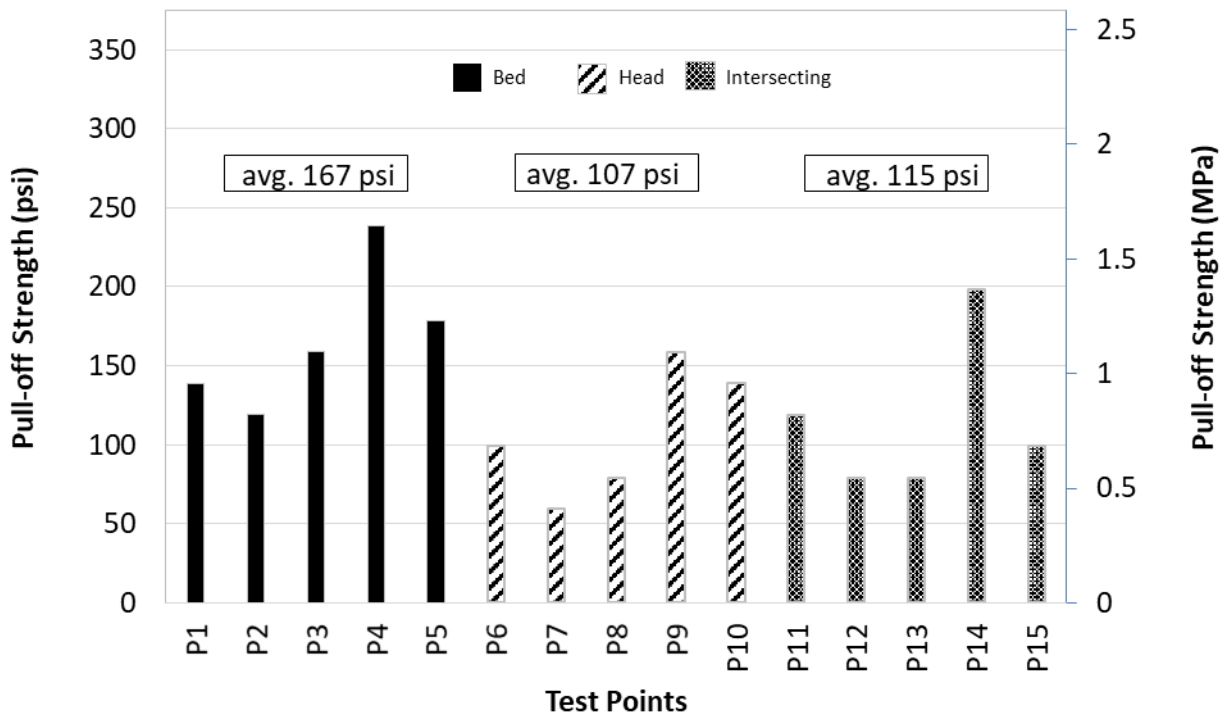
Figure 9.11 Pull-off strength at mortar joints in CMU wall

9.13 CFRP Strengthened Wall

A total of 98 pull-off tests were conducted to assess the CFRP-CMU bond of the two walls. The intent was to conduct an identical number of tests in each wall. However, because of unforeseen factors, e.g. incorrect dolly installation, the number of tests differed. A total of 54 tests were conducted on Wall 2 and 44 on Wall 3.

A general layout of the locations of the dollies is shown in Figure 9.12. An overview of all the results is summarized in Table 9.3 through Table 9.6. Individual results from the five series of tests on the wall face (center and corner of the CMUs), bed joints, head joints and intersecting joints are plotted in Figure 9.13 through Figure 9.17.

Since CFRP surfaces became less protected over part of the repair through the loss of the top resin coating Figure 9.8, tests were further sub-divided between regions that had greater

exposure to sun and those that did not (shade). Of the 54 tests conducted on Wall 2, 24 were in the shade and 30 in the sun. The corresponding numbers for Wall 3 were 18 (shade) and 26 (sun) for the 44 tests. These include tests conducted at the center of the blocks, at the corners and across the bed, head, and intersecting joints.

Figure 9.12 Dolly layout out in wall 3 (tonen).
On CFRP surface, over bed, head and intersecting joints

Table 9.3 Summary of CFRP/CMU results at face (42)

Description	Wall 2 Henkel			Wall 3 Tonen		
	# of tests	psi	MPa	# of tests	psi	MPa
Shade- center	5	226	1.6	5	179	1.2
Shade- corner	6	215	1.5	5	175	1.2
Average	11	220	1.52	10	177	1.22
Substrate Failure	20			18		
	90.9%			90%		
Shade average psi (MPa)	199 (1.37)					
Sun-center	6	152	1	5	151	1
Sun-corner	5	171	1.2	5	147	1
Average	11	161	1.11	10	149	1.03
Sun average psi (MPa)	155 (1.07)					
Overall average psi (MPa)	177 vs 234 (CMU) (1.2) (1.6)					

Table 9.4 Summary of CFRP/CMU results at bed joints (18)

Description	Wall 2 Henkel			Wall 3 Tonen		
	# of tests	psi	MPa	# of tests	psi	MPa
Shade	2	179	1.5	-	-	-
Sun	8	138	0.95	8	165	0.95
Average	10	146	1	8	165	0.95
Overall average psi (MPa)	154 vs 167 (CMU) (1.1) (1.15)					

Table 9.5 Summary of CFRP/CMU results at head joints (22)

Description	Wall 2 Henkel			Wall 3 Tonen		
	# of tests	psi	MPa	# of tests	psi	MPa
Shade	6	139	0.95	5	131	0.9
Sun	7	113	0.8	4	136	0.9
Average	13	125	0.9	9	133	0.92
Overall average psi (MPa)	129 vs 107 (CMU) (0.9) (0.7)					

Table 9.6 Summary of CFRP/CMU results at intersecting joints (16)

Description	Wall 2 Henkel			Wall 3 Tonen		
	# of tests	psi	MPa	# of tests	psi	MPa
Shade	5	91	0.63	3	99	0.7
Sun	4	97	0.67	4	102	0.7
Average	9	94	0.65	7	101	0.7
Overall average psi (MPa)	97 vs 115 CMU (0.7) (0.8)					

9.13.1 Results for CFRP-CMU Surface

To assess whether the location of a pull-off test on a concrete block had any influence, tests were conducted at the middle of blocks and near corners in close proximity but not touching the mortar joints. A total of 22 tests were carried out on Wall 2 and 20 tests on Wall 3 (Table 9.3).

Half of the tests were conducted at shaded locations and half at sunny locations. The results of the tests are summarized in Figure 9.13 (center) and Figure 9.14 (corner). Over 90% (38/42) were cohesive failures in the concrete substrate addressed later; the performance of both epoxies was comparable.

Inspection of Figure 9.13 Figure 9.14 shows that pull-off values were generally higher in the shaded region (shown in black) in both walls. (Table 9.3) provides average values. For Wall 2 they were 220 psi (1.52 MPa) in the shade and 161 psi (1.11MPa) in the sun. The corresponding values for Wall 3 were 177 psi (1.22 MPa) in the shade and 149 psi (1.03 MPa) in the sun. The marked difference in the pull-off strength between shaded and sunny locations reflects the effect of damage caused by the sun that led to a disintegration of the protective epoxy coating (Figure 9.8).
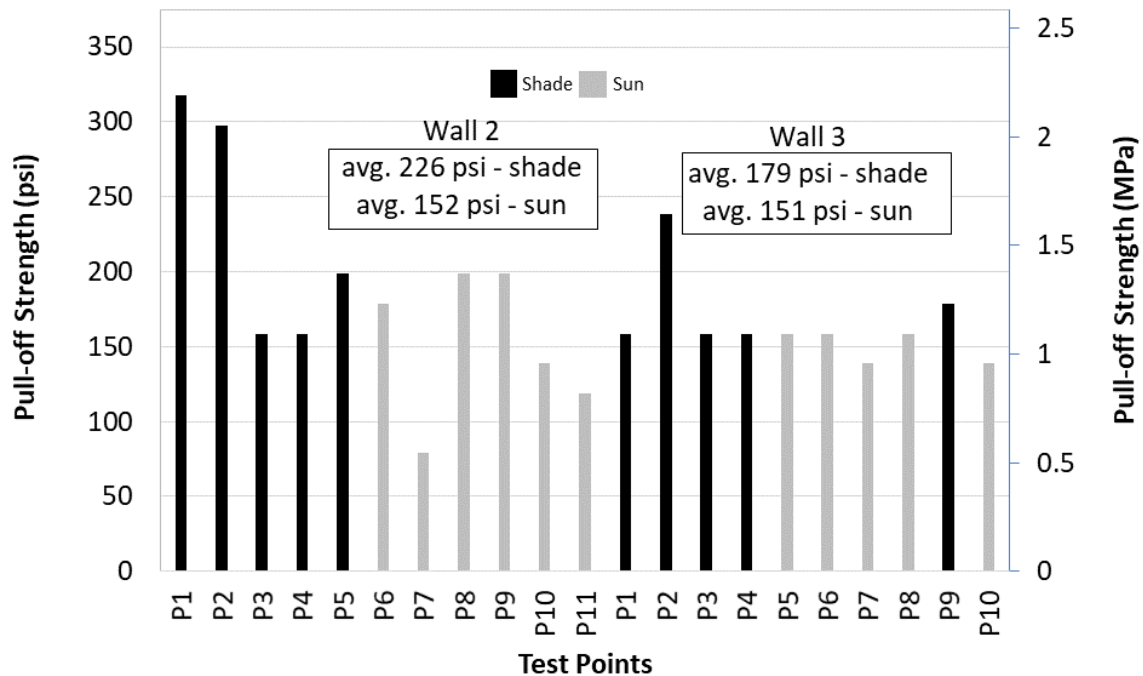
Figure 9.13 Pull-off strength at CFRP-CMU face-center
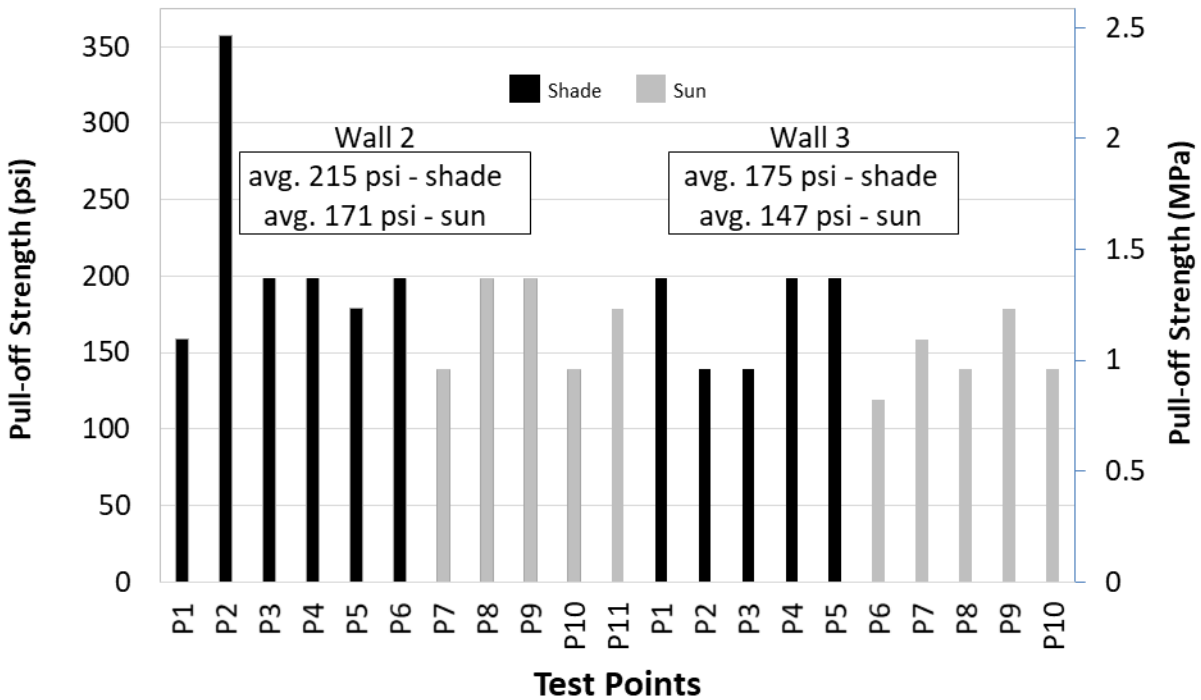
Figure 9.14 Pull-off strength at CFRP-CMU face-corner

9.13.2 CFRP-CMU Mortar Joints

A total of 56 tests (32 in Wall 2 and 24 in Wall 3) were conducted at bed, head and intersecting joint locations in the CFRP strengthened walls Table 9.4 through Table 9.6. The largest number of tests was conducted across head joints (22) followed by bed joints (18). Typically, low values correspond to the measured strength at debond locations.

9.13.3 CFRP-CMU Bed Joints

Figure 9.15 shows the results for tests across bed joint locations in Walls 2 and 3. The majority of the tests were conducted at sunny locations based on the findings of the non-destructive evaluation. Average values for shaded and sunny regions are shown in the same plot. The overall average value from all 18 tests for CFRP was 154 psi (1.1 MPa), somewhat smaller than the 167 psi (1.15MPa) value for CMU (Table 9.4).
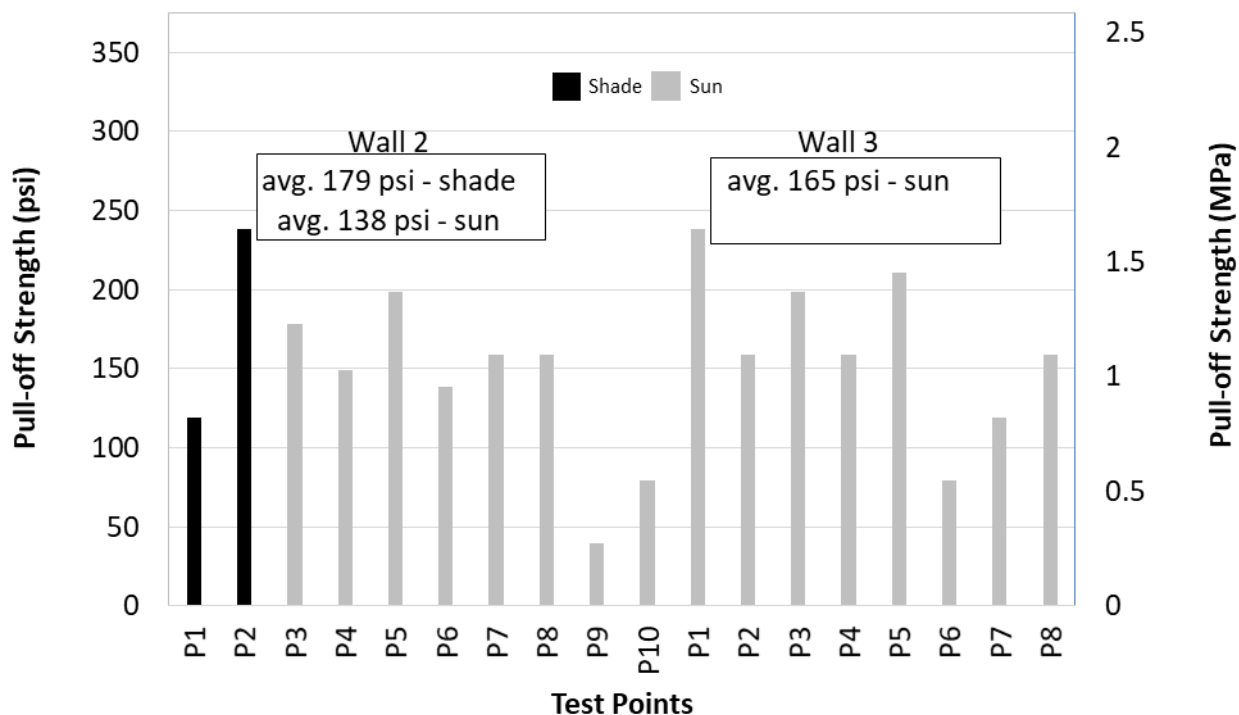
Figure 9.15 Pull-off strength at CFRP-CMU bed-joints

9.13.4 CFRP-CMU Head Joints

Figure 9.16 shows a plot of the results for head joint locations in Walls 2 and 3. An overall summary of the results is presented in Table 9.5. The average pull-off values from 22 tests was 129 psi (0.9MPa). This was higher than the 107 psi (0.7MPa) value for masonry but lower than that for the bed joints (154 psi (1.1MPa) in Table 9.4. The results for shaded and sunny locations were mixed. It may be seen from Figure 9.16 that values were lower at sunny locations in Wall 2 (113 psi (0.8 MPa) vs 139 psi (1 MPa in the shade) but higher for Wall 3 (136 psi (0.93 MPa) in sun vs 131 psi (0.89 MPa) in the shade). The values were considerably higher than the average 107 psi (0.74 MPa) recorded for the masonry wall Table 9.2.
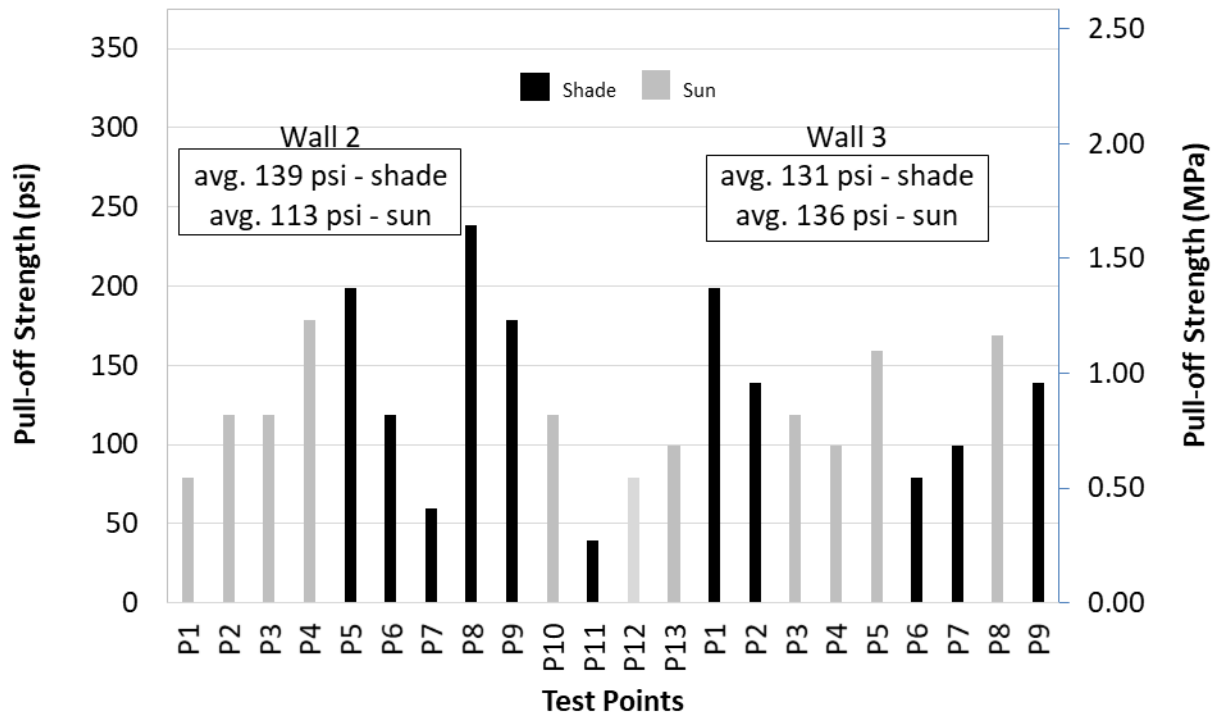
Figure 9.16 Pull-off strength at CFRP-CMU head-joints

9.13.5 CFRP-CMU Intersecting Joints

Figure 9.17 plots the individual results for tests conducted at the intersecting joint locations for the CFRP strengthened Walls 2 and 3. Table 9.6 provides a summary of the results. The pull-off strength of intersecting joints was lower than that for the bed and head joints. The overall average pull-off value from 16 tests was 97 psi (0.7 MPa) a little lower than the 115 psi (0.8 MPa) CMU value. As for head joints, there was no marked difference in bond values in the shade and in the sun.

9.13.6 Comparison of Failure Modes

Figure 9.18 provides side-by-side images of the failure modes in the bare masonry and CFRP from the four different locations that were tested (i.e. wall surface and bed, head and intersecting joints). For each series, two representative photographs corresponding to high and low

89

bond values are shown. As noted earlier Table 9.3, failure modes on the CMU surface were pre-dominantly cohesive. Of 42 tests, 38 failed in the concrete substrate.
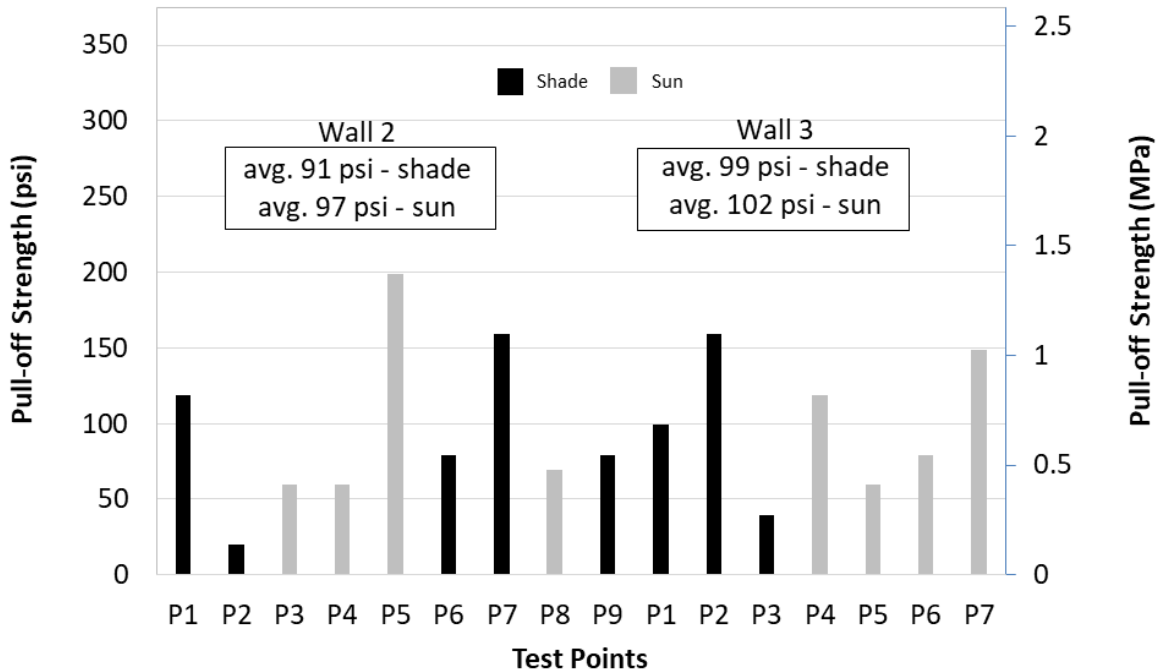
Figure 9.17 Pull-off strength at CFRP-CMU intersecting-joints

Inspection of Figure 9.18 shows that the CFRP bond values at mortar joints were comparable to those on the block face of the masonry. This was most likely because the mortar joints were not flush with the wall (Figure 9.4) and therefore the bond values provided a measure of the area that was in contact with wall face, e.g. for a 1.25 in. (3.18 cm) dolly with a 3/8 in (9.5 mm) bed joint at its center, the area in contact is approximately 60% of the dolly area. In contrast, the contact area for CFRP was the entire dolly area. Low values at CFRP joints indicated that they were measured at debond locations. Variability reflected the geometric positioning of the joint relative to the dolly.
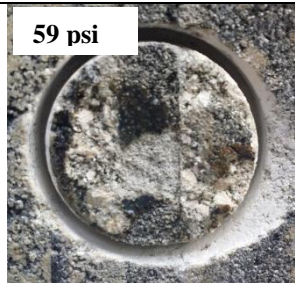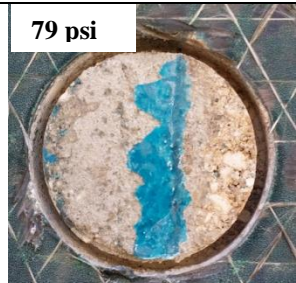
CMU		CFRP	
High	**Low**	**High**	**Low**
Surface			
277 psi	158 psi	198 psi	119 psi
Values higher when aggregates were engaged in the failure plane			
Bed Joint			
238 psi	158 psi	238 psi	79 psi
CMU bed joint values comparable to those at wall face. CFRP values lower when debonded			
Head Joint			
100 psi	59 psi	169 psi	79 psi
Head joint values lower than bed joints for both CMU and CFRP			
Intersecting Joint			
119 psi	79 psi	159 psi	39 psi
Values least at intersecting joints			

Figure 9.18 Comparison of CMU and CFRP failure modes

9.14 Discussion

Non-destructive evaluation played a critical role in defining the scope of the destructive testing. Visual inspection showed that the top resin coating had disintegrated more in areas having prolonged exposure to sunlight Figure 9.8. Thermocouple readings provided information on the spatial variation in temperature across the CFRP region Figure 9.6. This indicated that the temperature on the surface of the carbon repair could be more than 10F (5.5C) higher than the ambient temperature. The spatial distribution of the destructive tests Figure 9.12 was influenced by this finding. Despite the loss of the top coat, the CFRP material remained well bonded to the masonry. The average bond value from 42 tests was 177 psi (1.2 MPa, Table 9.3).

Unlike concrete, masonry is characterized by well-defined planes of weakness along horizontal and vertical mortar joints. Since these joints were not flush with the block surface, (Figure 9.4), the expectation was that these locations would yield lower bond values. This was largely borne out by the test results (Table 9.2 and Table 9.4 through Table 9.6).

The results showed that bond values were consistently higher in tests conducted across the bed joints compared to those across head and intersecting joints. The consolidating effect of the weight of wall above the bed joint may have contributed to a higher strength.

To assess the impact of poorer bond across the mortar joint it is instructive to calculate the development length of CFRP, ACI 440.7R-10,. Using material properties provided by the manufacturer ((Hartley, 1995), the development length of the CFRP is:

$$\ell_d = \sqrt{\frac{E_f t_f}{50(0.1)f_m'}} = \sqrt{\frac{(33,000,000)(0.00433)}{50(0.1)(1500)}} = 4.36 in \ (110.7 mm) \tag{1}$$

where,

l_d = development length

E_f = FRP modulus of elasticity

t_f = FRP thickness

f'_m = masonry compressive strength

The development length is 4.36 in. (110.7 mm) and is small compared to the 8 in. (200 mm) half-block width. Since mortar joints are only 3/8 in (9.5 mm) wide, the lower bond strength will not affect load transfer as long as the CFRP material remains bonded to the concrete block face. This was found to be the case from testing (Figure 9.13 and Figure 9.14).

ACI 440.2R-08 requires the minimum compressive strength of concrete to be 2500 psi (17.2 MPa). This corresponds to the minimum strength permitted in structural applications in ACI 318. Since structural masonry applications require the use of type S mortar, the same principle could also be used to set a corresponding lower limit in masonry for consistency. Similarly, the ACI code sets a limit of 200 psi (1.37 MPa) for minimum tensile strength of concrete to ensure that loads could be transferred to the FRP. Given the well-defined planes of weakness such a requirement would be meaningless for masonry. Nonetheless, in tests, the 1900 psi (13.1 MPa) concrete masonry was found to have an average direct tensile strength of 234 psi (1.61 MPa) (Table 9.2, Figure 9.10 and Figure 9.11), higher than the 200 psi (1.37 MPa) ACI minimum.

The relatively high residual bond (177 psi (1.2 MPa in Table 9.3) after 20 years exposure to an aggressive environment is not surprising. Water is primarily responsible for bond degradation, (Dolan, et al., 2009), and its accumulation at the bond line results in degradation in the material properties of the epoxy and its interface with concrete. In vertical elements such as walls, water cannot collect but drains over the CFRP surface even though there were air gaps along the bond line. On the other hand, it was sunlight that led to degradation and measures should be and normally would be taken to periodically apply a protective coating to minimize damage from UV radiation.

9.15 Limitations

The intent of the original study was to explore the feasibility of CFRP to repair settlement damage and no attempt was made to establish a baseline bond strength. This was both good and bad: it provided unaltered wall specimens for this durability assessment, but did not provide exact quantification of the actual degradation in bond over time (values would be marginally lower and would reflect the lower concrete strength after 28 days versus after 20 years). However, 90% of the pull-off failure modes were cohesive where the masonry strength, not CFRP bond controlled (Table 9.3). Moreover, the CFRP material was not under load since the applied settlement and the vertical roof loads were removed after the testing was completed. Nonetheless, the results are very encouraging given that both epoxies performed equally well in an extreme environment for over 20 years.

9.16 Conclusions

This study provides findings on the performance of CFRP-CMU bond after 20 years exposure to an aggressive sub-tropical environment. Given the uniqueness of the test site considerable attention was paid to non-destructive evaluation prior to destructive testing. Detailed investigation by (Ross, 2013) was followed by additional studies conducted more recently. In these investigations, visual inspection and tap tests were complemented by active and passive thermal imaging coupled with microscopic investigation of the CFRP surface. Based on the findings, the following conclusions may be drawn:

1. Active thermal imaging accurately identified poor bond along the mortar joints (Figure 9.9), that was confirmed by pull-off testing. Visual inspection augmented by the use of a portable microscope was able to identify damage caused by disintegration of the top epoxy coat Figure 9.8.

94

2. The average pull-off tensile strength of the 1900 psi CMU block was 234 psi (1.61 MPa), Table 9.2. This suggests that the 200 psi (1.37 MPa) ACI requirement for sound substrate may also be valid for concrete masonry. But given the lower tensile strength of mortar joints such a limit may not be as meaningful.

3. Thermocouple data showed that ambient temperatures were lower than those on the masonry and CFRP surface. Since spatial wall temperature distribution was non-uniform Figure 9.6, destructive tests were conducted at shaded and sunny regions. Results showed that bond values were lower in sunnier regions on the wall face (Figure 9.13 and Figure 9.14). This effect was less pronounced at mortar joint locations (Table 9.4 through Table 9.6, Figure 9.15 through Figure 9.17).

4. The CFRP-CMU pull-off strength was generally lower at mortar joint locations (Figure 9.15 through Figure 9.17, Table 9.4 through Table 9.6). The exception was bed joints, where bond values were high (Figure 9.15). This may be because of the beneficial effect of the wall weight on mortar strength. Head joints (Figure 9.16) had a lower strength than bed joints. Intersecting joints were the weakest (Figure 9.17). Lower mortar joint strength is not expected to affect load transfer because of the good bond between CFRP and masonry face (Figure 9.13 and Figure 9.14) and the relatively small development length compared to the block width.

5. The performance of the two commercially available epoxy systems (Table 9.1) used in the repair was comparable (Table 9.3). However, the surface condition Figure 9.8 highlighted the importance of the periodic application of coatings on CFRP-repaired surfaces to protect them against the effect of solar radiation.

After over 20 years exposure to Florida's environment, the residual CFRP-CMU bond for the masonry face (Table 9.3) exceeded 150 psi (1.2 MPa). As water cannot accumulate in voids along mortar joints in vertical walls, moisture-induced strength reduction was minimal. Therefore, the findings may not be directly transferable to repairs on horizontal elements such as beams or slabs.

CHAPTER 10: FRP-CONCRETE BOND IN TIDAL WATERS

10.1 Note to Reader

This chapter has been accepted for publication in ASCE, Journal of Composites for Construction and is reproduced with permission from the publisher ASCE.

10.2 Abstract

The Friendship Trail Bridge linking St. Petersburg to Tampa FL was demolished in 2016. This was the site of thirteen FRP repairs of corroding reinforced concrete piles undertaken in three separate demonstration studies completed in 2003-04, 2006, and 2008. The repairs used carbon or glass fiber, wet layup or prepreg, and epoxy or polyurethane resins. Installation was by shrink wrap in the initial series and by pressure bagging in the next two. Residual FRP-concrete bond was evaluated in 2015-16 through 120 pull-off tests conducted on ten representative repaired piles. Results showed wide variation in the measured pull-off strength depending on the resin type, the number of FRP layers, the prevailing conditions at the time the epoxy was mixed and how it was placed. Ambient conditions at installation influenced bond in epoxy-based systems. The highest residual bond was recorded in epoxy-based repair on piles that were installed by pressure bagging in 2008.

10.3 Introduction

Corrosion of piles driven in tidal waters is a common problem in southeastern United States particularly in Florida with its long coastline and sub-tropical climate. Historically, repairs were conducted using conventional pile jackets but because they proved unsatisfactory.

Only "Lifejackets" incorporating cathodic protection are permitted nowadays. (Leng, 2000). Though effective, Lifejackets are a costly option, (Sen, et al., 2011)

Cost considerations made Florida more open to exploring alternate systems such as fiber-reinforced polymers (FRP) for corrosion repair of piles. To ensure rapid technology transfer, field applications were an integral part of the research. Three such demonstration projects were undertaken on corroding piles supporting the Friendship Trail Bridge, (Mullins, et al., 2004) (Mullins, et al., 2006) (Mullins, et al., 2007) (Sen, et al., 2007).

Its unexpected demolition provided a unique opportunity to evaluate in-situ FRP-concrete bond. In the initial phase, non-destructive evaluations were carried out. Subsequently, a total of 120 pull-off tests were conducted in 26 site visits spread over four months. This paper presents findings from the destructive pull-off tests.

10.4 Site Details

The 4.2 km (2.6 mile), 274 span Friendship Trail Bridge was completed in 1956 to connect Hillsborough and Pinellas counties. Following construction of a new bridge in 1997, it ceased to carry vehicular traffic and was used by pedestrians and cyclists. Tampa Bay's sub-tropical marine environment is very aggressive and provided an ideal site for evaluating the performance of FRP used for corrosion repair. The piles selected included unwrapped controls and FRP repaired piles in bents 99-101 and 103-104 on the Hillsborough side of the bridge. Individual piles are labeled A to F from north to south in Figure 10.1a. The test pile layout is shown in Figure 10.1b and details summarized in Table 10.1.
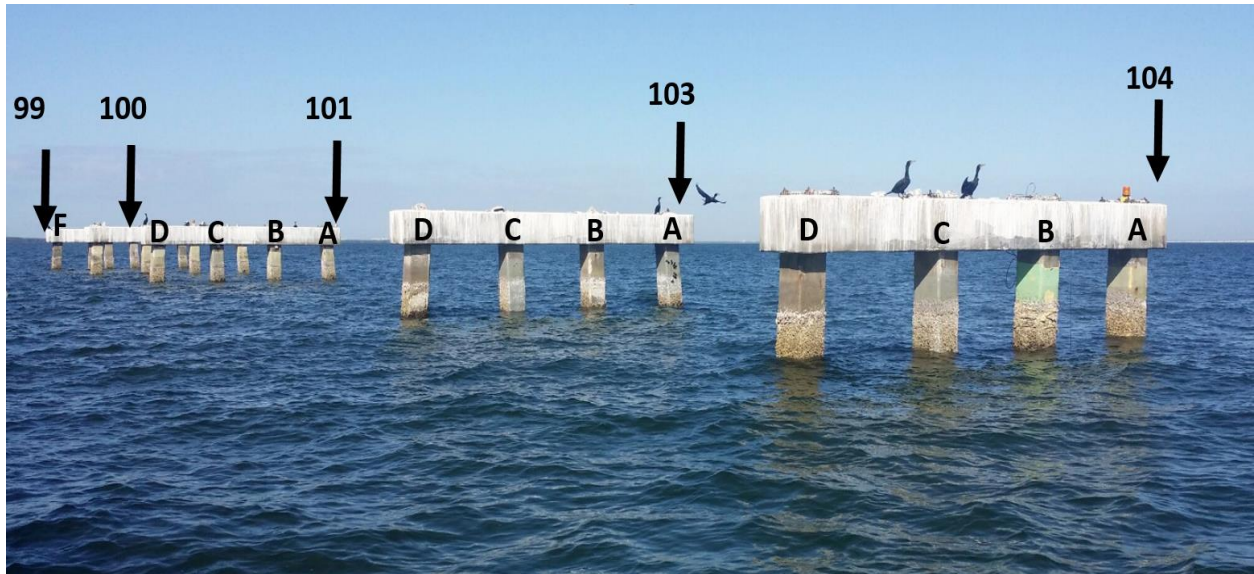
(a) Friendship Trail Bridge- view of pile bents evaluated during demolition

Bent-99 2003	Bent-100 2003	Bent-101 2004-06	Bent-103 2008	Bent-104 2008
A Control	A 3 Layers	A 6 Layers	A 2 Layers	A 4 Layers
B	B 3 Layers	B 2 Layers	B	B 2 Layers
C	C 6 Layers	C 2 Layers	C 2 Layers	C 2 Layers
D	D 6 Layers	D CP-Zn mesh	D Control	D CP-Control
E				
F				

N ↑
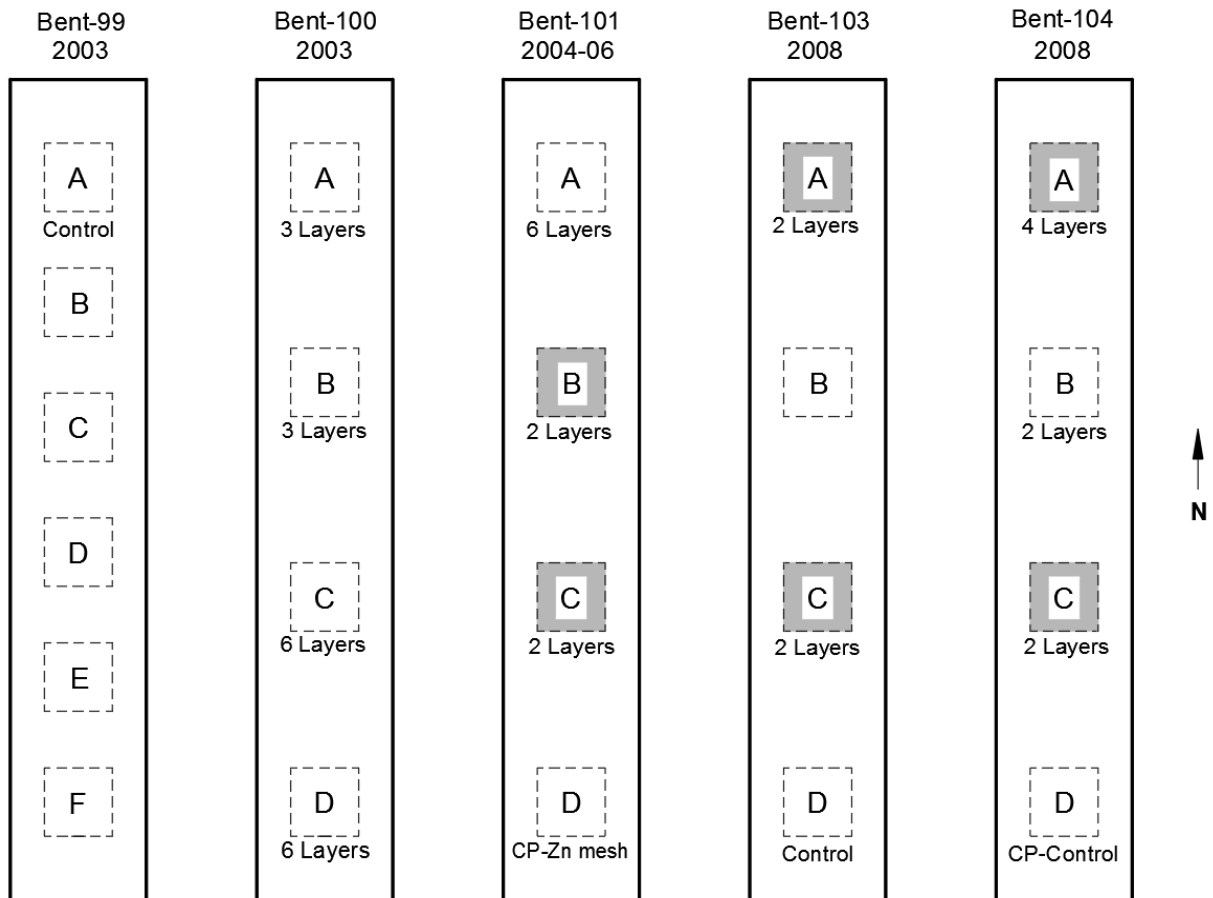
(b) Piles layout

All glass except 100A, B (carbon)
Highlighted piles (6) were pressure-bagged

Figure 10.1 View of pile bents and piles layout

A total of 13 piles - 11 glass and 2 carbon were repaired. The number of FRP layers used ranged from 2 to 6. The first repairs were carried out on piles supporting bents 100-101 in 2003-04. The second in 2006 used a pressure bagging system addressed later. The final repairs were completed in 2008 on piles supporting bents 103-104. These incorporated a sacrificial cathodic protection (CP) system within the FRP wrap.

Eleven piles were instrumented to monitor corrosion performance; six utilized an innovative pressure bagging system to enhance bond. Seven were repaired with polyurethane-based systems while the remainder utilized epoxy. The polyurethane resins are water-activated and pre-impregnated into the fibers. These were delivered to the site in hermetically-sealed pouches and installed over a surface primer. The epoxies were a Bisphenol-A resin combined with a proprietary curing amine and were applied to the concrete substrates. The primer for the polyurethane systems was also used as the UV coating.

Table 10.1 Repair summary

Bent	Pile [a]	Year of Installation	Wrap Layout [b]	Product Type	Fiber Material	Matrix Material	Bond Enhancement	Instrumentation (Pile Face)
100	100A	2003	1+2	Prepreg	Carbon	Polyurethane	-	East
	100B	2003	1+2	Prepreg	Carbon	Polyurethane	-	
	100C	2003	2+4	Prepreg	Glass	Polyurethane	-	
	100D	2003	2+4	Prepreg	Glass	Polyurethane	-	East
101	101A	2004	2+4	Two-part	Glass	Epoxy		East
	101B	2006	1+1	Prepreg	Glass	Polyurethane	Pressure bag	East
	101C	2006	1+1	Two-part	Glass	Epoxy	Pressure bag	East
	101D	2004	2+4	Two-part	Glass	Epoxy		East
103	103A	2008	1+1	Two-part	Glass	Epoxy	Pressure bag	West
	103C	2008	1+1	Two-part	Glass	Epoxy	Pressure bag	West
104	104A	2008	4+0	Prepreg	Glass	Polyurethane	Pressure bag	West
	104B	2008	0+2	Prepreg	Glass	Polyurethane		West
	104C	2008	1+1	Two-part	Glass	Epoxy	Pressure bag	West

[a] A – D designations denote pile position along pier from north to south.
[b] Indicates wrap layers in longitudinal + transverse directions.
Note: Piles 99A, 103D, 104D were controls.

10.5 Relevant Studies

The durability of FRP-concrete bond has been the focus of numerous laboratory and field investigations. Details on the performance of epoxy-based systems may be found in state-of-the-art reviews, e.g. (Myers, 2007) (Dolan, et al., 2009) (Sen, 2015) (Hamilton, et al., 2017). Fewer studies are available for polyurethane systems, e.g. (Bailey, et al., 2013).

Laboratory studies evaluate degradation in carefully prepared specimens. Specimens are usually prepared on flat rather than vertical surfaces so that gravity effects during cure are discounted. Environments are controlled, e.g. (Karbhari, 2009) reported a 26-61% reduction in pull-off strength after 24 month exposure to salt water solution at 22.8°C (73°F); (Dolan, et al., 2009) measured a 19-40% reduction after a 12 month exposure to salt water solution at 50°C (122°F). Since field installation and ambient conditions differ from that in laboratories it is not surprising that the failure modes in laboratory and field specimens differ as was observed by (Tatar, et al., 2016). This disparity can be expected to be greater for polyurethane resins that release carbon dioxide during cure. In laboratory studies, researchers applied rollers for ten minutes to prevent voids caused by gases trapped within the bond layer, (Haber, et al., 2012). This is not an option in field repair of partially submerged piles where void volume is significantly greater, (Walker, 2007).

Field data for marine applications are scarce. (Long, et al., 2012) evaluated a FRP-strengthened quay wall in Dunkerque Port, France installed using both prepreg and wet layup CFRP. After eight months, average residual bond from 40 pull-off tests varied between 1.86 and 2.74 MPa (269 and 397 psi). Other available studies in marine settings only utilize pull-off testing to verify installation and conduct long-term evaluations using non-destructive methods.

Excepting for studies conducted by the authors, e.g. (Sen, et al., 2007), field studies incorporating destructive evaluations are only for FRP applied to dry surfaces under dry conditions. Their findings are not applicable for this study where specialist resins designed for application on wet surfaces were used. Nonetheless, limited comparisons are presented to provide a measure of the variability in FRP field test data for columns.

10.6 Background

10.6.1 Chloride Content

Pull-off tests are conducted on the pile surface and therefore the chloride content at this location can impact results. Chloride measurements in the 75 mm (3 in.) concrete cover were undertaken for nine test piles Table 10.2. Chloride content was highest nearer the surface (0-25 mm or 0-1 in. layer) and closest to the pile cap. Their magnitude more than exceeded the 0.59-1.19 kg/cu. m (1-2 lb/cy) chloride threshold for concrete surrounding reinforcement (50-75 mm or 2-3 in.) indicating that the passive layer that protects steel in concrete was destroyed (Mindess, et al., 2003). These values were consistent with corrosion potential measurements that indicated a 95% probability of corrosion, (Mullins, et al., 2004) (Mullins, et al., 2006) (Sen, et al., 2010).

Table 10.2 Chloride profile in concrete cover

Pile	Location from underside of pile cap		0-25 mm 0-1 in.		25-50 mm 1-2 in.		50-75 mm 2-3 in.	
	mm	in.	kg/cu. m	lb/cy	kg/cu. m	lb/cy	kg/cu. m	lb/cy
99A	75	3	10.96	18.58	5.17	8.77	1.22	2.07
99A	533	21	8.70	14.74	4.56	7.73	2.62	4.44
103A	125	5	3.44	5.83	2.08	3.52	0.94	1.96
103B	125	5	4.57	7.74	2.78	4.71	1.42	2.4
103C	125	5	3.61	6.12	1.90	3.22	1.06	1.8
103D	125	5	3.16	5.35	2.55	4.32	1.71	2.89
104A	125	5	7.23	12.25	2.87	4.86	2.08	3.52
104B	125	5	6.00	10.18	2.70	4.57	1.64	2.78
104C	125	5	7.35	12.46	4.30	7.29	2.92	4.95
104D	125	5	5.72	9.69	4.01	6.79	3.60	6.10

10.6.2 Instrumentation and Cathodic Protection

Eleven wrapped piles were instrumented to monitor the efficacy of FRP corrosion repairs, (Suh, et al., 2008). (Aguilar, et al., 2010). Instrumentation varied; in the initial study, two embedded rebar probes were used to measure corrosion current, (Mullins, et al., 2004) Piles repaired in 2008 incorporated a sacrificial cathodic protection system within the FRP repair, (Aguilar, et al., 2009), (Sen, et al., 2010). This system was designed to provide 30 years of protection. It required eight embedded zinc anodes and a submerged bulk zinc anode. The performance of this system was monitored using two silver-silver chloride reference electrodes that measured the anodic current drawn from the embedded and submerged anodes.

Installation of instrumentation required holes to be drilled and grooves to be cut on the pile surface for the required wiring and junction boxes that were located on the accessible east and west faces. These were also the two faces where all destructive and non-destructive testing was carried out. The implication of disturbance to the bonding surface is addressed later.

10.6.3 FRP Wrap Design

The FRP wrap was designed to fully recover an assumed steel cross-section loss of 20% while simultaneously limiting transverse expansion caused by the formation of corrosion products. The epoxy system used unidirectional fibers in all repairs. Bidirectional fibers were used by the prepreg system in the transverse direction in 2003 and in both longitudinal and transverse directions in 2008. FRP properties used in the calculations are summarized in Table 10.3and Table 10.4, (Mullins, et al., 2004) (Mullins, et al., 2007), (Aguilar, et al., 2009). More layers were required for the lower strength of fibers used in the prepreg system Table 10.1.

103

Table 10.3 Properties of prepreg system

Fibers	Type	Tensile Strength (MPa)	(ksi)	Tensile Modulus (GPa)	(ksi)	Load / ply (kN/m)	(lb/in.)
Glass	Unidirectional	586	85	35.8	5,200	420.3	2,400
	Bidirectional	324	47	20.6	3,000	210.2	1,200
Carbon	Unidirectional	827	120	75.8	11,000	595.4	3,400
	Bidirectional	586	85	22.1	3,200	420.3	2,400

Table 10.4 Properties of epoxy-based system

Property	Value SI	USCS
Tensile strength	0.58 kN/mm	3.3 k/in.
Tensile modulus	20.89 GPa	3030 ksi
Ultimate elongation	2.2%	2.2 %
Laminate thickness	1.27 mm	0.05 in.
Dry fiber thickness	0.36 mm	0.014 in.

10.6.4 Pressure Bagging

In-situ bond measurement of piles repaired in 2003-04, showed that conventional installation practice of using shrink wrap during curing (Figure 10.2) led to significant bond variability, (Sen, et al., 2007). Laboratory studies indicated this variability could be lowered by using pressure or vacuum bagging to reduce voids while the epoxy cured, (Winters, et al., 2008), (Aguilar, et al., 2009). Pressure bagging involves the use of a pressurized cuff which surrounds and restrains the FRP wrap during curing. This configuration was found in a previous study to be a more effective tool for enhancing bond in piles than vacuum bagging since an airtight envelope is not required around the FRP. The effect of pressure on voids was also numerically modeled by (Grunenfelder, et al., 2010). In essence, uniform pressure increased interfacial frictional resistance in repairs of vertical elements that prevented the resin-saturated fabric from slipping. All USF pile repairs conducted after 2004 were pressure bagged.
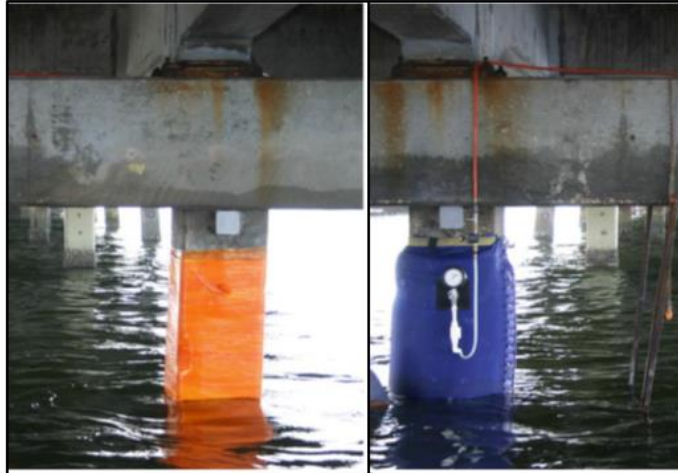
Figure 10.2 Shrink wrap (left); pressure bag (right)

10.7 Exposure

Since the wraps were installed at different times, ambient conditions differed. Temperatures varied from 12 °C (54 °F) to 30 °C (86 °F) and humidity from 69% to 83%. Heat indices ranged from 22 °C (72 °F) to 34 °C (94 °F). Where available the heat index, the combined effect of air temperature and humidity, is included in Table 10.5 the temperature range for all the piles is identical since both maximum and minimum temperatures were recorded the same year in 2010.

Table 10.5 Pile installation and service ambient conditions

| Installation Date | Piles | Conditions at Installation | | | | | Temp. Range, °C (°F) [b] |
		Temperature, °C [a]	Temperature, °F [a]	Rel. Humidity, % [a]	Heat Index, °C	Heat Index, °F	
10/30/2003	100A	25	77	69	28	82	-4-37 (25-98)
10/30/2003	100B	25	77	69	28	82	
10/30/2003	100C	25	77	69	28	82	
10/30/2003	100D	25	77	69	28	82	
s2/27/2004	101A	12	54	83	-	-	

105

Table 10.5 (Continued)

2/27/2004	101D	12	54	83	-	-	
9/26/2006	101B	29	85	65	34	94	
9/26/2006	101C	30	86	63	34	94	
7/30/2008	104B	28[c]	83[c]	71[c]	22	72	
12/17/2008	104A	23	74	76	-	-	
12/17/2008	104C	22	72	81	-	-	
12/18/2008	103A	24	75	71	-	-	
12/18/2008	103C	24	75	71	-	-	

[a] Indicates conditions at installation; [b] From installation date to April 2016 ; [c] Average for the day; Maximum relative humidity for all ranges was 100%; Temperature data from weather underground website (reference provided)

10.8 Objectives

The goal of the research project was to obtain new information on the FRP-concrete bond by evaluating residual FRP-concrete bond following exposure of up to 12 years. All testing was conducted at the accessible east and west faces of the wrap in dry and splash zones Figure 10.3. Since field inspectors evaluate bond through visual inspection and tap tests, all wrapped piles were similarly evaluated prior to destructive testing. The intent was to assess the reliability of such inspection methods. Given the diversity of the repairs in terms of systems, number of layers, adhesives, installation methods and ambient condition, the investigation sought to obtain answers to key questions. These include the role of surf and ambient conditions during installation, the relative performance of the epoxy and polyurethane adhesives, the effectiveness of pressure bagging, and the overall performance of repairs after over 7, 9 and 12 years of exposure.

Pile Cap

15.24 cm (6 in.)

Dry Zone

45.72 cm (18 in.)

111.76 cm (44 in.)
(Practical range
for testing)

▼ High Water
Line

167.64 cm (66 in.)
(Length of wrap)

Splash Zone

106.68 cm (42 in.)

Submerged
Zone

▼ Low Water
15.24 cm (6 in.) Line

Instrumented Pile

Pile Cap

Dry Zone

60.96 cm (24 in.)

111.76 cm (44 in.)
(Practical range
for testing)

▼ High Water
Line

182.88 cm (72 in.)
(Length of wrap)

Splash Zone

106.68 cm (42 in.)

Submerged
Zone

▼ Low Water
15.24 cm (6 in.) Line

Non-instrumented Pile

Figure 10.3 Definition of dry, splash and submerged zones

10.9 Bond Evaluation Program

Field testing was initiated after the contract for the demolition of the bridge had been awarded. As a result, there was a constant race against time to complete testing before the bridge was demolished. Unfortunately, conditions were not always favorable when the research team was ready and able. Despite 26 site visits, not all testing could be completed in time. Additional testing was therefore required after the bridge had been demolished and the test piles carefully moved on-shore. These are referred to as "land" tests.

10.9.1 Non-Destructive Evaluation

Non-destructive evaluation comprising acoustic sounding, visual inspection, and thermal imaging were completed in seven site visits. The role of this evaluation was to identify locations that were deemed to have either an apparent good (intact) or poor (debonded or delaminated) bond

for follow-up confirmation by destructive testing. In this paper, only selected results from visual inspection are discussed.

Marine growth over the FRP wrap was first removed with a hand scraper and each surface of the wrap photographed to identify occurrences of discoloration, debonding, peeling, and rust stains.

Cracking of the protective UV coating was observed in all piles. Junction boxes housing wiring for cathodic protection and instrumentation installed close to the underside of the pile caps and were found to be intact. The boxes at piles 100D and 101C were observed to have expelled corrosion residue downward and onto adjacent wrap material.

Figure 10.4 shows photos of three pressure bagged piles 101B, 101C, 103C and one non-pressure bagged pile 104B taken as part of the visual inspection study. The photo suggests that the residual bond would be higher for the pressure bagged piles installed in 2006 (101B, C) and 2008 (103C). In contrast, the only non-pressure bagged pile, 104B, installed in 2008 showed clear signs of distress in which patches of FRP material had already delaminated. It exhibited low interlaminar bond strength as strips could be easily detached from the pile face by hand. This repair used glass and a proprietary polyurethane resin and was not installed by the USF research team.

10.9.2 Destructive Evaluation

Pull-off testing was conducted in accordance with ASTM D7522, ASTM 2009. An Elcometer 106 adhesion tester with 31.7 mm (1.25 in.) diameter dollies was used. Locations for pull-off testing in the dry and splash zones (Figure 10.3) were, by default, randomized along areas where both well-bonded and delaminated/debonded states were indicated by NDE. However, constraints such as surface waviness, marine growth, dolly spacing, candidate locations relative to

the water surface / boat, and the use of a drilling rig limited the available areas for scoring. Tests were restricted to east and west pile face locations at heights accessible from a boat.

Figure 10.4 Photos of FRP repairs in piles.
(left to right) 101 B, 101C, 103C and 104B

The FRP surface was scored using a 31.7 mm (1.25 in.) diameter diamond core drill bit to an approximate depth of 6.35 mm (0.25 in.) into the concrete cover. The drill was attached to a custom-built leveling fixture Figure 10.5, which was temporarily attached to the pile. This configuration had been utilized in previous studies and allowed for vertical face drilling while ensuring levelness and uniformity of the scoring process, even in moderately choppy waters. The scored areas were then sanded with medium-grit sand paper and cleaned with acetone. Dollies were adhered to the prepared surfaces with 3M Scotch-Weld DP-420 epoxy adhesive, which has a maximum tensile strength of approximately 15.5 MPa (2,250 psi). The dollies were then taped to the surrounding wrap to prevent slippage during setting and allowed to cure for a minimum of 24 hrs Figure 10.6. Logistics led to their positioning along a circular arc. After the dollies were installed, a spirit level was used to verify that they were at right angles to the bonding surface (Figure 10.6 right) before testing.

Figure 10.5 FRP scoring for dolly attachment
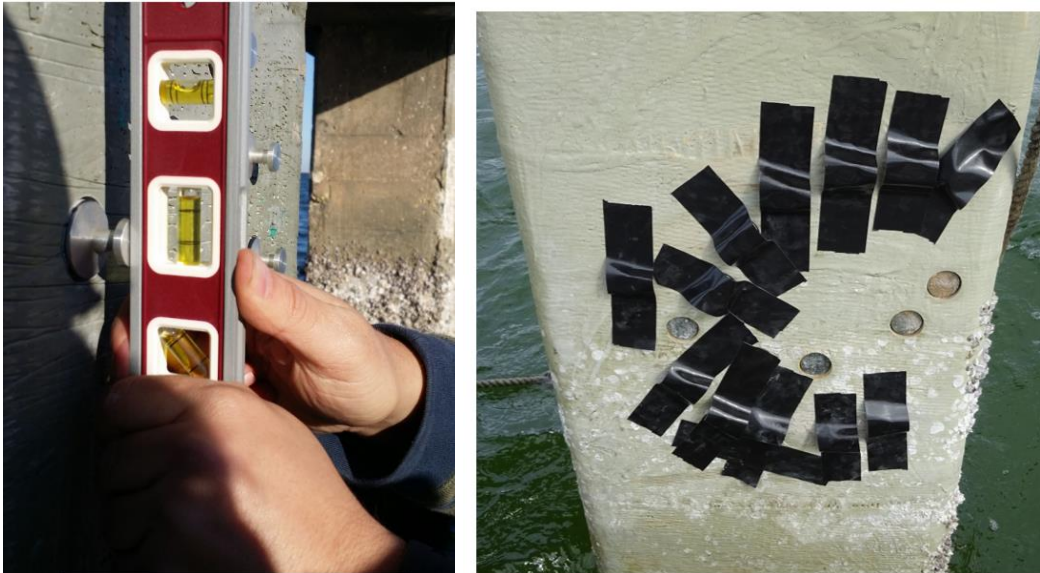
Figure 10.6 Taped dollies and check for correct alignment (right)

During scoring, several locations revealed delaminated conditions in which only 1-2 of the inner layers remained well-bonded to the substrate. To test these locations, dollies had to be re-designed and fabricated with the neck extended by 6.35 mm (0.25 in.) Figure 10.7. This provided sufficient height for the tester to properly engage the dolly head.
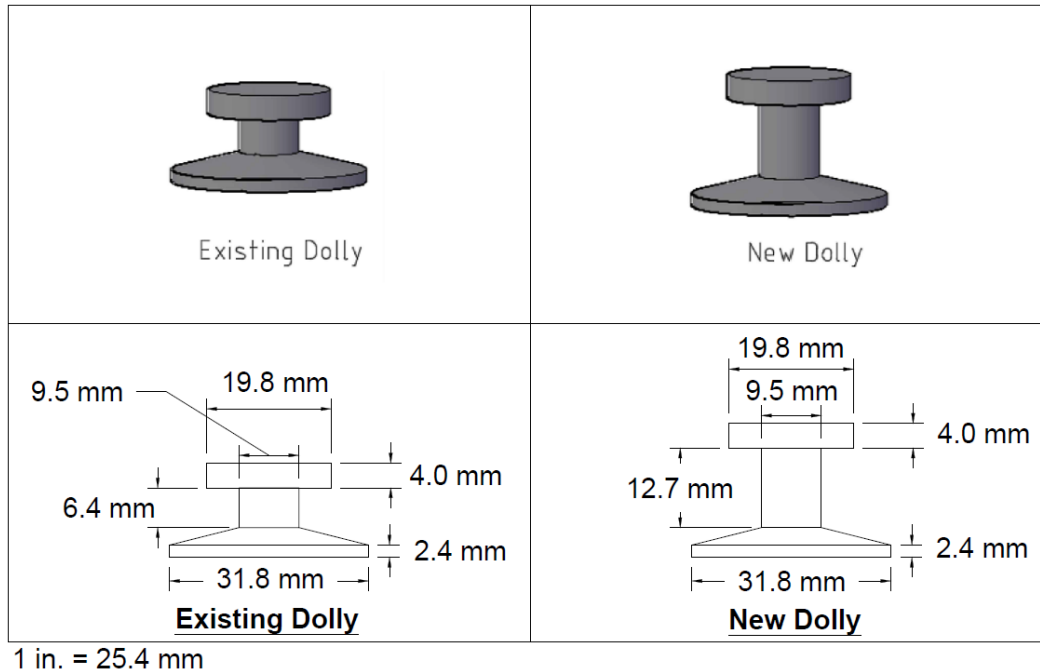
Figure 10.7 Dolly configurations

10.10 Pull-off Testing Results

A total of 16 piles – three controls and 13 wrapped (Figure 10.1b) – were available for testing. Of these, one control and 10 wrapped piles were tested to obtain representative results. Given logistic constraints, the test goal to obtain a minimum of five data points within the dry and splash zones was ambitious. As noted, because of the demolition schedule, not all the planned tests could be completed on site. Of the 120 tests, 76 were conducted on site and the remaining 44 conducted on land within two weeks of removal of the pile. These latter tests were carried out on sections of seven extracted piles (100A, 101A, 101B, 101C, 103A, 104A, 104B) that had been carefully removed by the contractor and moved offshore.

10.10.1 Overview

Table 10.6 is an overview of the results. It contains information on the pile, resin system, installation method, whether the test was carried out on site or on land, numbers of tests in the dry and splash zones (Figure 10.3), occurrence of inter-layer failure, and average bond values for

111

interlayer and interface failures. Of the 120 tests, 33 were on the piles wrapped in 2003-04, 40 on the piles wrapped in 2006 with the remaining 47 tests on piles wrapped in 2008. A required bond value will first be introduced to offer baseline comparisons with test results. The validity of the land site tests is then evaluated followed by a detailed description of the results summarized in Table 10.6.

10.10.2 Required Bond

ACI 440.2R-08 specifies a minimum 1.4 MPa (200 psi) bond. This was primarily set to ensure that the concrete material had sufficient strength to be repaired. However, the required bond for load transfer is lower because it must comply with fire resistance and debonding strain limits. In this study, FRP was required to make up for an assumed 20% steel cross-section loss. The following is based on measurements provided in Figure 10.3:

For a 508 mm x 508 mm (20 in x 20 in) concrete pile with a 75 mm (3 in.) cover reinforced by eight #8 bars uniformly distributed along its perimeter (3 per face), the tensile capacity required by the FRP can be approximated as 20% of the tensile force, T, in the outer steel. Using n as the number of bars, A_b as the cross-sectional area per bar, and f_y as the steel yield strength:

$$F_{Steel} = 20\%(T) = 20\%\left(nA_b f_y\right) \tag{1}$$

$$F_{Steel} = 0.2(3\ bars)(509.68\ mm^2/bar)(2.87\ MPa) = 126.5\ kN\ (28.44\ kips)$$

Since the effective depth for FRP is greater than that of the tensile steel, the tensile strength, F_{FRP}, required to generate the equivalent lost flexural capacity in the rebars, assuming a lever arm of 508 mm (20 in.), is approximated by:

$$F_{FRP} \approx F_{Steel}\left(\frac{d}{d_{FRP}}\right) \tag{2}$$

$$F_{FRP} \approx 126.5\ kN\left(\frac{431.8\ mm}{508\ mm}\right) = 107.5\ kN\ (24.1\ kips)$$

Dividing the force by the pile face width of 50.8 cm (20 in.) yields the force per unit width, $\overline{F_{FRP}}$, of 2.12 kN/cm (1.21 kips/in.). This requirement is satisfied by all installed systems. Assuming maximum metal loss is at 91.4 cm (3 ft) below the underside of the pile cap and using half of a 1.83 m (72 in.) longitudinal strip length, l_{bond}, the required bond can then be determined as:

$$\text{Req'd Bond} = \frac{\overline{F_{FRP}}}{l_{bond}} \tag{3}$$

$$\text{Req'd Bond} = \frac{2.12 \text{ kN/cm}}{(183 \text{ cm}/2)} = 0.23 \text{ MPa (33 psi)}$$

Values will be higher if the maximum steel loss occurred nearer to the pile cap because the available length is smaller. However, corrosion potential measurements suggested that corrosion was unlikely within 457 to 610 mm (1.5 to 2 ft.) of the pile cap, (Mullins, et al., 2004) (Mullins, et al., 2007) (Aguilar, et al., 2009).

Table 10.6 Breakdown of pull-off tests.

Repair Year	Pile	Installation	Site Test Dry	Site Test Splash	Land Tests Dry	Land Tests Splash	Total Data Points Dry	Total Data Points Splash	Total Interlayer failures Dry	Total Interlayer failures Splash	Pull-off test value MPa (psi), interlayer failure Average	Min.	Max.	Mean, Dry	Mean, Splash
Concrete	99A		-	-	4	6	**4**	**6**	-	-	-	1.1 (159)	2.6 (377)	2.25 (327)	1.63 (236)
2003	100A		4	1	1 (p5) [b]	4 (p2-p5)	**5**	**5**	2 (p3, p5)	1 (p2)	0.32 (46)	0	0.27 (40)	0.01 (13)	0.1 (20)
	100C		4	1	-	-	**4**	**1**	1 (p2)	1 (p1)	0.14 (20)	0.27 (40)	0.82 (119)	0.6 (93)	0.27 (40)
	100D		3	4	-	-	**3**	**4**	2 (p1-p2)	3 (p1-p3)	0.05 (8)	0.27 (40)	0.82 (119)	0.8 (119)	0.27 (40)
	101A		6	-	-	5 (p1-p5)	**6**	**5**	-	-	-	0	1.78 (258)	0.6 (87)	0.44 (64)
2006	101B	PB [a]	4	12	1 (p5)	5 (p13-p17)	**5**	**17**	-	5 (p1, p2, p4, p10, p13)	0.22 (32)	0	0.55 (79)	0.14 (20)	0.1 (20)
	101C	PB	8	5	5 (p9-p13)	-	**13**	**5**	1 (p1)	-	0	0	1.23 (179)	0.1 (20)	0.3 (44)
2008	103A	PB	4	3	-	5 (p4-p8)	**4**	**8**	-	-	-	0.21 (31)	1.47 (213)	1.32 (191)	0.56 (82)
	103C	PB	1	4	4 (p1-p4)	2 (p1-p2)	**5**	**6**	-	-	-	0.55 (79)	2.46 (357)	1.23 (179)	1.14 (165)
	104A	PB	4	3	5 (p5-p9)	5 (p4-p8)	**9**	**8**	4 (p1-p3, p7)	-	0.82 (119)	0	1.37 (198)	0.71 (103)	0.69 (100)
	104B		5	-	-	2	**5**	**2**	-	2	0.41 (60)	0	0	0	0
		Total (FRP)	**43**	**33**	**16**	**28**	**59**	**61**	**9**	**12**					
		Total	**43**	**33**	**20**	**34**	**63**	**67**							

Piles 100A to 100D, 101B, 104A, 104B used polyurethane; all others used epoxy

[a] PB = Pressure bagging

[b] Identities data point for a given pile referenced in Figure 10.9 through Figure 10.11

10.10.3 Validity of Land Site Results

All land site tests were carried out within two weeks of the extraction of the pile from water. It was possible that unknown factors may have influenced the behavior of the wrap systems during extraction, transport, and temporary storage that cannot be determined by a side-by-side comparison of site and land data sets.

If the on-land sample set were affected by unforeseen factors, the effects would present as statistical metrics which differ from those for the in-situ data. From this perspective the population means for the two data sets would need to be equal ($\mu_{land} = \mu_{site}$) for the on-land data to be used in the study. A t-test can provide a quantitative confidence level as to whether the difference between sample means is due to chance or not, (Walpole, et al., 2012).

Selecting the type of t-test is conditional on the number of data sets, sample size, inter-dependence, the possibility that a t-statistic could be found within one or both ends of a standardized t-distribution (one- or two-tail), and on an optional assumption that population variances for both sets are equal. Since the site / land comparison involves two independent data sets with differing sample sizes and without assuming the population variances are equal, the test of choice was Welch's two-tailed t-test. This test method is a variation of the popular student's t-test which is effective when working with sets of unequal variances and sample sizes. Here, the null hypothesis, H_0, is that the population means are equal.

Well-bonded data points – locations where bond exceeded the 0.23 MPa (33 psi) requirement – were used for each t-test with the exception of the sets for piles 100A, 101B, and 104B, which will be discussed. These data points represent the actual performance and degradation behavior of the bonded systems, which are in contrast to poor results – those not exceeding the bond transfer requirement - that may stem from a number of other influences (workmanship,

installation conditions, etc.). Before running the test, a normalization check was run for each data set to ensure robustness and applicability of the method, Ahad and Yahaya 2014. A confidence interval of 95% ($\alpha = 0.05$) was used for the tests. This interval states that there is a 95% chance that if the t-statistic lies between the negative and positive t-critical values, the population means of the two data sets are equal.

Table 10.7 Summary of two-sample t-tests, assuming unequal variances

Pile	Data Points (n)		Negative t-Critical (Two-Tail)	t-Statistic	Positive t-Critical (Two-Tail)	Result of Hypothesis Test
	In-Situ	On Land				
100A	1	3				Error [a]
101A	3	3	-3.182	1.834	3.182	Do not reject H_0
101B	1	6				Error
101C	3	2	-4.303	1.000	4.303	Do not reject H_0
103A	6	5	-2.365	2.051	2.365	Do not reject H_0
104A	7	9	-2.145	-0.026	2.145	Do not reject H_0
104B	0	0				Error

[a] Indicates an insufficient amount of well-bonded data points available for analysis

The results of the t-test for each pile, executed using MS Excel are summarized in Table 10.7 It shows that the criterion is met for all applicable test piles excepting piles 100A, 101B, and 104B. For these three piles (all prepreg polyurethane), insufficient well-bonded data points were available and the difference between sample means could not be tested. However, since four of the seven queried test piles indicated that no factors significantly influenced the data points when the piles were extracted, it is assumed that the remaining piles were similarly unaffected.

10.10.4 Concrete (Figure 10.8)

A total of ten tests were carried on the control pile (99A) – four in the dry region and six in the splash zone. The measured salt concentration in the cover for this pile is given in Table 10.2. The average pull-off strength reported in Figure 10.8 was 28% lower in the splash zone compared to that in the dry region. The cyclic effect of tidal cycles may have led to a degradation in concrete

properties in the splash. According to ACI 318-14 section 14.5.2.1, the tensile strength of plain concrete can be taken as $5\sqrt{f'_c}$. This translates to a concrete compressive strength of 29.5 MPa (4,290 psi) for the dry region and 15.4 MPa (2,237 psi) for the splash zone. This is consistent with the specified concrete strength for the piles of 27.6 MPa (4,000 psi).
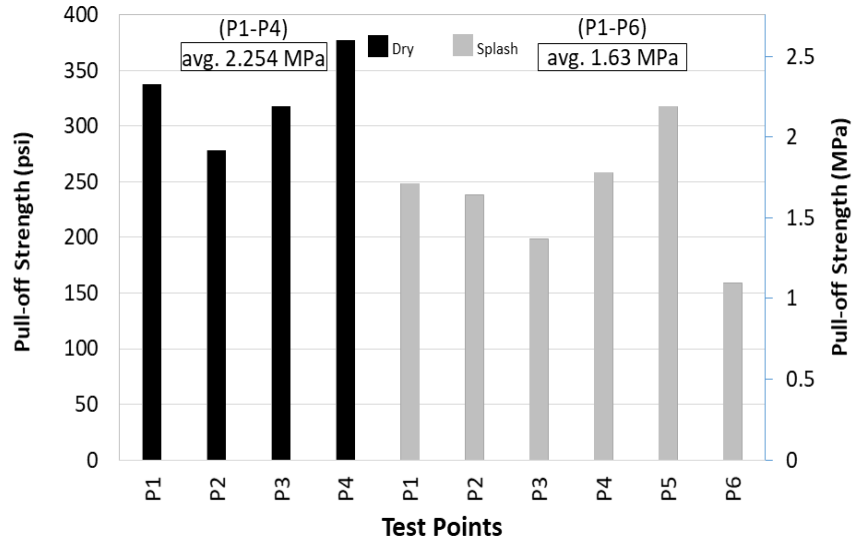
Figure 10.8 Pull-off values for concrete (pile 99A)

10.10.5 Piles Repaired 2003-04 (Figure 10.9)

No piles belonging to this series were pressure bagged. Three of the four piles were wrapped using polyurethane resin and one an epoxy resin that had been specially formulated for underwater applications (Pile 101A). A total of 33 tests were conducted in this series. While some bond values were high in both dry (1.7 MPa (258 psi) in 101A) and splash (0.9 MPa (129 psi) in 101A) zones, there were also twelve locations where bond was zero (8 in polyurethane, 4 in the epoxy).

117

Five of the eight zero values in the polyurethane system were a subset of ten interlayer failures – all in the polyurethane resin system. The average residual bond for these failures ranged from 0.05 (8) to 0.3 (46) MPa (psi) Table 10.6.

Since interlayer failures do not reflect FRP bond with the concrete substrate, they are excluded in the calculation of average residual values included in Figure 10.9. The interlayer failures suggest insufficient resin had been applied in the prepreg system.

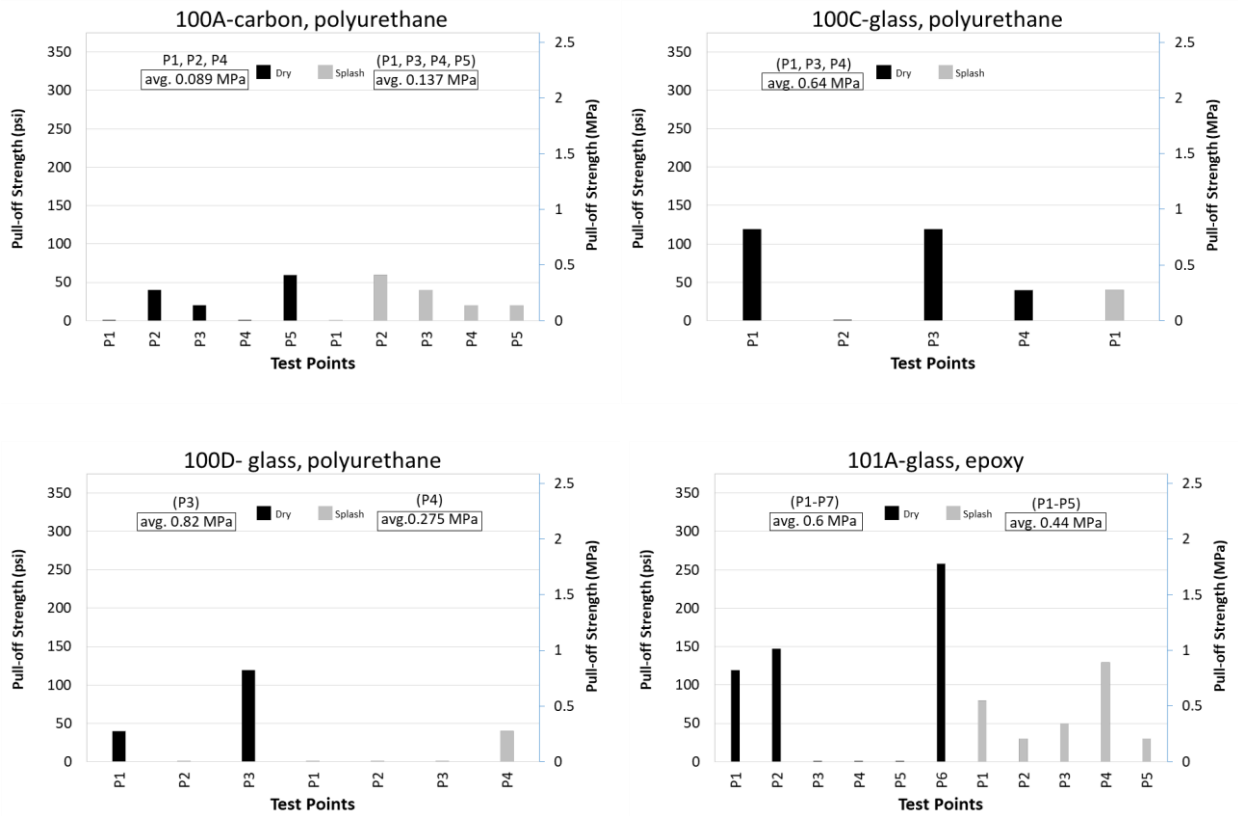Figure 10.9 Pull-off test results for repairs conducted in 2003-04

10.10.6 Piles Repaired 2006 (Figure 10.10)

Both piles – one epoxy and one polyurethane - repaired in this series were pressure bagged. Visual inspection (Figure 10.4) had suggested a high relative residual bond in these piles. A total of 40 tests were conducted – 22 for the polyurethane and 18 for the epoxy. There were 19 zero

bond values (12 for polyurethane and 7 for epoxy) and 6 interlayer failures (5 for polyurethane and 1 for epoxy). As before, interlayer failures are not included in the average values given in Figure 10.10. The highest residual bond was 0.41 MPa (60 psi) (101B – polyurethane) in the dry zone and 1.2 MPa (179 psi) in the splash zone (101C - epoxy).

Whereas limited improvement was expected for the polyurethane resin because it released carbon dioxide during the curing process, the epoxy resin was expected to deliver superior results. The reason for the poor outcome became evident from the failure mode that showed that not enough epoxy had been applied (discussed later). The results indicate that visual inspection is not a reliable method for identifying poor bond locations.
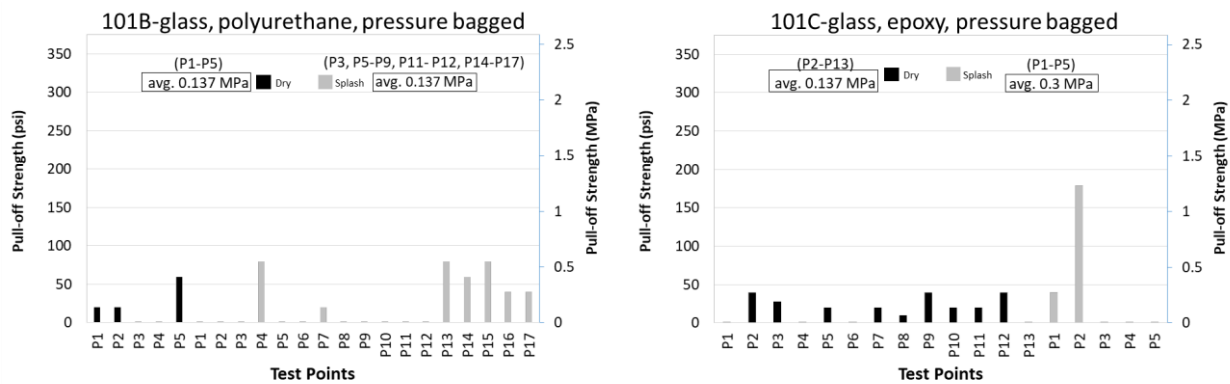
Figure 10.10 Pull-off test results for repairs conducted in 2006

10.10.7 Piles Repaired 2008 (Figure 10.11)

A total of five piles were repaired in this series. Four were pressure bagged, three using epoxy resin, and one using polyurethane. A fifth pile was not pressure bagged. This was installed by a sponsor and used a polyurethane resin. Thus, it was possible to make direct comparison of the performance of pressure bagged and non-pressure bagged piles.

A total of 47 tests were conducted, 24 for the polyurethane (104A, B) and 23 for the epoxy (103A, 103C). Results summarized in Figure 10.11 showed that the performance of the pressure

bagged piles was superior compared to the non-pressure bagged pile (104B). The average residual bond for epoxy (103A, 103C) was higher in the dry zone (1.3 MPa (191 psi), 1.2 MPa (179 psi)) vs 0.7 MPa (103 psi) for polyurethane (104A) and comparable in the splash zone (0.5 MPa (82 psi)), 1.1 MPa (165 psi) vs 0.7 MPa (100 psi) for polyurethane. Even though pressure bagging was used, there were four interlayer failures in the polyurethane system (excluded in the calculated average value included in Figure 10.11). However, the average residual bond (Table 10.6) for these failures was relatively high (0.8 MPa (119 psi)).

The performance of the non-pressure bagged pile 104B was distinctly poorer. The average bond was zero from five points in the dry zone but higher (0.4 MPa (60 psi)) in the splash zone where both failures were interlayer. As discussed, the latter tests were conducted on land and the mean value did not satisfy statistical criterion (see Table 10.7).
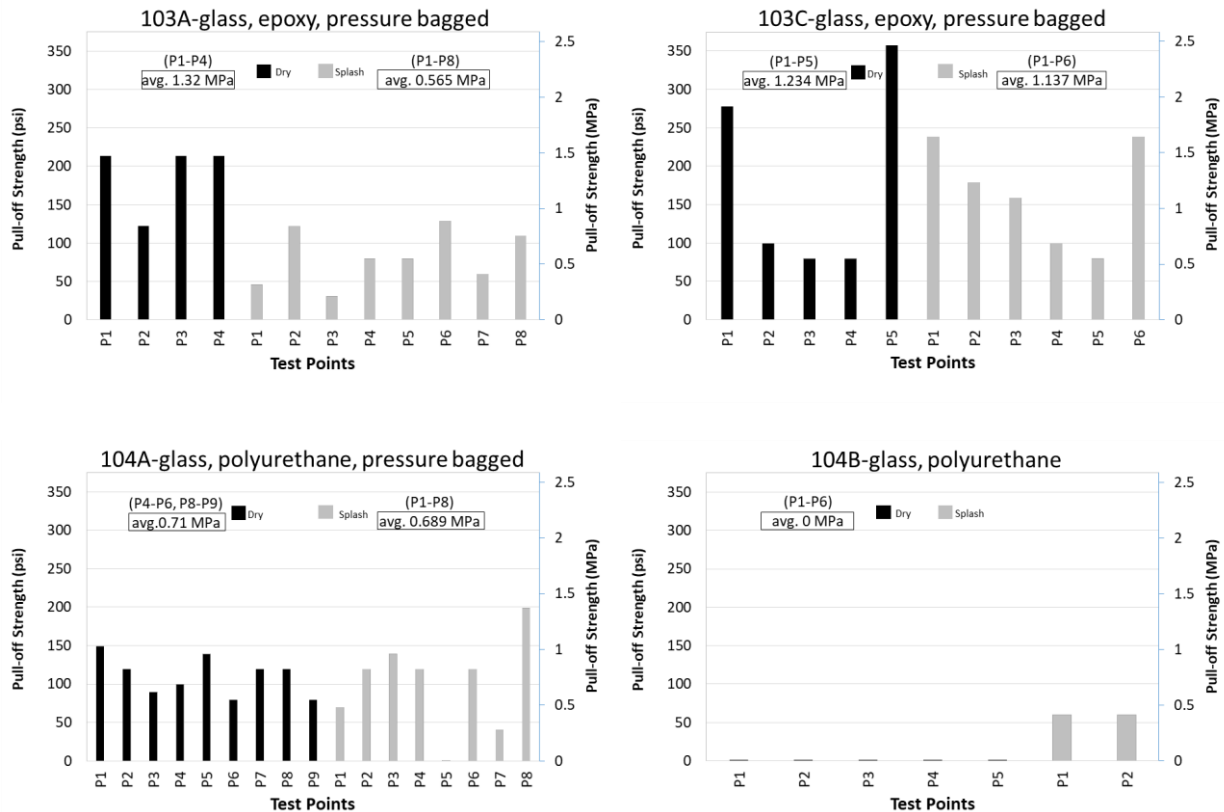

Figure 10.11 Pull-off test results for piles repaired in 2008

120

10.10.8 Failure Mode

The failure modes observed in the 120 tests were cohesive, mixed mode, adhesive and inter-layer failures. Cohesive failure in the substrate concrete during pull-off testing corresponds to Mode G in ASTM D7522 (ASTM 2009). Within the recorded data set, one specimen (0.85% of total points) exhibited a Mode G failure. A total of 13 specimens (10.7% of total points) exhibited Mode F, which is a mixed mode condition. The remaining 107 specimens exhibited Mode B (cohesive in laminate) or Mode E (adhesive at bond plane) failure modes. Figure 10.12 illustrates the failure modes encountered during testing.
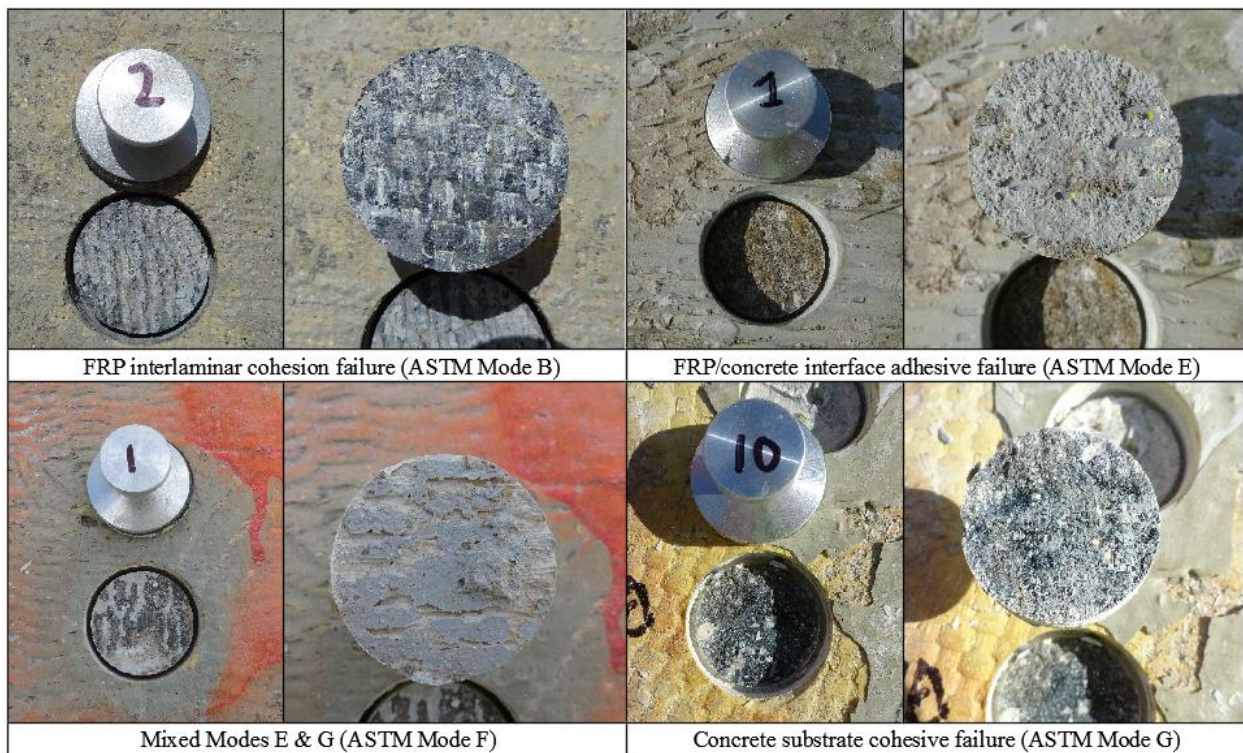

Figure 10.12 Representative failure modes

10.11 Discussion

Results of pull-off tests summarized in Table 10.6 and Figure 10.9 through Figure 10.11 showed wide variation. Bond values ranged from zero (37 occurrences – 26 with the polyurethane resin) to a high of 2.5 MPa (357 psi). Among piles pressure bagged in 2006 there were 19 locations

where the measured bond was zero, 12 for polyurethane resin and 7 for epoxy. For a similar installation in 2008 there was just a single instance of zero bond (polyurethane - 104A). The observed variability is common in field testing and has been reported by other researchers, e.g. (Banthia, et al., 2010), (Myers, et al., 2011).

(Banthia, et al., 2010) conducted tests on corrosion repair of columns after 13 years of exposure. Since FRP was applied to a vertical surface and tests conducted after 9 and 13 years comparisons are more appropriate. The variation in bond ranged from 0.12 MPa (17 psi) to 4.95 MPa (718 psi). The higher value reflects the higher compressive strength of concrete used in the columns but the lower value is comparable to those obtained in this study. Though maximum and minimum values may be deemed to be similar if adjustments are made for compressive strength, reported mean values of 0.83 (120 psi) to 3.54 MPa (513 psi) were higher. This reflects the better control that can be exercised in land installations and on dry surfaces compared to marine environment.

10.11.1 Cause of Poor Bond

Research has proven that water intrusion is the most likely reason for poor bond in epoxy-based systems, e.g. (Judd, 1977), (Myers, 2007), (Dolan, et al., 2009) (Sen, 2015). The extent to which water can diffuse to the bond line or between FRP layers is a function of surface preparation, workmanship and the type of resin. Since the same surface preparation and the same resin was used in all the applications their effect can be discounted. The highest strengths were in piles pressure bagged in 2008 where the bonding surface was heavily scarred to install sacrificial anodes and reference electrodes (see Figure 10.13).

FRP installations in marine environments are recognized to be problematic. (Walker, 2007) reported that voids of 5-8% are the norm for such applications adding that they can be even higher.

Voids provide a direct pathway for moisture to reach the concrete substrate or accumulate between

FRP layers.

Figure 10.13 Instrumented face for hybrid FRP-CP
Pressure bagged repair (2008)

The extent to which moisture can be transported or absorbed in voids depends on the degree

of cure of the epoxy. If epoxy does not fully cure moisture absorption is increased because the

unused polyamide hardener provides additional sites for hydrogen bonding by water molecules,

(Sharp, 2015). Ambient temperature at the time the two-part epoxy is mixed controls pot life and

therefore the time available for on-site fabric saturation.

Figure 10.14 shows three photos providing evidence of water intrusion at the bond line and

incomplete fabric saturation. They were taken from different piles. The first picture (Figure

10.14a) shows moisture in the bond plane; the second, water stored between two layers being

drained during scoring (pile 101A repaired in 2004). The accumulation of water between

layers led to marine growth and voids between layers (Figure 10.14b). Figure 10.14c shows

incomplete fabric saturation in specimen 101C that was pressure bagged in 2006. There was no

similar evidence for piles 103A, 103C that used the same epoxy and were also pressure bagged in 2008.

10.11.2 Performance of Epoxy System

Epoxy repairs were carried out in 2004, 2006 and 2008. Results (Figure 10.9 and Figure 10.10) were comparatively poorer in 2004 (installed when conditions were cool) and 2006 (when conditions were hot) and likewise improved in 2008 (Figure 10.11) when conditions were moderate (see Table 10.5). Thus, the performance mirrored ambient condition at the time the two parts of the epoxy were mixed.

Cool conditions under which the epoxy was mixed for pile 101A inevitably delayed curing thereby allowing moisture to diffuse and accumulate between layers over time (Figure 10.14a). Conditions were hot and humid when pile 101C was pressure bagged. Illig (2016) reported the pot life to be as little as 10-15 minutes for repairs conducted on the nearby Sunshine Skyway Bridge in 2007. This was also the experience of USF researchers. Using ice to extend pot life (as used in the Sunshine Skyway repair) was not a viable option. The limited time available led to incomplete saturation of the FRP material (Figure 10.14c). Conditions were more favorable in 2008 when the ambient temperature was 75F (24C). There was sufficient time to saturate the fabric and place it on the pile. Measured residual bond was notably higher for piles 103A, 103C (Figure 10.11).

(a) Moisture in bond plane and between FRP layers

(b) Marine growth between FRP layers and voids between FRP layers
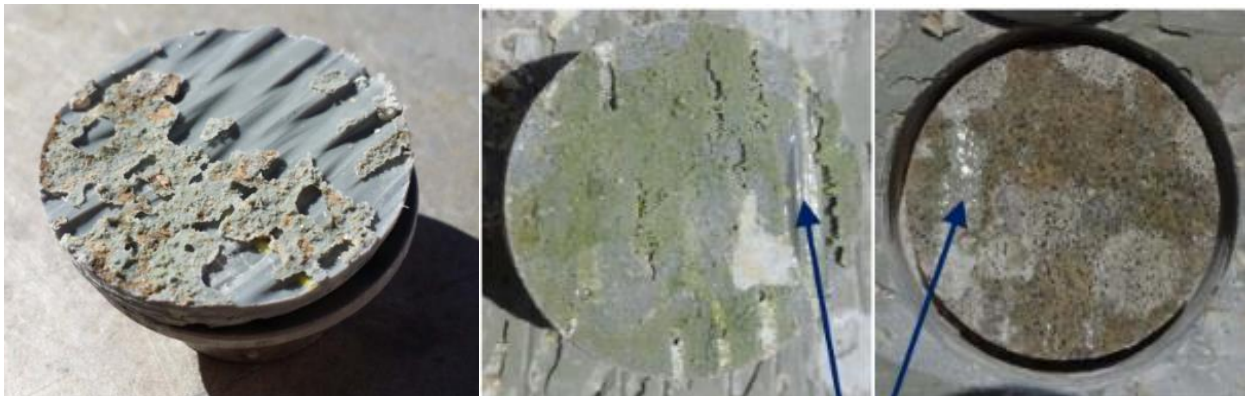
(c) Fiber not fully impregnated by epoxy; second and third photos are at the same location and show the dolly and the concrete surface to which it was bonded. Arrows point to locations with no epoxy. Dark regions point to regions with trace of epoxy.

Figure 10.14 Reasons for poor bond

10.11.3 Performance of Polyurethane Resin

The polyurethane resin requires water for curing and is therefore not as sensitive to ambient conditions. Since this resin system used lower strength fibers it required a greater number of FRP layers ranging from 2 in pressure bagged pile (101B) and 6 in non-pressure bagged piles 100C, 100D (Table 10.1).

During curing carbon dioxide is released that can lead to the creation of voids at the concrete interface and leave air pockets between layers if the gas is not permitted to escape. Not surprisingly, the zero bond values and interlayer failures were common for this resin system. There were a total of 26 tests that recorded zero bond (Figure 10.9 through Figure 10.11) and 21instances of inter-layer failure combining both zero and non-zero values (Table 10.6). This also suggests that the fabric may not have been adequately saturated in the factory.

Table 10.8 Pull-off test results by resin type

Year	Pile	Total data points		Pull-off test results [a]							
		Dry	Splash	Min.		Max.		Mean, Dry		Mean, Splash	
				MPa	psi	MPa	psi	MPa	Psi	MPa	psi
Polyurethane											
2003	100A	5	5	0	0	0.4	60	0.2	24	0.2	28
	100C	4	1	0	0	0.8	119	0.47	69	0.3	40
	100D	3	4	0	0	0.8	119	0.4	53	0.01	10
2006	101B[a]	5	17	0	0	0.5	79	0.1	20	0.15	23
2008	104A[a]	9	8	0	0	1.4	198	0.8	110	0.7	100
	104B	5	2	0	0	0.4	60	0	0	0.4	60
Total		31	37								
Epoxy											
2004	101A	7	5	0	0	1.8	258	0.6	87	0.44	64
2006	101C[a]	13	5	0	0	1.2	179	0.1	18	0.3	44
2008	103A[a]	4	8	0.2	31	1.5	213	1.3	191	0.56	82
	103C[a]	5	6	0.5	79	2.5	357	1.2	179	1.13	165
Total		29	24								

[a] **PB = pressure bagging**

Table 10.8 compares the maximum, minimum and mean values for the dry and splash zones for the two resin systems. A total of 68 tests were conducted for the polyurethane resin; 53 tests were conducted for the epoxy resin since there were fewer specimens. Inspection of this table indicates that the epoxy resin outperformed polyurethane.

10.11.4 Pressure vs Non-Pressure Bagged Piles

The performance of both piles pressure bagged in 2006 was worse than expected (Figure 10.10). For epoxy this was attributed to hot ambient conditions as discussed. For polyurethane it was likely due to pressure creating voids by trapping gases and preventing their escape during cure.

Figure 10.11 shows that pressure bagging led to a significantly higher residual bond compared to the non-pressure bagged pile 104B. This was possibly because of a change in the application technique based on laboratory findings, (Sen, et al., 2010). Instead of applying an initial primer coating to the concrete surface as recommended, the resin was applied to the already saturated prepreg material that was then placed on the bare concrete surface. This reduced the incidence of air bubbles and improved bond. However, there was one case where the measured bond was zero (Figure 10.11).

10.11.5 Change In Bond: 2005 vs 2016 Results

Pull-off tests were conducted in 2005 on three piles 100A, 100C (both prepreg) and 101A (epoxy), (Sen, et al., 2007). None were pressure bagged. Two of the piles, 100C and 101A were re-tested in 2016, and therefore it was possible to assess changes in bond over this eleven year time period. In the 2005 tests, bond was measured at four locations in each pile, two in the dry zone and two in the splash zone. Bond values reported in (Sen, et al., 2007) included inter-layer failure values that are excluded in Table 10.6. Though the target was 5 tests per zone for the 2016

tests, this was only met for pile 101A, not 100C. For the latter pile, five tests were carried with only one in the splash zone. The spatial distribution showing the location of the tests for piles 100C and 101A is mapped in Figure 10.15.

All failures in 100C (prepreg) in 2005 were inter-layer. In 2016, two of the five failures were inter-layer for the same pile. In contrast, failures in the epoxy pile 101A were adhesive, mixed mode or cohesive in both 2005 and 2016.
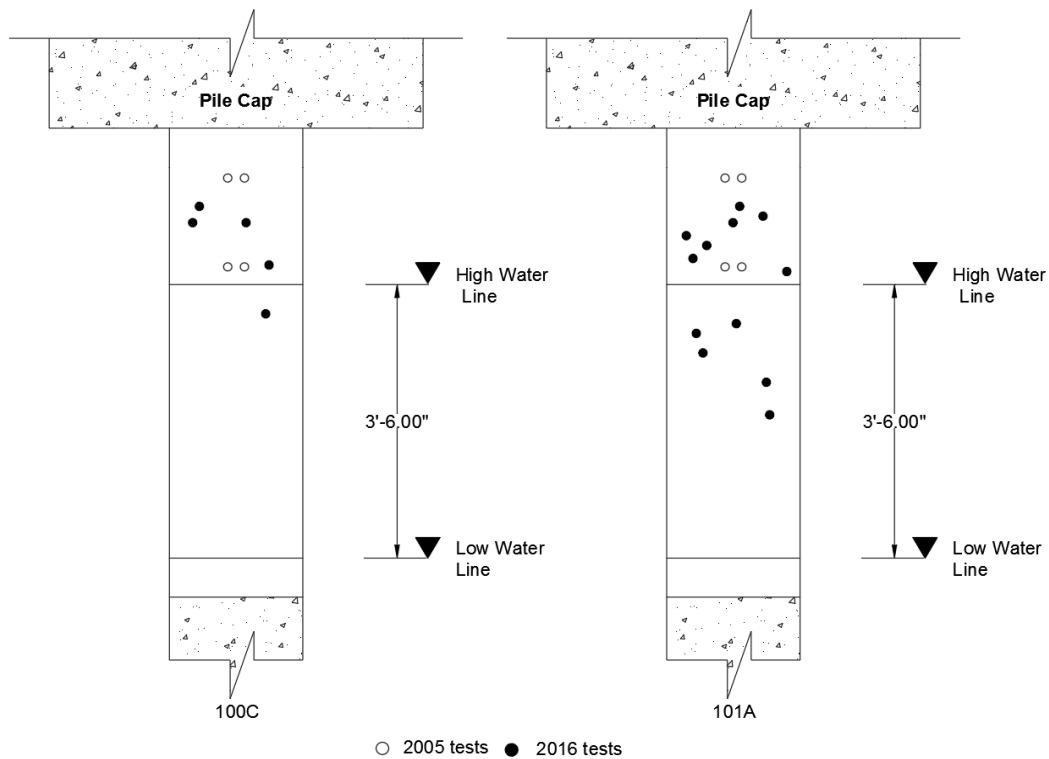

Figure 10.15 Spatial location of pull-off tests in 2005 and 2016

Figure 10.16 plots values of the residual bond for the two piles tested. This shows averages that include and exclude inter-layer failures for the 2016 tests. Since the tests were not conducted at the same locations there are differences in the measured values. Values were higher in the 2016 tests that were conducted closer to the rounded edges because of increased confinement. Because of the disparate failure modes, comparisons show increases in the dry zone in both piles. In

contrast, values in the splash zone were higher in 2005. The results portray the random variation in bond strength in non-pressure bagged piles. No underlying trend can be discerned.
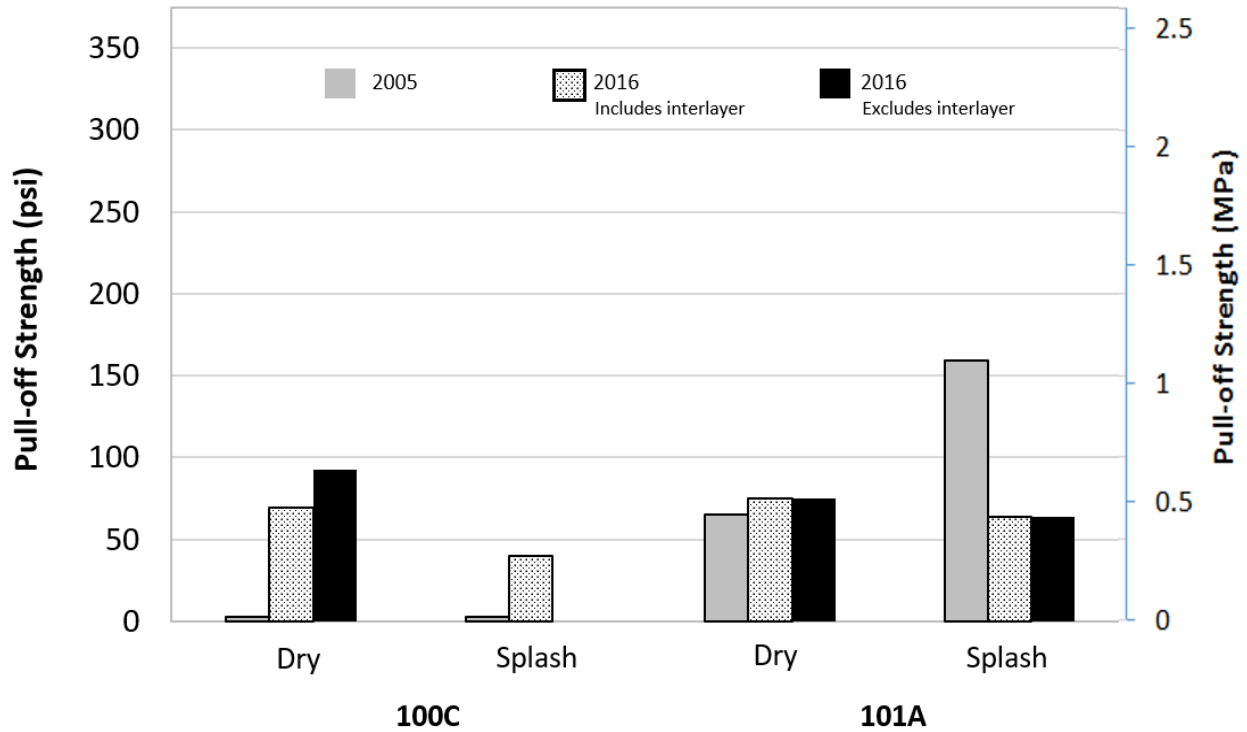

Figure 10.16 Results for piles tested in 2005 and 2016

10.12 Conclusions

This study presents results from a field evaluation in which the FRP-concrete bond was measured for two disparate FRP systems. One was a prepreg using polyurethane resin and the other a wet layup using specially formulated epoxy intended for application on wet surfaces. Of 13 piles that were repaired (Figure 10.1), 10 were tested. A total of 120 pull-off data points were collected in the dry and splash zones (Figure 10.3). Based on the foregoing results and discussion, the following conclusions can be made:

- Findings from visual inspection can be misleading (Figure 10.4).

- Bond was poor in epoxy-based systems when the two part resin was mixed in unfavorable conditions (Table 10.5). This reduced pot life or increased cure time and adversely impacted performance (Figure 10.9,Figure 10.10 and Figure 10.14). It is recommended to cool resins before mixing.

- Epoxy-based systems outperformed polyurethane-based systems in both the dry and splash zones (Table 10.8).

- Pressure bagged piles repaired in 2008 performed best for both resin systems (Figure 10.11).

- Epoxy-based, pressure bagged installations are comparably durable even when mixed in-situ and applied to wet surfaces in a marine environment.

Findings from destructive evaluation are based on studies conducted at the project site and do not necessarily apply to other installations. However, considerations of site evaluation logistics, the qualitative improvement in strength offered by pressure bagging, and the dangers of applying FRP during hot weather may be applicable to other projects.

REFERENCES

ACI (American Concrete Institute). (1992). "Building code requirements for masonry structures" ACI 530-92/ASCE5-92/TMS 402-92, Farmington Hill, MI.

ACI (American Concrete Institute). (2002). "Design and Construction of Externally Bonded FRP Systems for Strengthening Concrete Structures". ACI 440.2R-02, Farmington Hills, MI.

ACI (American Concrete Institute). (2003). "Guide for the selection of polymer adhesives with concrete". (Reapproved 1997, 2003), ACI 503.5R-92, Farmington Hill, MI.

ACI (American Concrete Institute). (2008). "Guide for the design and construction of externally bonded FRP systems for strengthening concrete structures." ACI 440.2R-08, Farmington Hills, MI.

ACI (American Concrete Institute). (2010). "Guide for the design and construction of externally bonded fiber-reinforced polymer systems for strengthening unreinforced masonry structures", ACI 440.7R-10, Farmington Hills, MI.

ACI (American Concrete Institute). (2014). "Building Code Requirements for Structural Concrete." ACI 318-14 , Farmington Hills, MI.

ACI (American Concrete Institute). (2017). "Guide for the Design and Construction of Externally Bonded FRP Systems for Strengthening Concrete Structures" ACI 440.2R-17, Farmington Hills, MI.

Aguilar, J., Winters, D., R., S., Mullins, G., & Stokes, M. (2010). Improvement in FRP-Concrete bond by external pressure. Transportation Research Record 2131, 145-154.

Aguilar, J., Winters, D., Sen, R., Mullins, G., & Stokes, M. (2009). Innovative underwater pile repair incorporating cathodic protection. University of South Florida. Tampa, FL: Final report Hillsborough County.

Aguilar, J., Winters, D., Sen. R., M. G., & Stokes, M. (2010). FRP-CP system for pile repair in tidal waters. Transportation Research Record 2150, 111-118

Ahad, N. A., and Yahaya, S. S. S. (2014). Sensitivity analysis of Welch's t-test. In AIP Conference Proceedings, Vol. 1605, No. 1, pp. 888-893, AIP.

.

Al Azzawi, M., Hopkins, P., Mullins, G., & Sen, R. (2018). FRP-Concrete bond after 12 year exposure in tidal waters. ASCE Journal of composites for construction. Accepted for publication.

Al Azzawi, M., Hopkins, P., Ross, J., M. G., & Sen, R. (2018). CFRP-CMU bond after 20 years outdoor exposure. ACI structural journal. Accepted for publication.

Aligizaki, K. K. (2005). Pore structure of cement-based materials testing, interpretation and requirements. CRC Press, Boca Raton, FL.

ASTM (American Society for Testing and Materials). (2009). "Standard test method for pull-off strength for FRP bonded to concrete substrate." ASTM D7522/D7522M-09, West Conshohocken, PA.

ASTM D7522-12 Standard test method for pull-off strength for FRP laminate systems bonded to concrete substrate, ASTM International, West Conshohocken, PA.

ASTM C642-13 standard Test Method for Density, Absorption, and Voids in hardened concrete, STM International, West Conshohocken, PA.

Attari, A., McNally, C., Richardson, & G., M. (2016). A combined SEM-Calorimetric approach for assessing hydration and porosity development in GGBS concrete. Cement and concrete composites, 68, 46-56.

Au, C., & Büyüköztürk, O. (2005). Peel and shear fracture characterization of debonding in FRP plated concrete affected by moisture. ASCE- Journal of composites for construction, 10(1).

Bailey, D. M., Hock, V. F., Noyce, P. A., & Restly, M. (2013). Polymer composite wrapping and cathodic protection system for reinforced concrete piles in marine applications (No. ERDC/CERL-TR-13-6). Engineer research and development center-construction engineering lab.

Balaras, C., & Agiriou, A. (2002). Infrared thermography for building diagnostics. Energy and buildings, 34(2), 171-183.

Banthia, N., Abdolrahimzadeh, A., Demers, M., Mufti, A. A., & Sheikh, S. A. (2010). Durability of FRP-concrete bond in FRP-strengthened bridges. Concrete International, 32, 45-51.

Blackburn, B. P., Tatar, J., Douglas, E. P., & Hamilton, H. R. (2015). Effects of hygrothermal conditioning on epoxy adhesives used in FRP composites. Construction and building materials, 96, 679-689.

Carloni, C., & Subramaniam, K. (2012). FRP-Masonary debonding numerical and experimental study of the role of mortar joints. Journal of composites for construction, 16(5), 581-589.

Chajes, M., Finch, J. W., Januszka, T. F., & Thomson, T. A. (1996). Bond and force transfer of composite material plates bonded to concrete. 98, 256-264.

Cho, S.-W. (2012). Using mercury intrusion porosimetry to study the interfacial properties of cement-based materials. Journal of marine science and technology, 20, 269-273.

Choi, S., Gartner, A. L., Etten, Van, N., Hamilton, H. R., & Douglas, E. P. (2011). Durability of concrete beams externally reinforced with CFRP composites exposed to various environments. Journal of composites for construction, 16(1).

Cromwell, J., Harries, K., & Shahrooz, B. (2011). Environmental durability of externally bonded FRP materials intended for repair of concrete structures. Construction and building materials, 25, 2528-2539.

De Lorenzis, L., Miller, B., & Nanni, A. (2001). Bond of Fiber-Reinforced Polymer laminates to concrete. ACI materials journal, 98, 256-264.

Delagrave, A., Bigas, J., OIlivier, J., Marchand, J., & Pigeon, M. (1979). Influence of the interfacial zone on the chloride diffusivity of mortars. Advanced cement based material, 5, 86-92.

Detwiler, R. J., Thomas, W., Stangebye, T., & Urahn, M. (2009). Variability of 4x8 cylinder tests, Vol., 31, No. 5, 2009, pp. 43-47.

Dolan, C., Tanner, J., Mukai, D., Hamilton, H., & Douglas, E. (2009). Research report for evaluating the durability of bonded CFRP repair/strengthening of concrete beams: technical data and discussion supporting the draft final report of NCHRP project. 12-73.

Engebretson, D., Sen, R., Mullins, G., & Hartley, A. (1996). Strengthening concrete block walls with carbon fiber. Materials for the new millennium, Proceedings of the materials engineering conference volume 2, ASCE, 2, 1592-1600.

Global historical climatology network. (2016, 10 11). Retrieved from National centers for environmental information: https://www.ncdc.noaa.gov/cdo-web/search

Grunenfelder, L., & Nutt, S. (2010). Void formation in composite prepregs - effect of dissolved moisture Composites Science and Technology. Composites science and technology, 70, 2304-2309.

Haber, Z., Mackie, K., & Zhao, L. (2012). Mechanical and environmental loading of concrete beams strengthened with epoxy and polyurethane matrix carbon fiber laminates. Construction and building materials, 26, 604-612.

Hamilton, H. R., Brown, J., Tatar, J., Lisek, M., & Brenkus, N. R. (2017). Durability evaluation of florida's Fiber-Reinforced Polymer (FRP) composite reinforcement for concrete structures. Final report for FDOT contract No. BVD31-977-01.

Hartley, A. (1995). Strengthening of concrete masonary walls using CFRP. MSCE thesis, University of South Florida, Tampa, FL.

Hartley, A., Mullins, G., & Sen, R. (1996). Repair of concrete masonry block walls using carbon fiber. Advanced composite materials in bridges and structures (Editor M. El-Badry), Canadian society of civil engineers, 795-802.

Hong Zhao, D. D. (1990). Quantitative backscattered electron analysis techniques for cement - based materials. Lawrence, Kansas: The University of Kansas.

Illig, G. (2016). Concrete repair, strengthening and protection. University of South Florida, Guest lecture, April, Tampa, FL.

Jean-Pierra Pascault, R. J. (2010). Epoxy polymers new materials and innovations. Wiley-VCH. Strauss GmbH, Mörlenbach, Germany.

Jelinski, L. W. (1985). Nature of the water-epoxy interaction. Macromolecules, 18 (6), pp 1091–1095.

Jovan Tatar, S. H. (2015). Bond durability factor for externally bonded CFRP systems in concrete structures. ASCE, Journal of composites for construction 20 (1), 04015027.

Judd, N. (1977). Absorption of water into carbon fibre composites. The British Polymer Journal, 9(1), 36-40.

Karbhari, V. M., & Ghosh, K. (2009). Comparative durability evaluation of ambient temperature cured externally bonded CFRP and GFRP composite systems for repair of bridges. Composites part A: Applied science and manufacturing, 40(9), 1353-1363.

Lau, D., & Büyüköztürk, O. (2010). Fracture characterization of concrete/epoxy interface affected by moisture. Mechanics of materials, 42(12), 1031-1042.

Leng, D. (2000). Zinc mesh cathodic protection systems. Materials performance, 39, 28-33.

Li, L., & Sagüés, A. (2004). Chloride Corrosion Threshold of Reinforcing Steel in Alkaline Solutions—Effect of Specimen Size. Corrosion the journal of science and engineering, 60, 195.

Long, M., C., D., Kesteloot, S., Bigourdan, B., Le Gac, P., & Szulc, J. (2012). Durability of CFRP-Concrete bonding in a marine environment. European conference on composite materials, 1-8.

Lucas F.M. da Silva, A. O. (2011). Handbook of Adhesion Technology. Springer-Verlag, Berlin Heidelberg.

Maerz, H., Chepur, P., Myers, J., & Linz, J. (2001). Concrete roughness measurement using laser profilometry for fiber reinforced polymer sheet application. Transportation research board, 132-139.

Mehta, P. K., & Monteiro, P. J. (1993). Concrete microstructure, properties and materials.Prentice Hall, Englewood Cliffs, NJ.

Mehta, P. K., & Monteiro, P. J. (2006). Concrete microstructure, properties and materials. McGraw-Hill. NY, NY.

Miller, B. (1999). Bond between carbon fiber reinforced polymer sheets and concrete. University of Missouri-Rolla, Department of civil engineering, University of Missouri-Rolla.

Mindess, S., Y. J., & Darwin, D. (2003). Concrete. Prentice Hall, Englewood Cliffs, NJ.

Mirmiran, A., Shahawy, M., Nanni, A., Karbhari, V., Yalim, B., & Kalayci, A. S. (2008). NCHRP report 609-Recommended construction specifications and process control manual for repair and retrofit of concrete structures using FRP composites. Washington, D.C: National Cooperative Highway Research Program.

Momber, W. (1999). Surface preperation of concrete-the German experience. Conference of new application of water jet technology, 207-217. Isniomaki, Japan.

Mullins, G., Hartley, A., Engebretson, D., & Sen, R. (2000). Settlement repair of lightly reinforced concrete block walls using CFRP. Innovative systems for seismic repair and rehabilitation of structures. Proceedings of the second conference on seismic repair and rehabilitation of structures (SRRS2) Edited by Ayman Mosallam. Technomic publishing company, 171-180.

Mullins, G., Sen, R., Suh, K., & Winters, D. (2004). Underwater FRP pile wrap of the Friendship Trails Bridge. Final Report submitted to Hillsborough County Tampa, FL.

Mullins, G., Sen, R., Suh, K., & Winters, D. (2006). A demonstration of underwater FRP repair. Concrete international.

Mullins, G., Sen, R., Winters, D., & Schrader, A. (2007). Innovative pile repair. Final Report submitted to Hillsborough County, FL.

Myers, J. (2007). Durability of external fiber-reinforced polymer strengthening systems. Durability of composites for civil structural applications (editor V.M.Karbhari), Woodhead Publishing Limited, Cambridge, UK, 247-283.

Myers, J., & Muncy, N. (2011). Bond behavior of externally bonded fiber reinforced polymer laminates subjected to in-situ service loading and environmental conditioning. CDCC-11, durability and sustainability of fibre reinforced polymer (FRP) composites for construction and rehabilitation, Québec City, Québec, Canada.

Neville, A. (2011). Properties of concrete. Pearson, Edinburgh Gate, Harlow, England

Quan Yang, G. X. (2007). Hygrothermal ageing of an epoxy adhesive used in FRP strengthening of concrete. Journal of applied polymer science, Vol. 107, Issue 4, 2607-2617.

Ross, J. (2013). Evaluating CFRP-masonry bond using thermal imaging. MSCE Thesis, University of South Florida, Department of civil and environmental engineering, Tampa, FL.

Sen, R. (2015). Developments in the durability of FRP-concrete bond. Construction and building Materials, 78, 112-125.

Sen, R., & Mullins, G. (2007). Application of FRP composites for underwater piles repair. Comp. Part B: Eng., 38, 751-758.

Sen, R., & Mullins, G. (2010). Underwater FRP repair of corroding piles incorporating cathodic protection. Final report NCHRP-IDEA.

Sen, R., Mullins, G., & Shahawy, M. (2008). FRP repair and strengthening of structurally deficient piles. Journal of transportation research board, 221-230.

Sen, R., Mullins, G., Aguilar, J., & Winters, D. (2011). Advances in corrosion repair of piles using FRP. ACI SP-275-30, ACI, Farmington Hills, MI.

Sharp, N. (2015). Effects of moisture on the properties of epoxies and carbon-epoxy composite laminates. Ph.D dissertation, Purdue University West Lafayette, Indiana.

Shen, X. (2002). Effect of surface roughness and putty thickness on the bond performance of FRP laminates. University of Missouri-Rolla, Department of civil engineering, Rolla, Missouri.

Suh, K., Sen, R., Mullins, G., & Winters, D. (2008). Corrosion monitoring of FRP repaired piles in tidal waters. ACI SP-252, 137-156.

Tatar, J., & Hamilton, H. (2016). Comparison of laboratory and field environmental conditioning on FRP-concrete bond durability. Construction and building materials, 122, 525-536.

Tuakta, C., & Büyüköztürk, O. (2011). Conceptual model for prediction of FRP-concrete bond strength under moisture cycles. ASC, Journal of composites for construction, 15(5), 743-56.

Walker, L. (2007). Aerospace grade composite technology for infrastructure Paper 17B, 2007, Cobrae conference,University of Stuttgart, Stuttgart, Germany.

Walpole, R. E., Myers, R. H., Myers, S. L., & Ye, K. (2012). Probability & statistics for engineers & scientists (9 ed.). Boston: Pearson education.

Winslow, D. N., & Diamond, S. (1970). A mercury porosimetry study of the porosity in portland cement. Journal of Materials, 5, 564-585.

Winters, D., Mullins, G., Sen, R., Schrader, A., & Stokes, M. (2008). Bond enhancement for FRP pile repair in tidal waters. Journal of composites for construction, 10.1061/(ASCE) 1090-0268, 334-343.

Yoshizawa, H., Myojo, T., Okoshi, M., Mizukoshi, M., & Kliger, H. (1996). Effect of sheet bonding condition on concrete members having externally bonded carbon fiber sheet. Fourth materials engineering conference. Washington, D.C.: ASCE annual convention.

Zhenyu Ouyang, B. W. (2008). Modeling of moisture diffusion in FRP strengthened concrete specimens. ASCE, Journal of composites for construction, Vol. 12, 4, 425-434.

Zhou, A., Büyük€oztürk, O., & Lau, D. (2017). Debonding of concrete-epoxy interface under the coupled effect of moisture and sustained load. Cement and concrete composites, 80, 287-297

(2017, 4 14). Retrieved from Weather underground: https://www.wunderground.com/history/airport/KSPG/2008/12/18/DailyHistory.html?req _city=&req_state=&req_statename=&reqdb.zip=&reqdb.magic=&reqdb.wmo

(2017, 5 16). Retrieved from Campbell scientific: http://www.campbellsci.com/cr1000#specifications

APPENDIX A: PHOTOS AND CALCULATIONS

```
Tarmac / Titan America, LLC          1.62 CU FT                    DATE:          5/2/17
MIX DESCRIPTION:          USF Project                   0.00 % FLY ASH    SOUTHEAST
BATCH SIZE = E =                    0.060 CU.YD              WAT/CEM =      0.73
DESIGN STRENGTH:                    2500 PSI                CMNTS =        390
                          DESIGN WEIGHTS
                                                                  SOLID VOL.
   MATERIALS        WEIGHT    GRAVITY    MOISTURE    SOURCE
                                                                  1.98
Patras Cement         390       3.15                              0.00
Crystal River Fly Ash   0       2.41                              0.00
Masterlife SF 100       0       2.20      0.00                   11.26
Cemex #57 (87-089)   1680       2.39      1.90                    8.40
Cemex Sand (16-078)  1379       2.63      3.30                    4.54
WATER               34.00
Master Set 961R         3 OZ/CWT         11.70
Master Glenium 7500     0 OZ/CWT          0.00
Masterlife CL 30     0.00       1.00                              0.00
Master Air AE 90        3 OZ/YD                                   0.81
% AIR                3.00
SLUMP                5.00                            YIELD =      27.00
                                         TOTAL WT.PER YD=         3731.96
                                                                 138.22

            BATCH WT.      AT                    0.06 CUBIC YARD

                                          TARE                  TOTAL WT.

                                                                 23.40
Patras Cement        23.40 LBS  +                      =          0.00
Crystal River Fly Ash  0.00 LBS  +                     =          0.00
Masterlife SF 100     0.00                             =        102.72
Cemex #57 (87-089)  102.72 LBS  +                      =         85.45
Cemex Sand (16-078)  85.45 LBS  +                      =         12.35
WATER                12.35 LBS  +                      =
Master Set 961R      20.81 ML
Master Glenium 7500   0.00 ML
Master Air AE 90      5.34 ML
VMA (tail)            0.00
```

Figure A.1 Group 15 mix design

```
Truck        Driver      User        Disp Ticket Num   Ticket ID   Time   Date
1615         330468      user        801299            7910        10:26 2/28/17
Load Size    Mix Code       Returned    Qty          Mix Age    Seq    Load ID
1.00  CY     CAL05R10                                            D      8292
Material    Design Qty    Required    Batched      % Var    % Moisture   Actual Wat
#57 C         1650 lb      1605 lb     1740 lb  )   3.29%    2.10% M        4  gl
SND C         1283 lb      1335 lb     1360 lb      1.83%    4.10% M        5  gl
CEM PT        620.0 lb     620.0 lb    630.0 lb     1.61%
WATER         33.50 gl     28.04 gl    28.00 gl    -0.22%                  20.03 gl
AE90          2.00 oz      2.00 oz      .00 oz    100.00%
700N          19.00 oz     19.00 oz    20.00 oz     5.26%
Actual          Num Batches:  1                                Manual   10:26:00
Load Total:   3690 lb      Design 0.451  Water/Cement 0.444  T     Design 33.5 gl      Actual 30.7 gl   To Add:  2.8  gl
Slump:   5.00  in      Water in Truck: 0.0 gl   Adjust Water: 2.0 gl  / Load   Trim Water: -3.0 gl/ CY   Note: Manual feed ec


LOAD START TIME:      LOAD END TIME:
  10:26:00 AM          10:27:32 AM
```

Figure A.2 Group 35 mix design

```
Truck        Driver      User        Disp Ticket Num   Ticket ID   Time   Date
1615         330468      user        801301            7911        11:13 2/28/17
Load Size    Mix Code       Returned    Qty          Mix Age    Seq    Load ID
1.00  CY     SSR05P12                                            D      8294
Material    Design Qty    Required    Batched      % Var    % Moisture   Actual Wat
#57 C         1235 lb      1261 lb     1260 lb     -0.07%    2.10% M        3  gl
SND C         1353 lb      1408 lb     1460 lb  )   3.66%    4.10% M        7  gl
CEM PT        1081.0 lb    1081.0 lb   1100.0 lb *  1.76%
WATER         33.00 gl     17.25 gl    17.00 gl    -1.42%                  17.00 gl
951R          22.00 oz     22.00 oz    22.00 oz     0.00%
7920          32.00 oz     32.00 oz    32.00 oz     0.00%
Actual          Num Batches:  1                                Manual   11:13:52
Load Total:   3965 lb      Design 0.255  Water/Cement 0.250  T     Design 33.0 gl      Actual 27.0 gl   To Add:  6.0  gl
Slump:   8.00  in      Water in Truck: 0.0 gl   Adjust Water: 0.0 gl  / Load   Trim Water: -6.0 gl/ CY   Note: Manual feed oc


LOAD START TIME:      LOAD END TIME:
  11:13:52 AM          11:16:15 AM
```

Figure A.3 Group 50 mix design

P1	P4	P5
14 mm	17 mm	17 mm

A15-control-side view

P1	P4	P5

A15-Control-top view

Figure A.4 Failure mode A15-Control

| P1 | P3 | P5 |
| 16 mm | 15 mm | 17 mm |

B15-control-side view

| P1 | P3 | P5 |

B15-control-top view

Figure A.5 Failure mode B15-control

P2	P3	P5
10 mm	9 mm	11 mm

A15-Wet-side view

P2	P3	P5

A15-Wet-top view

Figure A.6 Failure mode A15-wet

P1	P2	P5
10 mm	13 mm	11 mm

B15-Wet-side view

P1	P2	P5
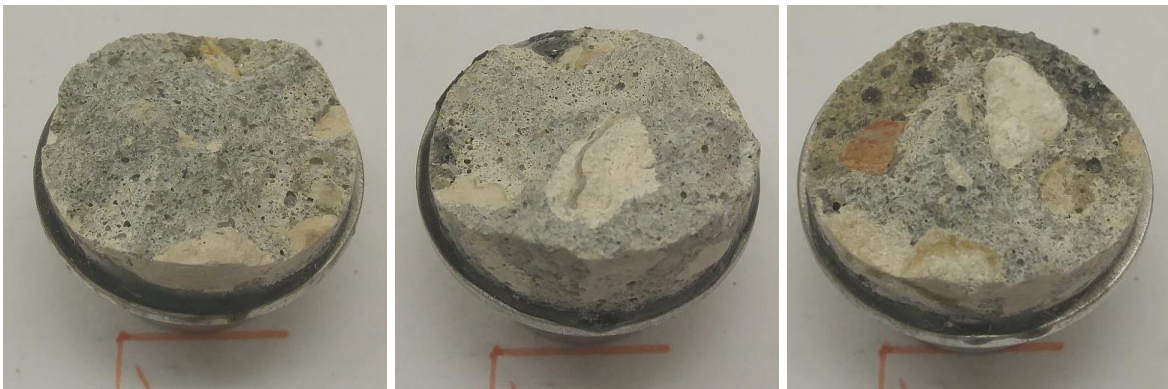
B15-Wet-top view

Figure A.7 Failure mode B15-wet
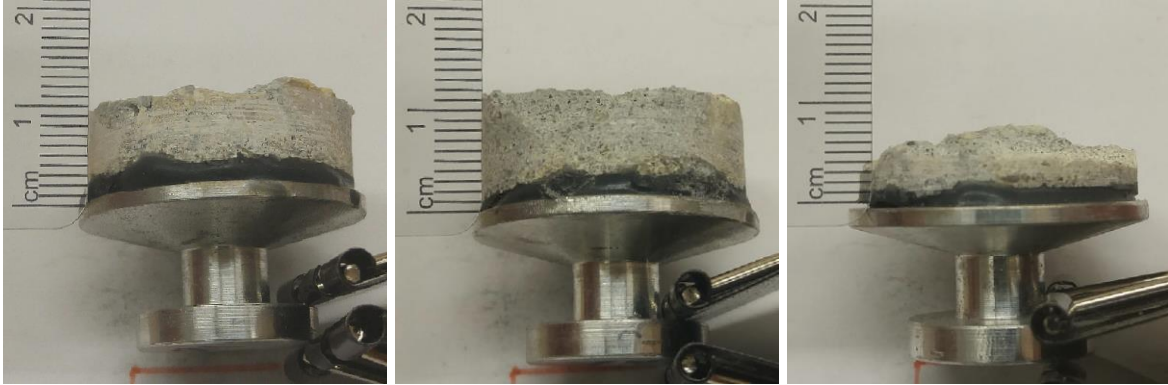
P1	P5	P6
13 mm	11 mm	8 mm

A15-Dry-side view

P1	P5	P6

A15-Dry-top view

Figure A.8 Failure mode A15-dry
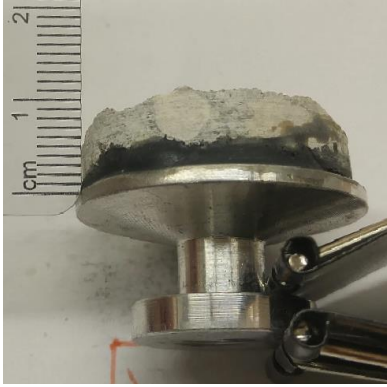
P3	P4	P5
10 mm	13 mm	9 mm

B15-Dry-side view

P3	P4	P5

B15-Dry-top view

Figure A.9 Failure mode B15-dry
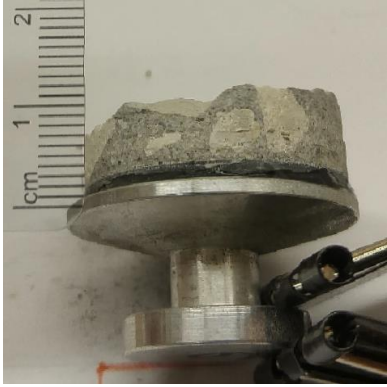
| P2 | P3 | P5 |
| 11 mm | 9 mm | 10 mm |

A35-Control-side view

| P2 | P3 | P5 |

A35-Control-top view
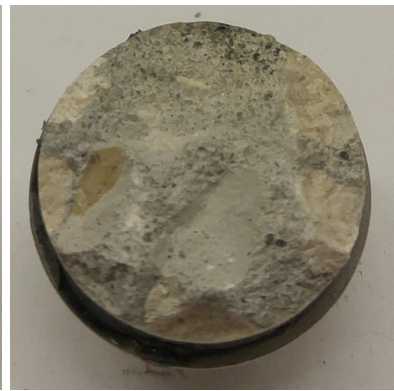
Figure A.10 Failure mode A35-control

| P2 | P4 | P6 |
| 10 mm | 9 mm | 12 mm |

B35-Control-side view
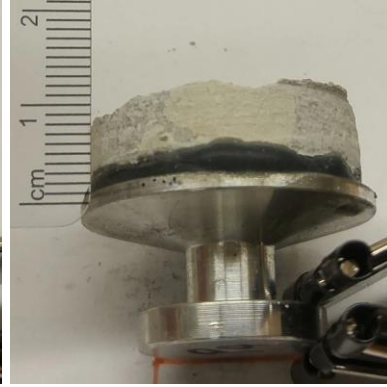
| P2 | P4 | P6 |

B35-Control-top view

Figure A.11 Failure mode B35-control

P2	P3	P6
4 mm	3 mm	5 mm

A35-Wet-side view

P2	P3	P6

A35-Wet-top view

Figure A.12 Failure mode A35-wet

P2	P4	P6
4 mm	3 mm	2 mm

B35-Wet-side view
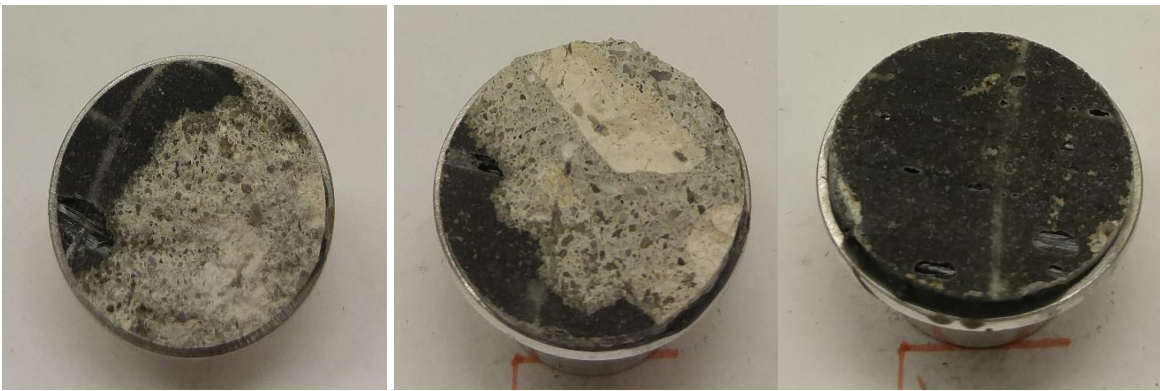
P2	P4	P6

B35-Wet-top view

Figure A.13 Failure mode B35-wet
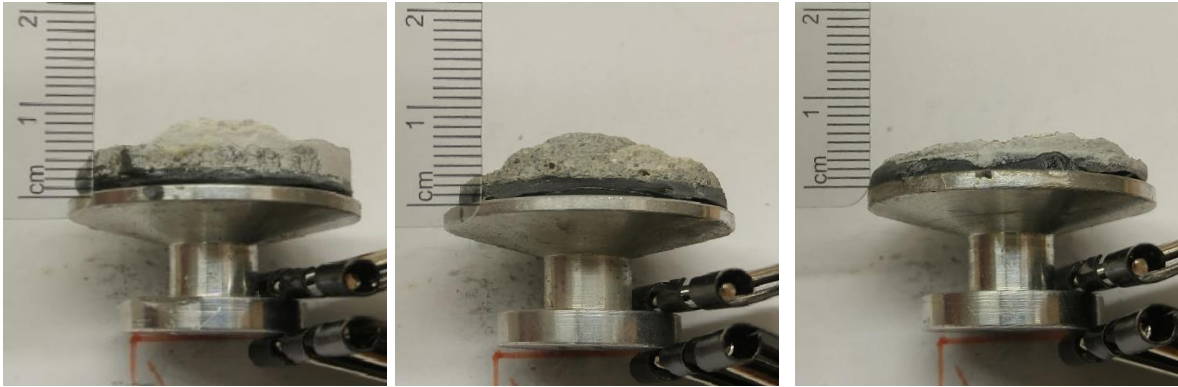
| P1 | P4 | P5 |
| 8 mm | 7 mm | 4 mm |

A35-Dry-side view

| P1 | P4 | P5 |

A35-Dry-top view

Figure A.14 Failure mode A35-dry
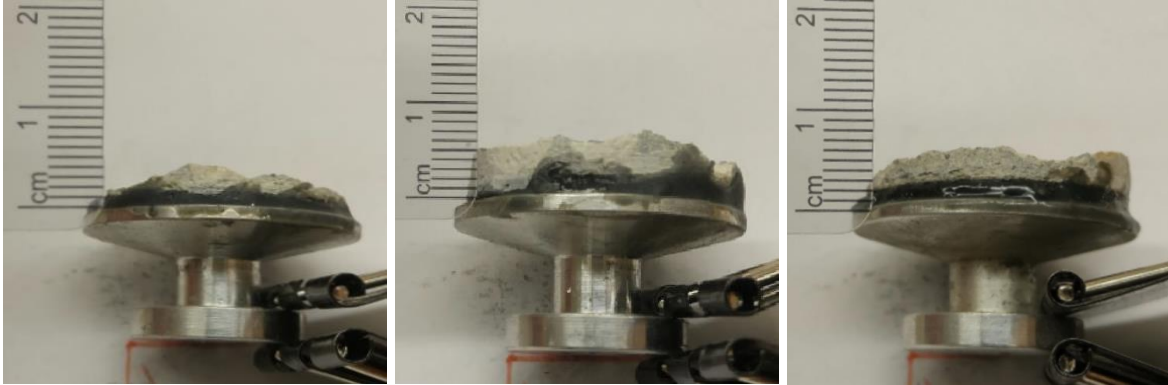
P1	P3	P4
4 mm	6 mm	5 mm

B35-Dry-side view

P1	P3	P4

B35-Dry-top view

Figure A.15 Failure mode B35-dry

| P1 | P3 | P4 |
| 9 mm | 8 mm | 9 mm |

A50-Control-side view

| P1 | P3 | P4 |

A50-Control-top view
Figure A.16 Failure mode B50-control
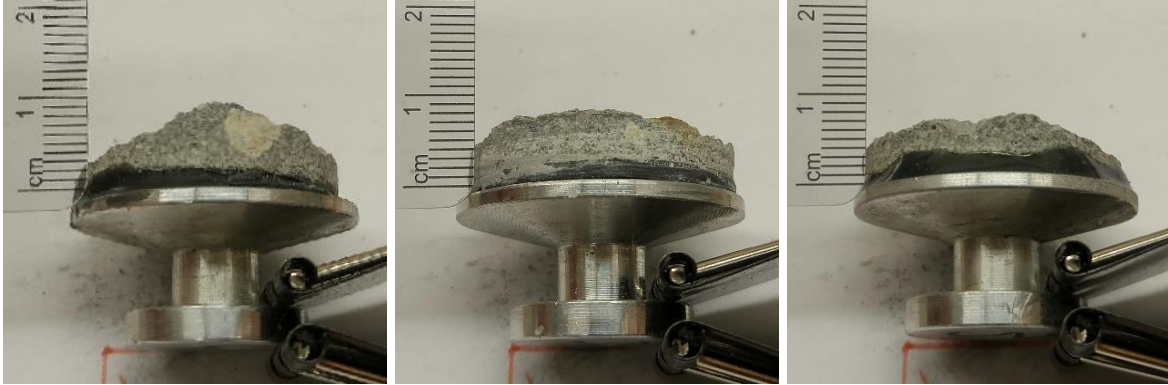
| P3 | P4 | P5 |
| 9 mm | 8 mm | 7 mm |

B50-Control-side view

| P3 | P4 | P5 |

B50-Control-top view

Figure A.17 Failure mode B50-control

P1
3 mm

P2
2 mm
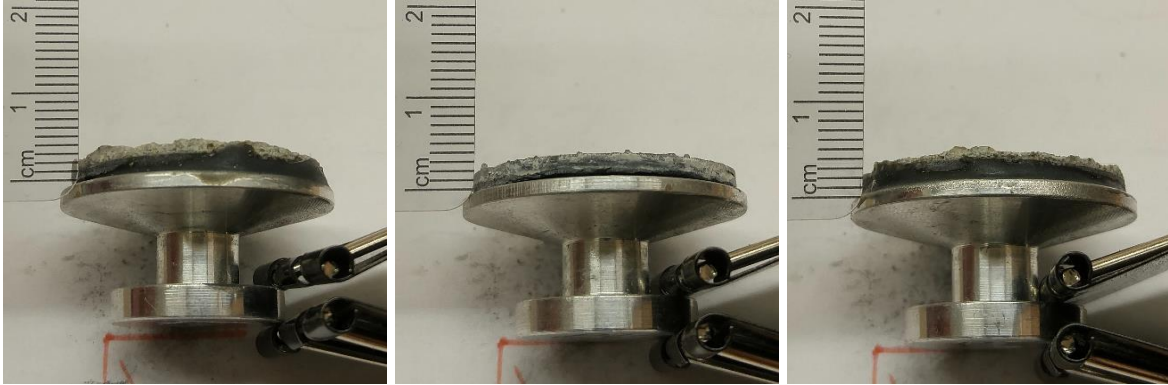
P6
3 mm

A50-Wet-side view

P1

P2

P6

A50-Wet-top view

Figure A.18 Failure mode A50-wet
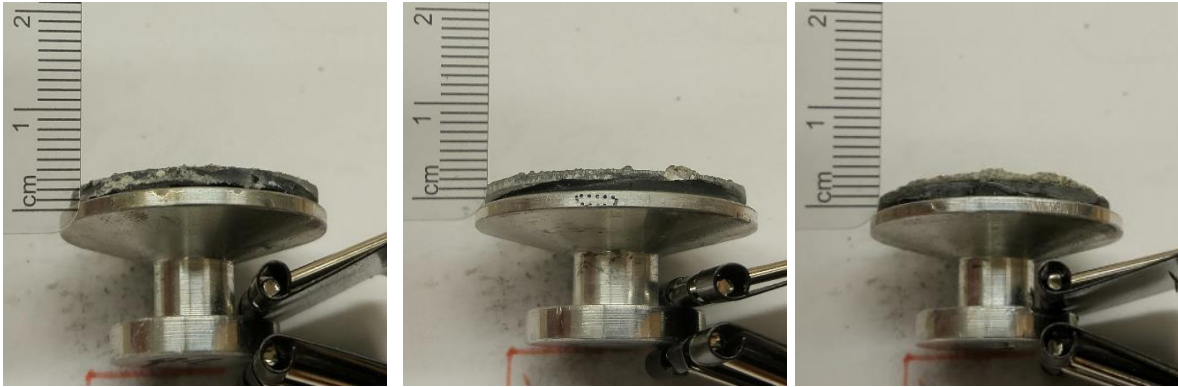
| P1 | P4 | P6 |
| 2 mm | 2 mm | 3 mm |

B50-Wet-side view

| P1 | P4 | P6 |

B50-Wet-top view

Figure A.19 Failure mode B50-wet

P5	P3	P2
3 mm	3 mm	4 mm

A50-Dry-side view
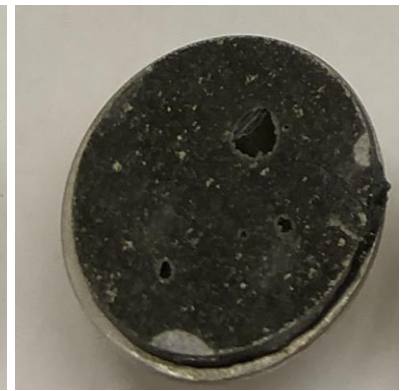
P5	P3	P2

A50-Dry-top view

Figure A.20 Failure mode A50-dry
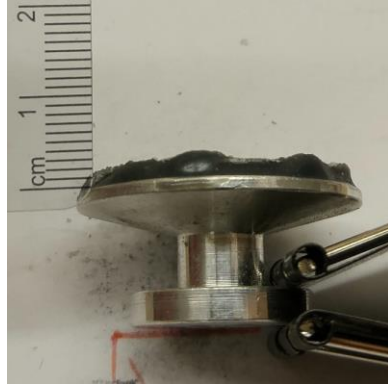
P1	P2	P6
4 mm	6 mm	5 mm

B50-Dry-side view

P1	P2	P6

B50-Dry-top view

Figure A.21 Failure mode B50-dry
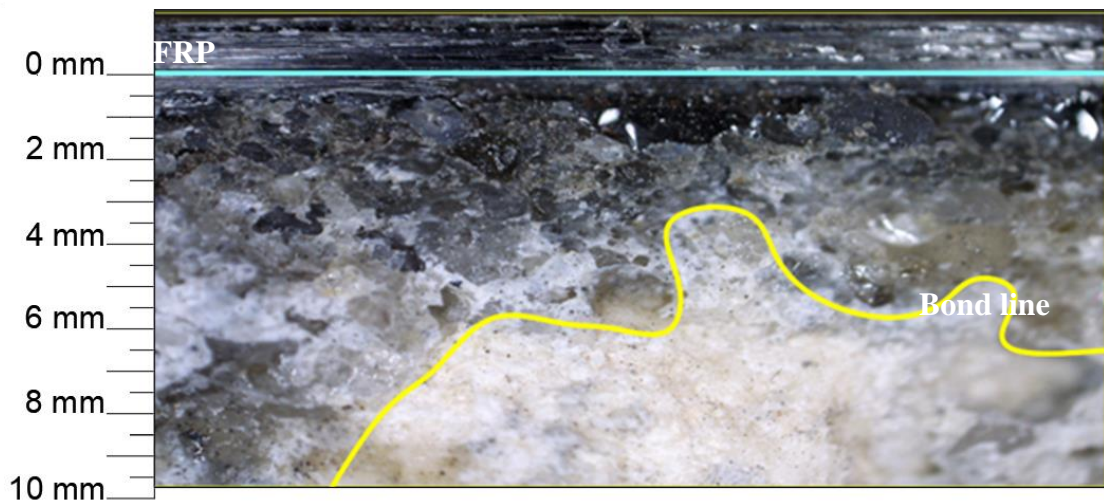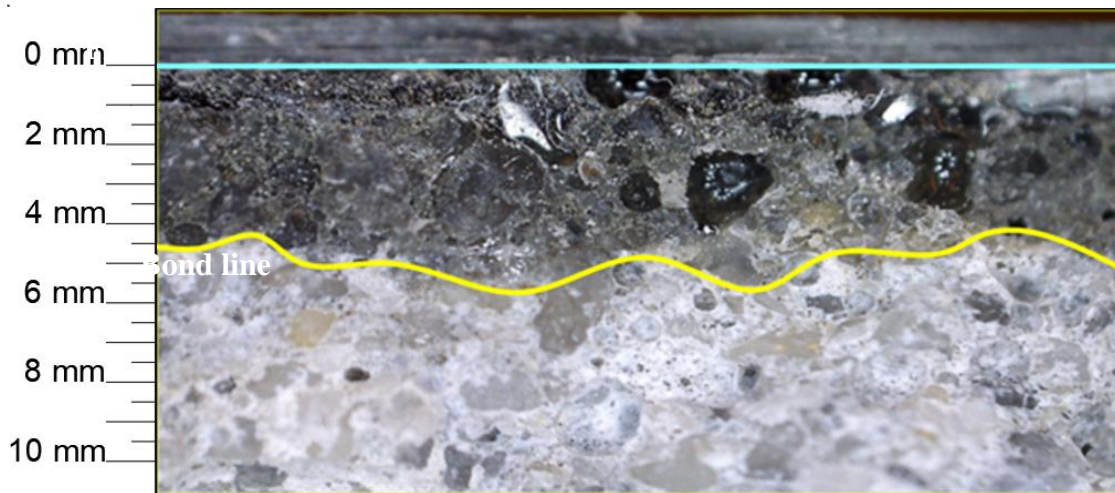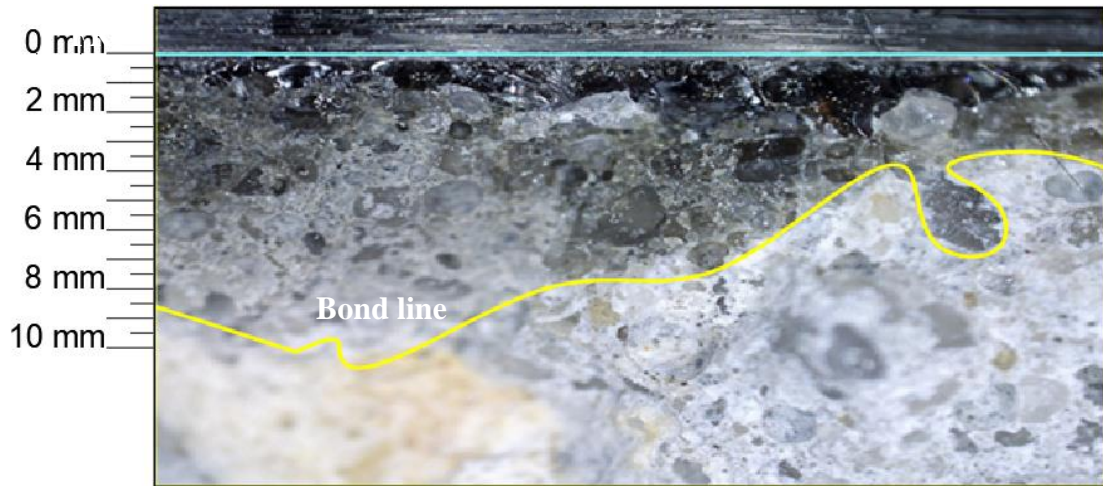
Figure A.22 Group 15 bond line images
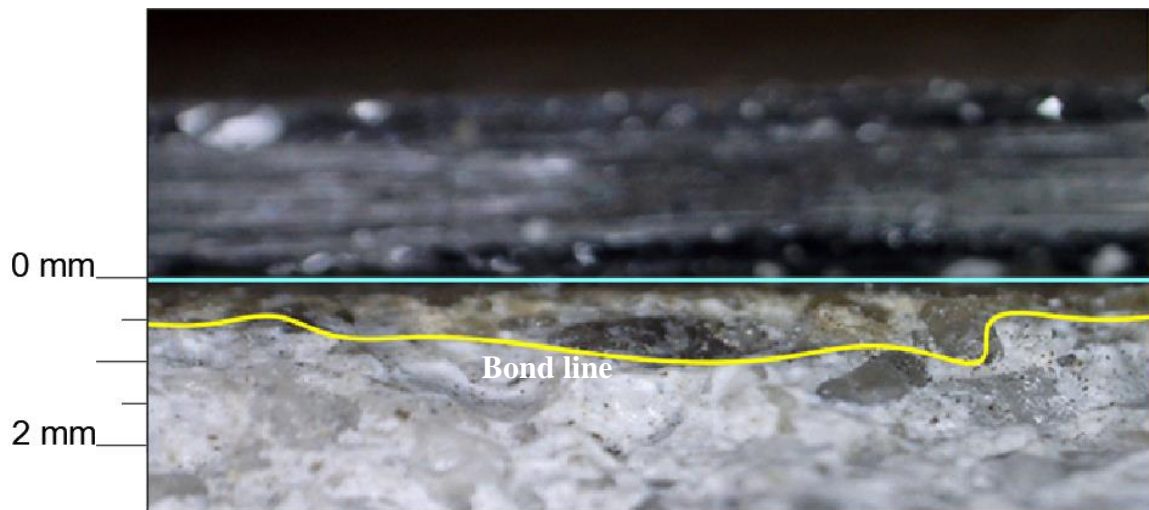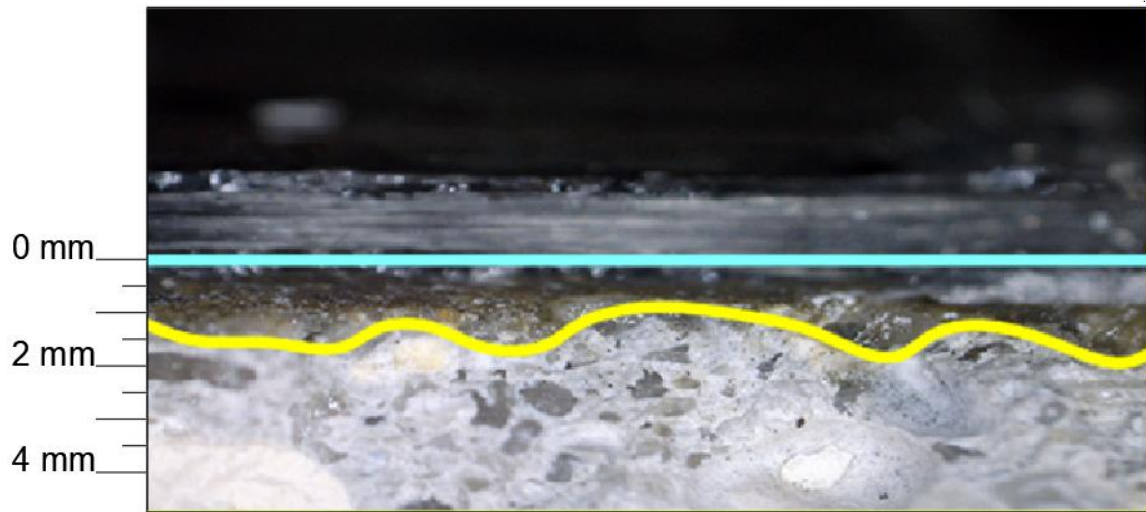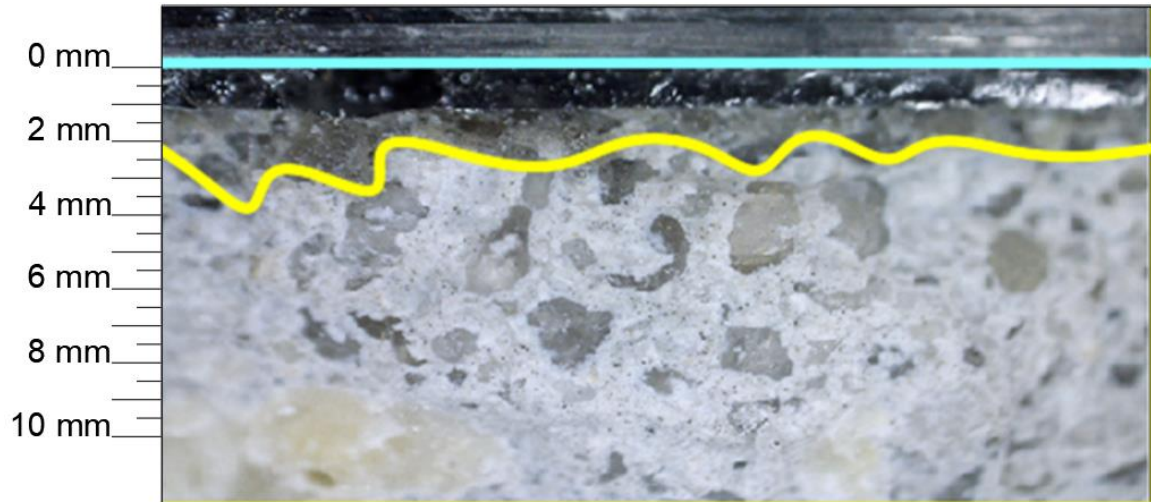
Figure A.23 Group 35 bond line images
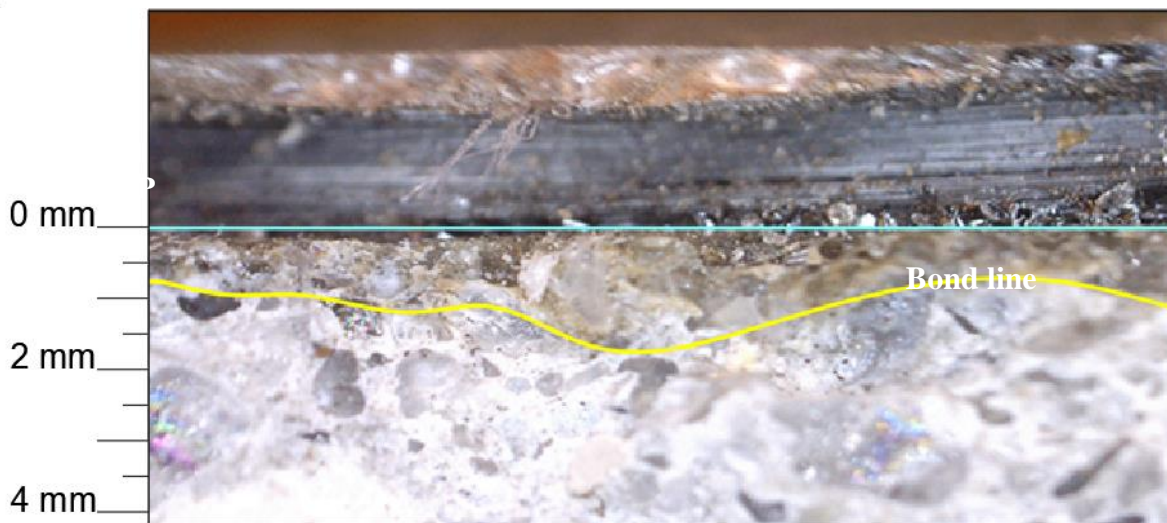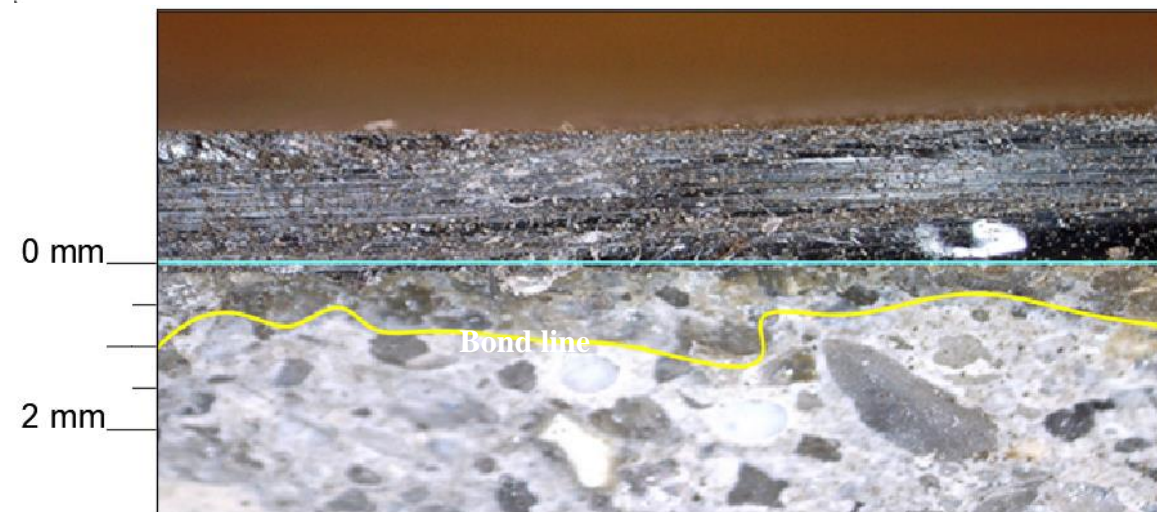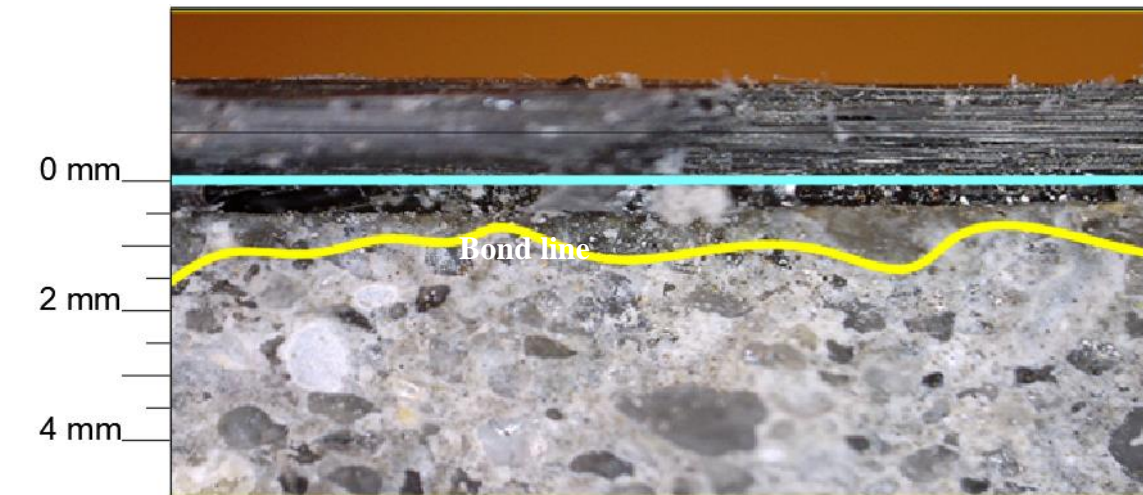
Figure A.24 Group 50 bond line images

APPENDIX B: COPYRIGHT PERMISSIONS

The permission below is used for Figure 2.1.

The National Academies of
SCIENCES · ENGINEERING · MEDICINE

National Academies Press
Rights & Permissions

April 5, 2018   Reference #: 04051800

Mostfa Al Azzawi
College of Engineering
Department of Civil and Environmental Engineering
University of South Florida
4202 E Fowler Avenue, ENB 118
Tampa, FL 33620

Dear Mr. Azzawi,

You have requested permission to reproduce the following material copyrighted by the National Academy of Sciences in a dissertation:

Attachment C, Figure C-6, page C-9, Report 609: Recommended Construction Specifications and Process Control Manual for Repair and Retrofit of Concrete Structures Using Bonded FRP Composites, 2008

Your request is granted for the material cited provided that credit is given to the copyright holder. Nonexclusive rights are extended for noncommercial use of this material.

Suggested credit (example):
Reprinted with permission from (title of publication), (publication year) by the National Academy of Sciences, Courtesy of the National Academies Press, Washington, D.C. (This credit may be edited pursuant to the publisher's house style and format so long as the essential elements are included).

Thank you,

Hannah Kenton
Permissions Coordinator
National Academies Press

161

The permission below is used for chapter 9.

Copyright Transfer Form

MS Number: S-2016-440.R1

Authors: Mostfa Al Azzawi, Philip Hopkins, Joseph Ross, Gray Mullins, Rajan Sen

Title: CFRP-CMU Bond after 20 years outdoor exposure

Transfer of Copyright by Contributors to ACI

It is the policy of ACI to safeguard all author-contributed works by copyrighting them in the name of ACI. To do so, ACI must obtain a written transfer of copyright ownership from contributing authors. The assignment of copyright will allow ACI to publish and reprint your article and to continue making arrangements for the various abstracting, indexing, copying, translating, and other services. These services are essential to the continued dissemination of publications of ACI and the information available through ACI. Therefore ACI requests the signature of all the authors. The authors warrant and represent that they are all of the authors work identified above, and they are the sole owners of the work and of the copyright pertaining to it, that they have not transferred the ownership of the work or of the copyright in the work or any interest therein or any part thereof to any other person or entity. The work is the original creation of the authors and is not copied from any other work, except for the portions that are clearly indicated by credits contained therein.

The copyright to the article identified above including, without limitation, any photographs, charts, illustrations, or graphs contained therein (but excepting any portions identified as being used with the consent of others) is hereby transferred to ACI (for Government employees this provision applies only to the extent which copyright is transferable) effective upon receipt of this manuscript. In consideration of agreement to publish the work if approved after review within at least 24 months of this assignment, authors hereby assign exclusively to ACI the copyright pertaining to the work. This includes, but is not limited to, the right to publish the work, to reproduce it, and to disseminate it, either alone, collectively with other works, in excerpts from the work or in whatever fashion ACI deems appropriate. The authors reserve the following: all proprietary rights other than copyright such as patent rights and the right to use all or part of this article in future works of their own such as lectures, reviews, personal websites, text books, etc.

If ACI does not publish the work within 24 months, it hereby agrees to reassign the copyright back to the authors. The signed transfer of copyright statement must be received at ACI headquarters before the manuscript can be accepted for publication.

	First name	Middle initial	Last name		Date
Author 1	Mostfa		Al Azzawi		5/17/17
Author 2	Philip		Hopkins		5/17/17
Author 3	Joseph		Ross		5/17/17
Author 4	Gray		Mullins		5/17/17
Author 5	Rajan		Sen		5/17/17

For further information, contact Editorial & Production Department at 248-848-3753

Revised 3/28/05

The permission below is used for chapter 10.